COMPOSITE REPAIR OF FULL-SCALE TIMBER BRIDGE CHORD MEMBERS THROUGH THE PROCESS OF SHEAR SPIKING

Travis A. Burgers
Richard M. Gutkowski, Ph.D., P.E.
Donald W. Radford, Ph.D.
Jeno Balogh, Ph.D.

December 2005

ACKNOWLEDGEMENTS

This report was prepared with funds provided by the U.S. Department of Transportation to the Mountain-Plains Consortium. MPC universities include North Dakota State University, Colorado State University (CSU), University of Wyoming, and University of Utah.

The authors appreciate the extensive assistance of Steve Babcock during the construction, fabrication, and other aspects of the specimen preparation. CSU students Misty Butler, Elliot De Jongh, Charles Manu, Rob Suarez, and Karl Wolfswinkel Helped at various times during this study, as well. Kathryn Sednek provided the clerical assistance needed in the preparation of the report and is graciously acknowledged for that work. Patrick Pellicane and Miklós Ivanyi provided very helpful reviews of the content of this report.

Abstract

Investigations into the effects of the addition of vertically-oriented shear spikes with fiberglass reinforced polymer rods have shown that the shear spikes increased the effective stiffness of the stringers of a full-scale timber bridge chord specimen. This was previously found to be true on dimension lumber and medium-sized timber. This report presents the results found from the flexural load testing of a full-scale timber bridge chord laboratory specimen. The bridge chord specimen was intentionally damaged to simulate degradation. Reinforcement was provided with 19 mm (3/4-inch) diameter fiberglass reinforced polymer shear spikes bonded to the wood by an epoxy resin. Shear spikes were installed in pairs vertically from the top of the member into pre-drilled holes to provide horizontal shear resistance and to improve the flexural effective stiffness. Results from the testing showed that with the insertion of five sets of shear spikes an average effective stiffness of 91.6 percent was recovered in the four stringers of the chord.

TABLE OF CONTENTS

LIST OF TABLES

LIST OF FIGURES

1. INTRODUCTION

1.1 Introduction

A significant number of the timber trestle railroad bridges built before World War II are nearing the end of their lifetimes because of deterioration, "wear and tear," or both. The advances made in the railroad industry have led to loads which exceed those used by the original bridge designers. Many of these bridges are no longer able to support contemporary design loads, much less the 10-20 percent axle load increase anticipated in future railroad traffic (Oomen and Sweeney [32]). Annual replacement costs of crossties on Class 1 railroads exceed $400 million, so alternatives to replacement need to be considered (Davalos, Zipfel, and Qiao [11]). As a result, there has been extensive research on methods to strengthen timber bridges. Some of this research includes replacing deteriorated members (Uppal and Otter [47]), wrapping members with fiberglass (GangaRao, Sonti, and Superfesky [14]) or carbon fiber sheets (Johns & Lacroix [27]), and installing fiberglass reinforced polymer (FRP) rods longitudinally near the tension or compression faces (Gentile, Svecova, and Rizkalla [16]). All these methods are very expensive ways to reinforce a crosstie or timber member. As an alternative to these methods, "Z-spiking" is being considered. Z-spiking is a method in which vertically-oriented shear spikes are installed in timber members to reinforce or strengthen them. This technique is the basis for the laboratory work conducted and for the research described here.

1.2 Standard Open-Deck Timber Trestle Bridges

In an American Railway Engineering and Maintenance of Way Association (AREMA (formerly AREA)) publication (Chapter 6: Timber Structures [1]) railway materials, specifications, design procedures, and maintenance for standard open-deck timber trestle railroad bridges are described. The geometry of a standard bridge is shown in Figure 1.1. It is composed of two main components: the substructure and the superstructure.

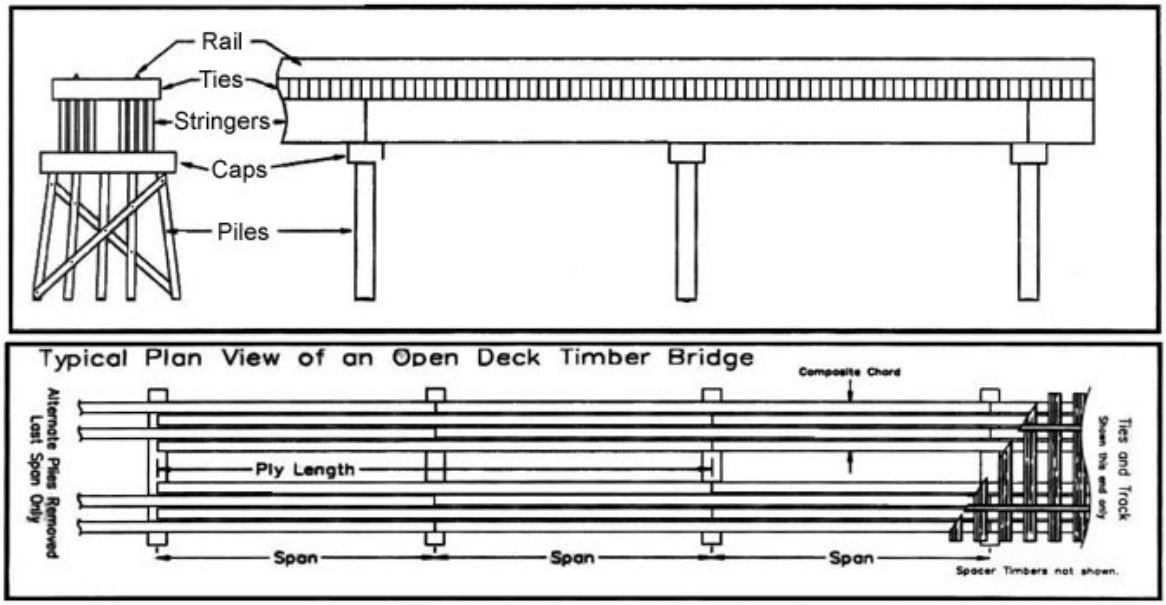

Figure 1.1: Schematic of a standard open-deck timber trestle railroad bridge

The open-deck type of bridge consists of two chords. The bridge is mirrored about its longitudinal center line and each half of the bridge is designated as a chord. The chord consists of the following:

- half the number of piles
- half of the length of the cap
- the entire length of half of the number of stringers
- half the length of the crossties
- the entire length of one of the two steel rails

The chord carries essentially half of the load of the bridge because it carries one line of the train wheels.

The railroad train rides on steel rails. Each steel rail sits on steel rail plates which rest on the crossties. The plates distribute the loads to the crossties. The rail is connected to the railroad ties (or crossties) by railroad spikes through holes in the plates.

The crossties rest on the stringers of the superstructure and are aligned perpendicular to them. They distribute the track load to the stringers. The crossties vary in dimension from bridge to bridge, but usually have about a 203 mm x 203 mm (8 inch x 8 inch) cross section. The crossties span the full width of the bridge and are typically about 3.04 m (10 feet) long.

The superstructure is composed of the stringers of the chords, the railroad ties (loosely, the ties), and the rail. Stringer widths vary from 178 to 244 mm (7 to 10 inches) and their heights vary from 406 to 408 mm (16 to 20 inches). Three to five stringers run longitudinally under each rail. They are spaced laterally between 24-102 mm (1-4 inches) in the open-deck configuration. An important feature of railroad bridges is that the stringers are two-span continuous (where the stringers extend over two spans) and are staggered so that adjacent stringers do not cross the same two spans. In the end spans, alternate stringers are single span, simply supported members.

The stringers are often laterally connected by transverse tie rods. These steel rods are usually about 19 mm (¾-inch) in diameter. A single tie rod is located at mid-depth at each midspan. Two tie rods are located about 180 mm (7 inches) from the center line of each pile cap. These two tie rods are spaced at the third points in the depth of the stringer. Each tie rod passes through metal spacers that keep the stringers at their specified spacing.

The bridge substructure consists of the piles, pile bracing, and caps. In a trestle bridge, the piles are made of timber and typically have a diameter of about 304 to 346 mm (12 to 14 inches). There are usually three to six piles per bent. The pile bracing connects the piles diagonally and restricts the lateral movement of the bridge. The cap rests atop the piles. The cross-sectional dimensions of the cap are typically 304 x 346 mm (12 inch x 14 inch) or 346 x 346 mm (14 inch x 14 inch). The cap is long enough to extend past the outer piles on each bent. The substructure supports the superstructure.

1.3 Objective of the Study

The objective of this study is to examine the possibility of using of vertically-oriented fiberglass reinforced polymer (FRP) rods (Z-spikes) in the strengthening and rehabilitation of the main load-bearing members of a timber trestle railroad bridge. The Z-spikes were used in combinations with an epoxy resin that bonded them to the timber beams. Prior studies by Radford et al. [38] and Schilling et al. [41] showed that shear spikes can significantly increase the

stiffness of dimension lumber and small- and medium-size wood members. The study included load tests of an intentionally damaged, full-scale open-deck timber trestle bridge chord test specimen when vertically-oriented shear spikes were used to repair it.

1.4 Z-spikes

In a prior study using Z-spikes, Radford et al. [38] used 3.2 mm (1/8-inch) diameter Z-spikes to reinforce nominal "2x4"s (actual dimensions 38 mm x 89 mm (1.4 x 3.4 inches)). In a subsequent study by Schilling et al. [41], 13 mm (1/2-inch) diameter Z-spikes were used to reinforce 164 mm x 203 mm (6.4 inch x 8 inch) cross-section timbers. Both were demonstrated to be highly effective in restoring or adding significant stiffness to the members.

Figures 1.2 and 1.3 show the shear spikes and the inserted Z-spikes used in the research described herein. The shear spikes used in this study had a 19 mm (¾-inch) diameter and a 406 mm (16 inch) length.

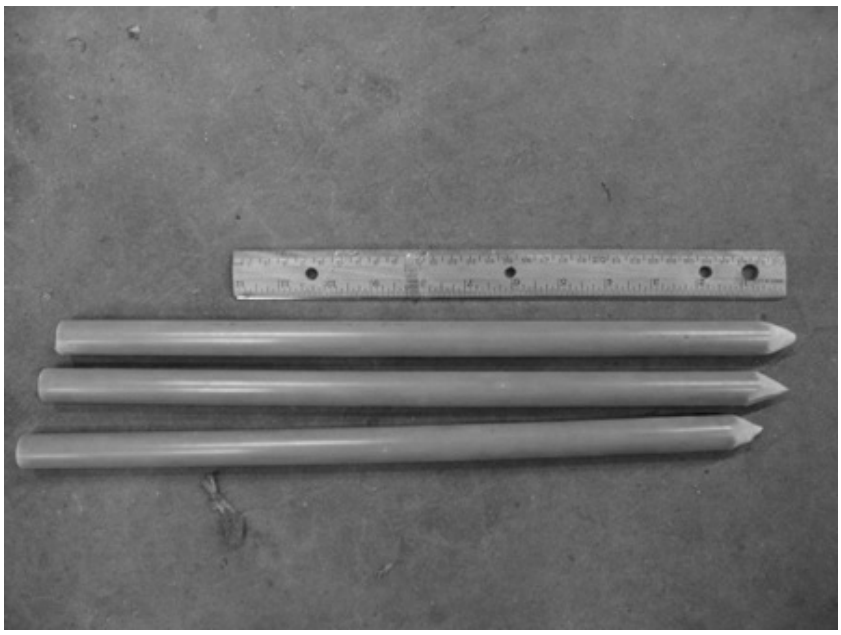

Figure 1.2: Z-spikes: 19 mm (¾-inch) diameter, 406 mm (16 inch) length

Figure 1.3: Photograph of inserted Z-spikes

2. BACKGROUND

2.1 Background to the Study

Researchers at Colorado State University (CSU) have been involved in a number of studies involving open-deck timber trestle railroad bridges and members in both the field and the laboratory (Gutkowski et al. [18, 19, 20, 21, 24, 24] and Radford et al. [37, 39, 40]). Several of those studies most relevant to the study described in this report are reviewed.

2.2 Field and Full-Scale Laboratory Bridge Testing

2.2.1 Gutkowski, Peterson, Robinson, Uppal, Oliva-Maal, and Otter

In 1999, field load tests were performed on three open-deck timber trestle bridges by CSU in cooperation with the American Association of Railroads (AAR) via its Transportation Technology Center, Inc. (TTCI) (Gutkowski et al. [22]). These tests were done to assess the load paths in the bridges. This work involved static and ramp vertical load testing, rolling wheel vertical load testing, and sinusoidal dynamic testing.

Three different bridges were chosen. The first bridge was a 31-span right bridge over the Poudre River located in Fort Collins, Colo. This bridge provided the opportunity to apply loads at many different locations. The second bridge was a four-span bridge located 402 m (1/4-mile) from the first in Fort Collins; it spans an irrigation ditch and has longer spans than typical and skewed intermediate pile bents. The third bridge was a three-span right bridge located in Pueblo, Colo. This bridge differed from the other two in that it was longitudinally curved in plan and that it had packed stringers, which means that there were no spaces between the stringers. All three bridges were considered in good condition with no signs of rot or member distress.

In the testing, static loads were provided by the test train which consisted of a locomotive, an instrumentation car, and a track loading vehicle (TLV). The TLV has special actuator-mounted intermediate axle on the car so it is capable of applying a ramp load to the bridges. A pair of hydraulic actuators mounted to the intermediate axle are used to apply the maximum vertical load. The applied load was 347 kN (78 kips) for the axle, as specified by the AAR team. In the static load tests, the three-car train was moved along the bridge and positioned in specified locations for the purpose of recording various displacement responses for each position. Numerous different loading positions were used. The displacements of the stringers, caps, and piles were measured electronically and optically relative to the ground. The major observations of this research were as follows:

- There was no consistent pattern for the deflections of the interior versus exterior stringers in a chord.
- An empirical approach was used to determine the load sharing between the stringers. This approach showed that an individual stringer within a four-stringer chord typically takes between 17 percent and 34 percent of the load, meaning that sometimes one stringer can carry twice the load of another.
- The two chords of the bridges did not displace identically. This was attributed to differing MOE values, differing end bearing conditions of the individual stringers, and relative member movements.
- Relative movements of the members because of gaps between the stringers and caps or incomplete bearing surfaces have significant effects.

- There were very small differences in the deflection ranges of the packed versus spaced stringers.

Rolling train tests were also performed and deflection data were recorded as the test train passed over the bridge at different estimated speeds. It was observed that the moving load produced approximately the same magnitude of the absolute maximum deflection peaks as observed in the previous static load tests. The major conclusion was that virtually no dynamic impact effect was evident at the speeds used for the tests. Local government regulations limited the speeds to 16.1 km/hr (10 mph) or less on the bridges in Fort Collins.

2.2.2 Gutkowski, Shigidi, Tran, Uppal, and Otter

A continuation project to the field load testing of the bridge, located in Pueblo, Colo., was subsequently conducted by CSU and the TTCI (Gutkowski et al. [23]). The objective of the testing was to investigate the effectiveness of additional (helper) stringers added to an existing bridge to increase stiffness and strength of the superstructure. The bridge was strengthened by adding a helper stringer on the outside of both of its chords.

The bridge was instrumented to enable more displacement measurements than were taken when the bridge was pre-tested (Gutkowski et al. [22]). Rolling-train tests were conducted at speeds ranging from 3.22 to 32.2 km/hr (2 to 20 mph). The pre- and post-strengthening bridge responses were compared.

The results of the field tests showed that the addition of helper stringers is a cost-effective way to increase the load capacity of the bridge. In the four-stringer chord, the maximum load an individual stringer carried was 34 percent, which is 10 percent higher than the idealized 24 percent. In the five-stringer chord, the maximum load carried was 29 percent, only 9 percent higher than the idealized 20 percent. The rolling-train tests indicated that the displacement responses for the 3.22 to 32.2 km/hr (2 mph and 20 mph) train speeds were essentially the same. In other words, no significant dynamic impact effect was evident at these train speeds.

2.2.3 Doyle, Gutkowski, Criswell, Pellicane, and Balogh

CSU researchers also conducted load testing a full-scale timber bridge chord in the laboratory (Doyle et al. [12]). This research analyzed the effects of adding a helper stringer to one-span, two-span, and three-span bridge chords. First, the specimen was assembled into three spans; then it was disassembled and reassembled into a two spans; then again into one span. Vertical displacements were measured at the mid-span and quarter-span points and near the piles. The specimens were ramp-loaded using single and two point loads. The additional exterior stringer added to the single span chord was effective in taking significant proportions of the load share.

The results of the testing were compared to model created by a commercial structural analysis software package, Axis VM (InterCad [26]). The laboratory specimen had flaws in the setup as uplift occurred at the end supports. Researchers recommended that this uplift be prevented in future testing of this and similar test specimens.

2.3 Shear Spikes

2.3.1 Radford, Peterson, and VanGoethem

Radford et al. [38] initially examined the effect of adding pultruded "shear spikes" to layered dimension lumber members. The concept of shear spiking comes from the aerospace industry (Cox [8] and Steves & Fleck [44]). The spikes are analogous to nails connecting two layered 2x4s (actual dimensions 38 mm x 89 mm (1.4 x 3.4 inches)) into a single beam, making it much stiffer than that of layered 2x4s without interconnection. The advantages of shear spiking are high performance, low cost, and compatibility of material properties with the wood.

First groups of two layered, nominal "2x2"s (actual dimensions 38 mm x 38 mm (1.4 inches x 1.4 inches)) were joined with twelve pairs of vertically-oriented nails symmetric about the center of the boards. This produced an average increase in flexural stiffness of 81 percent relative to the unattached, layered 2x2s. Then, twelve pairs of 3.2 mm (1/8-inch) diameter, vertically-oriented shear spikes were bonded with epoxy resin and inserted incrementally to additional 2x2s. The shear spikes were added in pairs at 76 mm (3 inch) spacings along length of the members. The average increase in flexural stiffness relative to the unattached, layered 2x2s was observed to be 160 percent with the shear spikes and resin.

After the 2x2s were tested, pairs of 3.2 mm (1/8-inch) diameter shear spikes were inserted in individual nominal 2x4s loaded about the strong axis. No significant increase in stiffness was found. Then additional 2x4s were sawn longitudinally along the centroidal axis from the ends to within 41 mm (2 inches) of the center (midspan) of the beam. This was done to simulate severe splitting damage to the wood specimens. Pairs of shear spikes were again inserted incrementally so that there were six sets of two on each side of the centerline. The testing showed that the stiffness returned to the level of the undamaged 2x4, effectively increasing the stiffness 100 percent relative to the damaged specimen. The insertion order of the shear spikes is shown in Figure 2.1, where R1 was inserted first, then R2, and lastly R6.

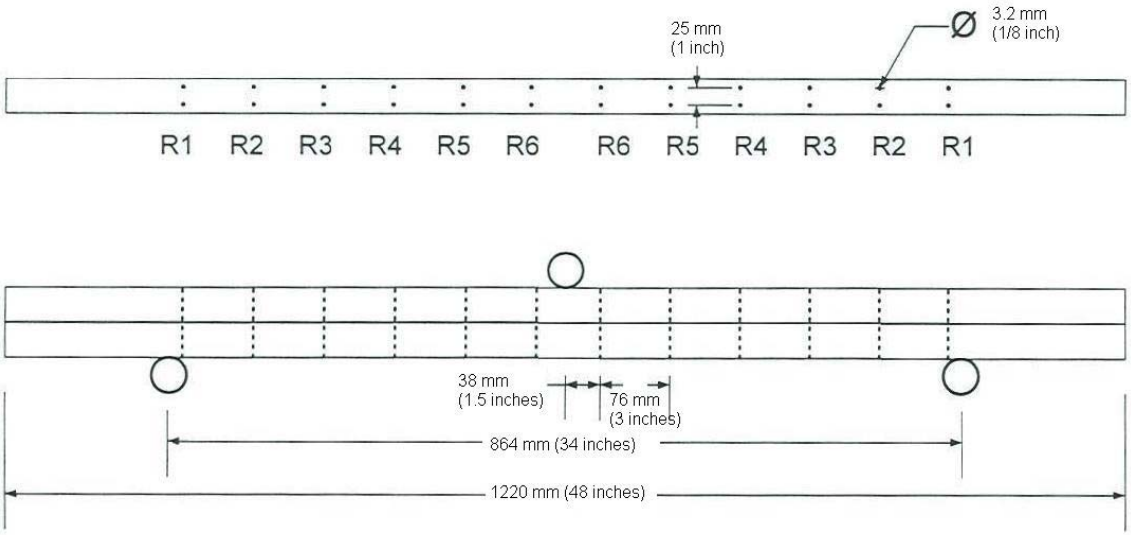

Figure 2.1: Insertion order of shear spikes

The researchers concluded from the testing that repair is directly related to the location and number of shear reinforcing rods and that the epoxy was highly effective. The method was deemed successful and it was recommended that this testing be done on larger-scale members.

2.3.2 Schilling, Gutkowski, and Radford

Schilling et al. [41] continued the research done by Radford et al. [38]. Schilling et al. used 13 mm (1/2-inch) diameter fiberglass reinforced polymer (FRP) shear spikes in deteriorated railroad crossties to increase the flexural stiffness. Their research was intended to be an intermediate step, with the ultimate goal being the repair of much larger timber beams.

Thirty-five Douglas fir timber crossties were sorted by both appearance and flexural stiffness. The appearance rating incorporated the size of the horizontal cracks and the number of longitudinal faces that showed obvious deterioration. The flexural stiffness rating ranked the crossties based on the measured values of flexural stiffness determined by load testing. In each sorting method, the crossties were rated in one of the following categories: high, medium, or low. Then the ratings from both methods (appearance and flexural stiffness) were combined to rate the crossties as either high, medium-high, medium, medium-low, or low. Based on these ratings, a group of 10 low-quality and a group of 10 medium-high quality crossties were selected for the flexural stiffness strengthening and testing program.

The flexural effective stiffness of the crossties was measured by applying a ramp loading at midspan of the crosstie. The maximum load was 28.9 kN (6.4 kips) and the load and deflection were measured at each 4.44 kN (1 kip) increment during the loading and unloading. The effective stiffness, EI, was calculated from the simple beam bending equation relating the load to the midspan displacement. This was done both before and after the shear spikes were inserted.

The shear spikes were installed in a procedure similar to that used by Radford et al. Pairs of spikes were incrementally installed symmetrically about the center of the crosstie, starting from 183 mm (7.2 inches) from the end of the beam and working towards the center. In each pair, the two spikes were located at the third points of the crosstie width. The first pairs of shear spikes were inserted near the supports and then pairs were added at a 183 mm (7.2 inch) longitudinal spacing moving from each end toward the centerline. An entire row was installed on one day, the epoxy was allowed to cure for two days, and the flexural stiffness was measured. Then the process was repeated for the next increment of spikes. The epoxy was used to bond the FRP rods to the crosstie and was injected into the holes prior to the spike being inserted using refillable caulking tubes.

The shear spikes improved the interlayer shear resistance by reconnecting the sound wood of the upper and lower portions of the crosstie. This resulted in an increased flexural stiffness. In both groups of crossties, five rows of paired shear spikes were sequentially added on each side of the centerline. For the medium-high quality group the average flexural stiffness increase with all the spikes inserted relative to before the shear spikes were inserted was 41.0 percent. In the low quality crosstie group, the corresponding average increase in flexural stiffness was 64.8 percent.

An approximate cost analysis was also performed. The total cost of the repair procedure was $67.49 per crosstie. This included the specimen preparation time and materials required for the installation of the shear spikes. The material cost was $23.74 and the labor cost was $43.74 for a repaired crosstie. As a reference, the labor cost for a five-person crew to replace a bridge stringer would be approximately $2400 per stringer. Using the shear spike method, it would cost approximately $242 for labor and $134 for materials per stringer for a total of $387 per stringer.

3. LITERATURE REVIEW

3.1 Timber Reinforcement

3.1.1 Wrap and Side Reinforcement

In 1996 GangaRao, Sonti, and Superfesky [14] conducted research on timber beams reinforced with a Glass Fiber Reinforced Composite (GFRP) "wrap," The wrap completely surrounded the four longitudinal faces of the beam. One group of wood crossties was wrapped with a GFRP fabric placed parallel to the longitudinal axis and one group was wrapped perpendicular (transverse) to the longitudinal axis. To minimize the amount of fabric used per tie, only one layer of GFRP was used. The GFRP wrap successfully increased the modulus of elasticity (MOE) by 14 percent to 41 percent and the modulus of rupture (MOR) by 14 percent to 31 percent. Ductility of the beams was also maintained as the ties could carry additional load and experienced more deformation relative to other beams that were not wrapped.

In 1998 GangaRao and Vijay [13] applied a carbon fiber fabric wrap and plates in the longitudinal direction of concrete beams with 1.38 percent tensile steel reinforcement. In this configuration, a carbon fabric plate was bonded to the tensile face using epoxy resin for a longitudinal reinforcement area of 0.124 percent. It was observed that the increase in ultimate strength of the beams was proportional to the number of longitudinal wraps. The maximum ultimate strength increase relative to the unwrapped concrete beam was 100 percent. The researchers claimed this method was more effective than strengthening the concrete beams with steel plates.

In 1999, Davalos, Zipfel, and Qiao [11] utilized a finite element (FE) model to compute how to minimize the volume of composite reinforcement in wrapping timber beams with GFRP fiber. Their study showed that the wrap need not be uniformly placed over the entire length of the beam. The wrapping technique was optimized by determining the most effective GFRP thickness and wrap locations to be used along the crosstie length. Four-point load tests showed that the linear load versus deflection responses of the wood and wood-GFRP wrap samples could be successfully predicted using FE analysis.

One disadvantage of the use of wood as a structural material is that it has poor strength in tension perpendicular to the grain. Triantafillou [46] conducted research in 1997 based on using FRP wraps to strengthen wood in that direction. FRP reinforcement was applied in the longitudinal and vertical directions, using either one or two 0.167 mm (0.00648 inch) thick plies of reinforcement in the shear-critical areas. Bending tests were then performed on 21 beam specimens. Using the test results, Triantafillou demonstrated that the contribution of the FRP could be readily calculated by a mechanics equation and experimental results correlated well with estimates, as they overestimated the shear failure loads by only 3 percent to 10 percent. Results of a parametric study suggested that the shear strength varied almost linearly with increasing reinforcement area.

Research on FRP reinforcement of wood members is not limited to the United States. In 2000, Canadian researchers Johns and Lacroix [27] used carbon fiber (CF) composite reinforcement to strengthen matched samples of dimension lumber. In the matched sample technique, two 1.68 m (4.4 foot) nominal 2x4 boards were cut from the same 3.66 m (12 foot) board. This method

allowed the researchers to remove knots in either end or from the middle of the 3.66 m (12 foot) board when cutting the 1.68 m (4.4 foot) boards. It also results in two boards that are similar in terms of density, grain, and growth patterns. Each board was nondestructively tested for its MOE values. The MOR was calculated using known correlations between the modulus of elasticity and the MOR. If the MOE of two boards from the same sample varied by more than 10 percent, they were excluded from the test. The matched samples were separated into three groups. In two groups, CF reinforcement was applied to the bottom of the beam; in the third group, GFRP was wrapped in a U-shape sleeve, covering the bottom and sides of the member. Four-point bending tests were performed and the failure mechanism was recorded. The composite layer arrested crack development, bridged defects, and confined local rupture. The reinforced wood was observed to have a higher ultimate bending stress than the unreinforced wood. The strength of the weaker of the two matched beams tested increased by 40 percent to 100 percent relative to the calculated strength of an unreinforced beam. The strength was higher than the value predicted by transformed section analysis.

Gilfillan et al. [17] at Queen's University in Northern Ireland studied the use of FRP composites using a local species of wood in 2003. Five configurations of FRP reinforcement were tested: no reinforcement, FRP tension face reinforcement, FRP tension and compression face reinforcement, FRP tension face and compression (embedded in the top instead of on the exterior face) reinforcement, and steel tension face reinforcement. The elastic behavior of all the beams with tensile reinforcement was successfully predicted by use of conventional layered-beam theory. Embedded compression strips buckled at a load closer to the predicted failure than when the compression strip was placed on the compression face. Higher strength and stiffness values were measured when the same cross-sectional reinforcement area was placed only on the tension face compared to when it was divided between the tension and compression faces.

Dutch researcher van de Kuilen [48] did work in 1991 with the application of glass fiber plates to wood beams. Plates were added to either the tension face, the compression face, or both the tension and compression faces of the wood. The flexural stiffness of the beams was considerably increased in all cases. There was no significant difference in stiffness when plates were applied to the tension face versus to the compression face. The effect of putting plates on both the tension and compression faces was virtually the same as for putting twice the thickness of the plates on only one face. However, the procedure was deemed not economical, as timber beams with equivalent properties could be purchased for 2-2.4 times lower cost, not including the labor of the reinforcement installation.

3.1.2 Other Reinforcement Methods

One alternative method to reinforce timber is to insert the fiber-reinforced polymers longitudinally into timber. Gentile, Svecova, and Rizkalla [16] conducted such experimental research on creosote-treated, Douglas fir solid sawn timber beams in 2002. GFRP rods were inserted longitudinally over the length of the beam. In 22 4.3 m (14.1 ft) long beams, grooves were cut in the side faces 30 mm (1.2 inch) from the bottom face to simulate in situ application. Then 4.1 mm (0.20 inch) diameter bars were inserted. In the four 10.4 m (32.1 foot) beams, either four grooves were cut on the bottom face or one groove was cut in each longitudinal side face 40 mm (2.0 inches) above the bottom face. Either 10 mm (0.39 inch) or 13 mm (1/2-inch) diameter bars were inserted. A bead of epoxy was placed in each groove, the GFRP bars were placed in the groove, and additional epoxy was inserted to completely fill the groove. In the longer beams, the bars were held in place by staples inserted at 1-m (3.3 foot) intervals so that they would stay in place during the application of epoxy. The beams were load tested to find differences in stiffness, strain, and ultimate flexural strength.

The reinforced beams, relative to the unreinforced beams, showed increases in flexural stiffness, ultimate tensile strain, and ultimate flexural strength. The increase in flexural stiffness was 4 percent to 7 percent. The increase in ultimate tensile strain was 64 percent. The average increase in ultimate flexural strength was 18 percent to 46 percent for reinforcement ratios between 0.27 percent to 0.82 percent of the gross beam area. No debonding or delamination of the GFRP bars was observed. The GFRP reinforcement impeded crack opening, confined local rupture, and bridged local defects in the timber. The failure mode of the timber changed with the addition of the reinforcement from brittle tensile failure to ductile compressive failure.

Another alternative to strengthen timber is to locally apply epoxy to damaged areas. Avent [3] discussed difficulties with development of design criteria for using such epoxy repair of timber in 1986. It is complex to establish design criteria because needed computational methods for calculating allowable stresses are difficult to formulate. The actual glue line stress and an allowable glue line stress were defined using a number of reduction factors for commonly known effects including exposure conditions, duration of load, aging conditions, and natural variability of the wood. These methods were demonstrated using numerical examples.

In 1998, Uppal and Otter [47] summarized methods to extend the life of timber trestle railroad bridges. The strength of a timber trestle railroad bridge can be improved in a number of ways, many of which are obvious as they involve the replacement or repair of members. The use of helper stringers has been proven to reduce the overall deflection of the chord and assist in the load sharing between stringers. They also suggest adding helper stringers or reinforcing stringers with the addition of vertical or horizontal plates. Reinforcement plates made of steel and fiberglass have been proven to strengthen the bridges.

3.2 FRP-Wood Interface

Barbero, Davalos, and Munipalle [4] performed extensive research on the bond strength of adhesives used between FRP and wood. A finite element model was developed to try to predict the response of the interface under shear stress. The researchers state that mechanical fasteners create high-stress concentrations when they are used to attach reinforcement to wood. Adhesive bonding is an improvement because it creates a better shear transfer and has a larger contact area.

Experiments were conducted on yellow poplar wherein the ultimate shear strength was measured for different wood-wood (e.g. nature of the wood rather than the species) and wood-FRP interface combinations. Six interface combinations were used in the testing: sapwood-sapwood, heartwood-heartwood, sapwood-vinylester, sapwood-polyester, heartwood-vinylester, and heartwood-polyester. Three types of adhesives were separately used to bond the interfaces: resorcinol formaldehyde (RF), emulsion isocyanate, and epoxy. Each wood-wood or wood-FRP combination was bonded by at least one of the adhesives. A shear test was performed on 20 wet and 20 dry samples.

In the wet shear test, a vacuum-pressure-soak cycle accelerated the water absorption process. This cycle took place for one and a half hours, leading to increases in the moisture content of the wood as high as 100 percent. Wood is known to swell as it absorbs water, but FRP composites do not significantly change in volume with increasing water content. Thus, when joined by adhesives and subjected to water, the combination of the swelling of the wood and the constant volume of the FRP leads to stresses on the interface because the wood expansion is restricted by the FRP.

Barbero et al. observed that the ratio of shear strength of the wet specimens compared to dry specimens was 0.43. The FE modeling predicted wet-to-dry ratios of the average and maximum stresses of 0.48 and 0.46, respectively. In the FE model, the deterioration of the adhesive bond was considered insignificant; therefore, it was not taken into account.

Gardner, Davalos, and Munipalle [14] conducted research on the effectiveness of a vinylester FRP and wood interface in 1994. Their research showed that FRP composites can be adequately bonded to wood. RF adhesive was recommended for exterior applications while for interior applications, epoxy and RF were both recommended.

Little has been done to study the long-term performance and delamination behavior of FRP-wood composites. Davalos, Qiao, and Trimble [9] sought to examine these aspects in 2000. A high number of variables including types of adhesive, bonded materials, and coupling agents were involved. It was determined that a standard test could assess the effect of bonding parameters, but performance-evaluation tests were not sufficient to predict the effects of temperature, moisture, and service load conditions on delamination.

In a continuation of this research, Davalos, Qiao, and Trimble [10] evaluated fracture response of wood laminates. A contoured double-cantilever beam (CDCB) was used to analyze fracture toughness, which is an important quantity because it can be used to evaluate crack arrest and extension in delaminations. The CDCB specimen proved to be effective for obtaining fracture toughness values for Mode I failures.

4. EXPERIMENTAL TEST SETUP AND PROCEDURE

4.1 Experimental Test Setup

The laboratory test specimen was a full-scale representation of a chord of an open-deck timber trestle railroad bridge. A single chord was constructed and tested instead of the entire width of the bridge because of space limitations in the Structural Engineering Laboratory and the geometry of the testing frame. The train load is essentially equally shared by the two chords, so a single chord will get half of the train load. Thus, constructing and testing a single chord is the idealized case for imposed train loading. A single chord also allows for less construction material and half of the maximum load requirement.

Because the objective is to observe the effects of Z-spiking on the stiffness of large members, the stringers are the primary concern of this research. Therefore, it was decided that the stringers would be the only timber members, as opposed to all the members (e.g. rails, crossties), used in the test specimen. This is because they are the major load-bearing members in a timber trestle bridge and their individual use would reduce the number of variables involved in the results. The use of only the stringers also reduces the overall stiffness of the chord. For example, if the steel rail were included it would require much more load to deflect the bridge a given amount than in the present configuration.

A three-span, four-stringer bridge chord was constructed as shown in Figure 4.1. A schematic of the chord is shown in Figure 4.2. The timber materials were donated by the AAR in 1996 and had been used in a previous CSU research project (Doyle et al. [12]). In that previous project, the members were tested at loads well below their ultimate strength capacities, thus they were likely still intact after the load testing. However, for the objectives of this research, any damage that might have been inflicted would be advantageous.

Figure 4.1: Photograph of full-scale specimen

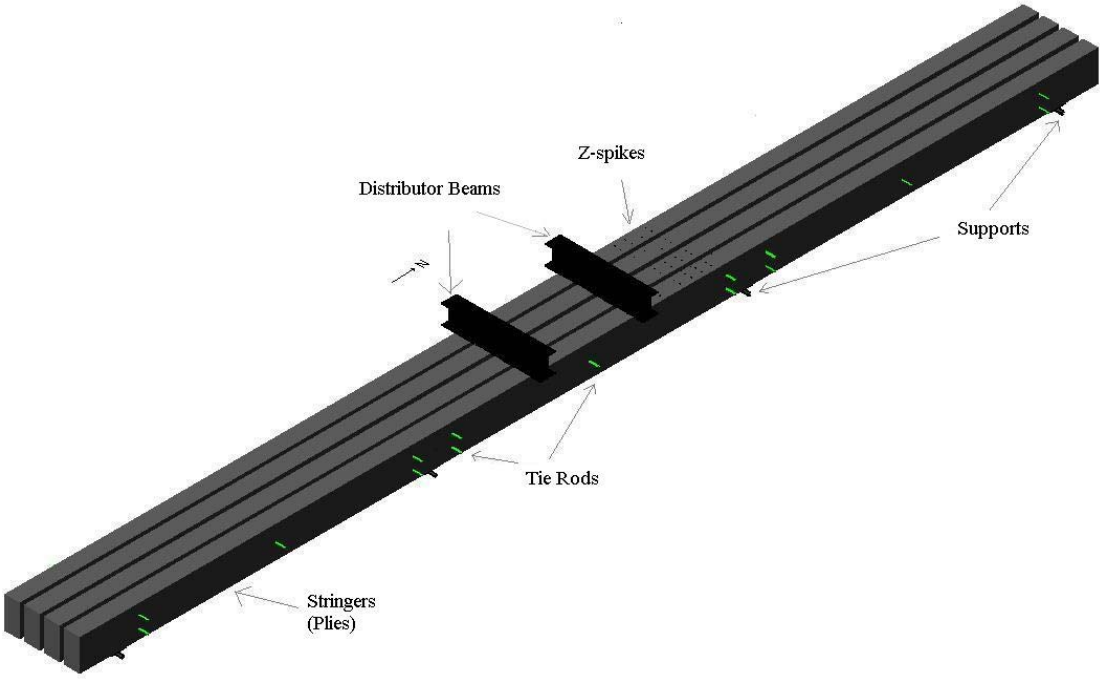

Figure 4.2: Schematic of specimen

It is also important for the specimen to be three spans because this allows for the two-span continuous members to be at least staggered in lateral placement while not having side-by-side one-span members, as would be the case in a two-span test specimen.

The four-stringer bridge chord was comprised of four two-span continuous members and four single-span members. As shown in Figure 4.3, each span was 4.013 m (13 feet 2 inches or 148 inches), center to center of the supports, which is less than the typical 4.27-4.47 m (14-14 feet). This shorter span distance was necessary because of the space restrictions involved in welding the interior column base plates to the steel members of the existing test frame. The cross sectional dimensions of each stringer varied slightly, but they were all approximately 203 mm (8 inches) wide and 406 mm (16 inches) deep. The single-span members were placed in the end spans and were alternated with the two-span continuous stringers.

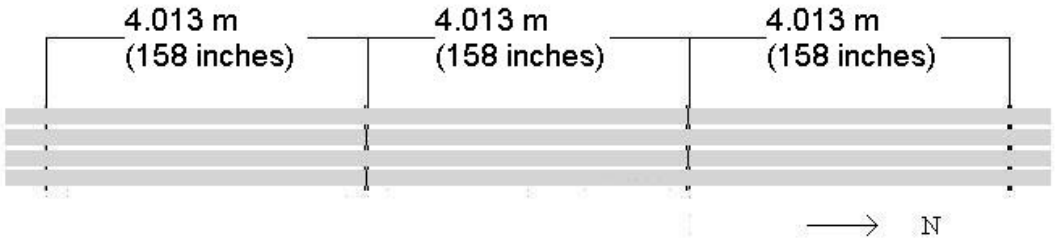

Figure 4.3: Plan view schematic of spans

The stringers in the chord were supported by steel crossbeams on the underside at the four support locations. The crossbeams were bolted to steel columns. The steel columns were then bolted to the laboratory floor. The steel columns were used to simulate the piles and the steel crossbeams served as the caps. The use of steel piles and caps allowed for the focus of the research to be on the timber stringers by eliminating support displacement uncertainties that could arise from using timber members for the substructure. These aspects are being examined in another ongoing CSU project.

At each support the stringers rest on 203 mm x 203 mm (8 inch x 8 inch), 13 mm (1/2-inch) thick steel plates. The steel plate is free to rotate as it rests on 41 mm (2 inch) diameter steel round stock. Each piece of round stock is located atop a steel crossbeam as shown in Figure 4.4.

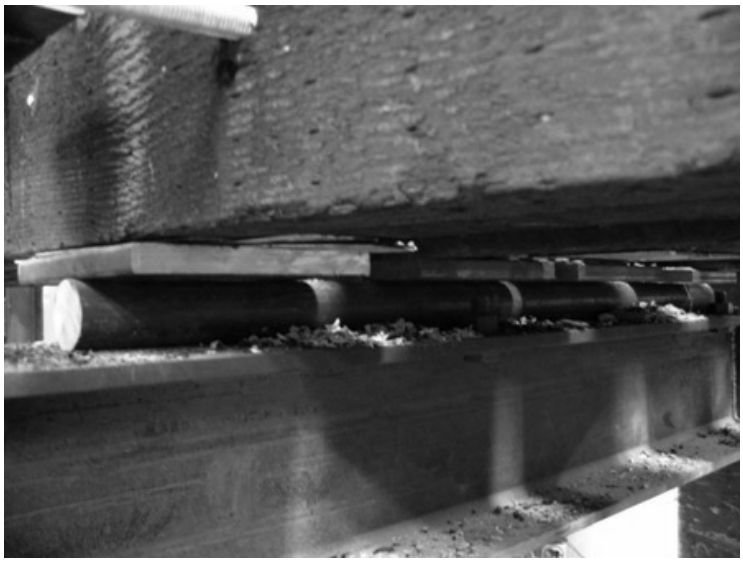

Figure 4.4: Timber stringer on steel crossbeam, round stock, and plates

Careful effort was made to tie down all the stringers at the supports to prevent uplift of the end spans which tends to occur under loading in the middle span. A schematic of the joint connection is shown in Figure 4.5. A rectangular steel tubular section (102 mm x 41 mm x 6.4 mm) (4 inch x 2 inch x 1/4-inch) was placed transversely over the top of the stringers. A 22 mm (7/8-inch) diameter hole was drilled in each end of the tubular section. A 13 mm (1/2-inch) thick L-section was bolted near the bottom of the stringers to each steel support column on either side of the test specimen. Each L-section had a 22 mm (7/8-inch) diameter hole drilled through its center and was strengthened by two welded diagonal stiffeners. A vertical 19 mm (3/4-inch) diameter steel threaded rod connected the steel tube and the steel angles. The steel tubular section was wide enough to hold down each stringer at the span joint and the configuration allowed for rotation at the joint. Because of the differing heights of the timber members, all the members were adjusted to be the same height using a varying number of metal shims placed between the timber member and the steel tubular section.

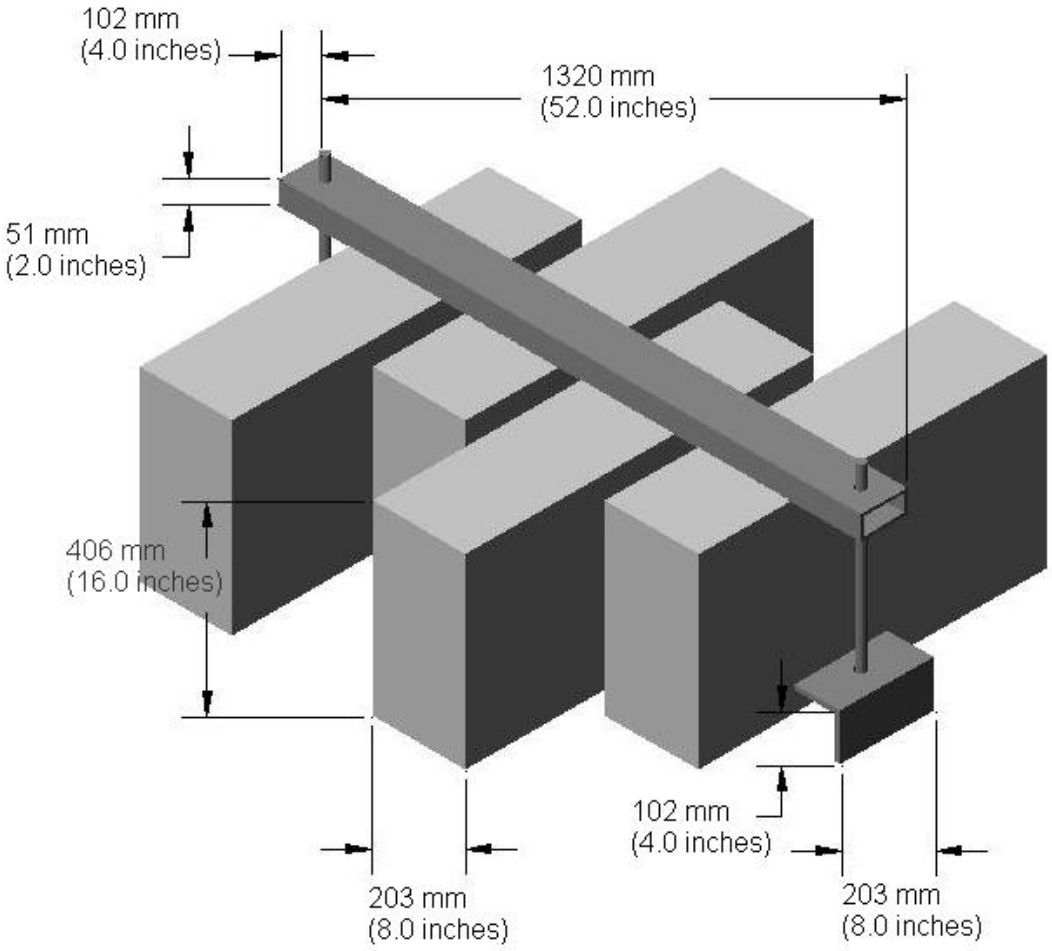

Figure 4.5: Schematic of joint connection

Transverse steel tie rods were used to laterally interconnect the four stringers to make the chord. The tie rod configuration is shown in Figure 4.6. The tie rods were 1.22 m (4 foot) long, 19 mm (3/4-inch) diameter threaded rods. This allowed them to go through each of the four stringers, as well as the 41 mm (2-inch) spacers used to keep the beams apart in the standard open-deck configuration. 24 mm (1-inch) diameter holes were drilled for the transverse tie rods. A total of 15 tie rods were used on the test specimen. Tie rods were placed at mid-depth at each of the three midspans. The width of the support columns dictated the end-span spacing so the two end-span tie rods were placed 244 mm (10 inches) from the end of the span and spaced at approximately the third points in the member depth. At each interior joint, four tie rods connected the single- and two-span members. Each transverse tie rod has a 41 mm (2-inch) outside diameter washer and a 19 mm (3/4-inch) diameter nut to secure the stringers, maintaining a 41 mm (2-inch) spacing in between each member. The spacers, shown between the beams in Figure 4.7, were made of a 19 mm (3/4-inch) inside diameter copper pipe welded to 41 mm (2-inch) outside diameter washers.

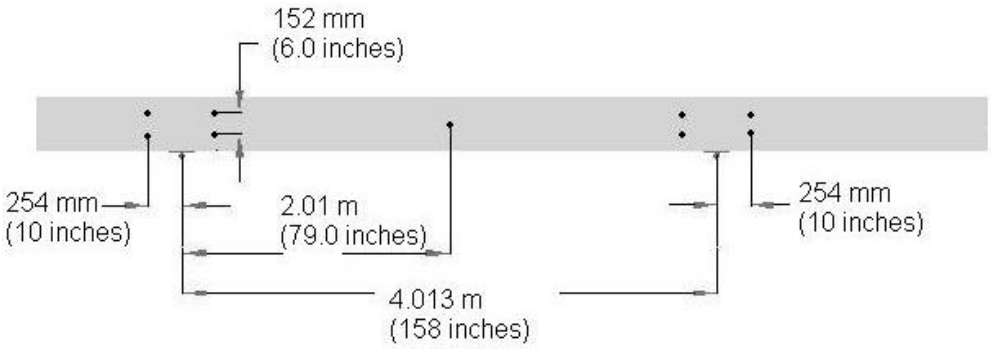

Figure 4.6: Elevation view of transverse tie rod configuration

Figure 4.7: Plan view of beams with spacers

4.2 Damaging the Timber Beams

The objective of the study is to rehabilitate or strengthen the members of a timber trestle railroad bridge. The beams used in this experiment were in good physical condition when the bridge was assembled. A bridge member in good condition would not need to be rehabilitated. For this reason, intentional damage was inflicted on the chord members.

The south half of the bridge chord was intentionally damaged by horizontally cutting the beams of the center span at mid-depth. A cut was made from the south interior support towards the loading point on only the center span. This was first attempted using a two-man saw with a thin blade, but this saw was not effective because the blade was twisting inside the two interior beams. Next, the handles were put on a wood-cutting blade. This blade worked only slightly better as it also twisted in the two interior beams. These blades are shown in Figure 4.8. The combination of these blades made a cut of approximately 203 mm (8 inches) in 8 hours. Thus, this method was abandoned.

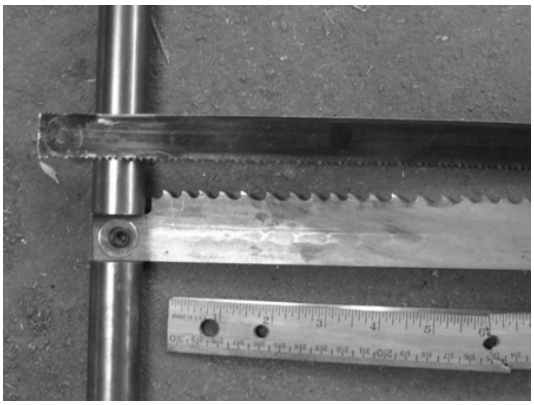

Figure 4.8: Handsaws

Finally, a chainsaw was used to inflict the damage, creating a much larger width of cut than originally intended. The chainsaw damage and shimming can be seen in Figures 4.9 and 4.10. The cut was shimmed so the gap would not close when load was applied to the specimen.

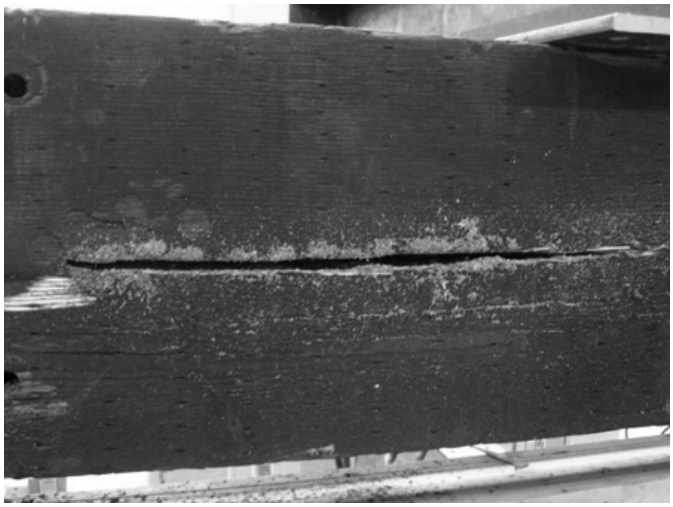

Figure 4.9: Chainsaw damage

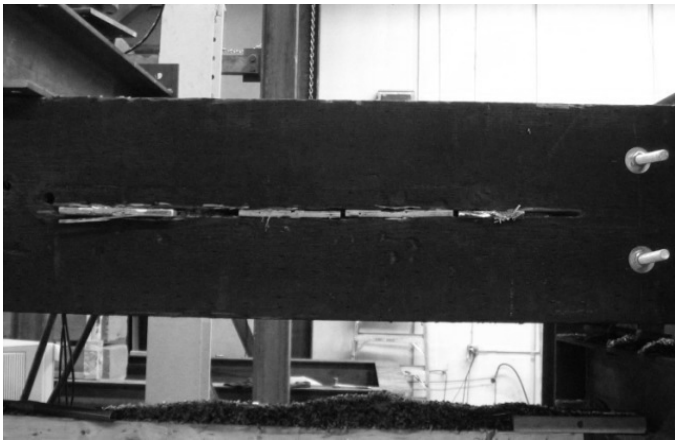

Figure 4.10: Shimmed chainsaw damage

The chainsaw was used on each side of the specimen to cut two stringers at a time, but the blade did not cut the inner 41 mm (2 inches) of the inner two stringers because of the length of the blade. The rest of the damage on the two inner stringers was done by loading the bridge and letting the load propagate the crack. However, the loading damaged the beam more than anticipated. A crack was initiated at the end of the cut and extended into the center third of the span, between the two load points.

The north half of the center span of the bridge chord was then cut using the chainsaw as described earlier. The remaining uncut segments of the two interior stringers were cut using the two-man wood-cutting handsaw.

4.3 Z-spike Installation

Z-spikes were each cut from a 1.40 m (49 inch) long base rod stock. Each rod was cut to a length of 406 mm (16 inches), the same as the depth of the timbers, leaving approximately 13 mm (1/2-inch) extending from the top face of the timber upon installation. An angle grinder was used to bevel a point out of the last 24 mm (1-inch) of the leading edge of the rod. This was done to reduce force that was required to drive the rods and so that the blunt end of the rod would not scrape the epoxy mix off of the sides of the hole during installation.

Pairs of Z-spikes were incrementally installed in the south half of the center span of the test specimen after an initial load test on the virgin specimen. In each increment, the two spikes were located at the third points of the crosstie width.

The progress of the damage and repair of the south half of the center span was measured 11 times. Short labels are given before the description and are used in the tables and figures in Chapter 5: Results.

1) No damage – The specimen was tested before any damage.
2) 8-inch cut (before crack) – An 203 mm (8-inch) cut was made that extended from 483 mm to 686 mm (19 inches to 27 inches) from the south support. During the load test to measure the effective stiffness of the 203 mm (8-inch) cut, there was a loud crack.
3) 8 inch cut (after crack) – Upon inspection of the specimen, it was evident that visible damage had occurred, particularly in the two beams on the east side, so the specimen was retested with the 203 mm (8-inch) cut.
4) Full cut completed – The cut was completed; it extended from 203 mm (8 inches) to 1320 mm (42 inches) from the south support.
5) Z-spikes in end – One set of Z-spikes was placed at 304 mm (12 inches) from the south support.
6) Repaired center beams (south) – Then the region between the two distributor plates was repaired. First the south half was repaired. In the repair of the south half, four sets of Z-spikes were placed at approximate 127 mm (4-inch) spacings from the midspan to the south distributor beam.
7) Repaired center beams (north) – Then the north half of the region between the distributor beams was repaired. Three sets of Z-spikes were placed at approximate 127 mm (4-inch) spacings from the midspan towards the north distributor beam.
8) 1st set of Z-spikes – Next, the Z-spikes were added to the cut. The first set of Z-spikes was placed 813 mm (32 inches) from the south support.
9) 2nd set of Z-spikes – The second set of Z-spikes was placed 447 mm (18 inches) from the support.

10) 3rd set of Z-spikes – The third set of Z-spikes was placed at 1220 mm (48 inches) from the support.
11) Repaired center beams (south2) – Next, the region between the two distributor beams was further repaired. A total of three sets of Z-spikes were added between the four sets already in place between the midspan and the south distributor beam. Two sets were also added to continue the approximate 127 mm (4-inch) spacing under the south distributor beam. The repair locations between the distributor beams are shown in Figure 4.11. In the figure, the dimensions above on the south half label the Z-spikes used in the first repair. The dimensions on the north half label the Z-spikes used in the second repair. The dimensions below on the south half label the Z-spikes used in the third repair.

On the north half of the specimen, Z-spikes were placed in the following order (the locations are shown in Figure 4.12):

1) at the center point of the damage, 787 mm (31 inches) from the support
2) at the three-quarters point of the damage, (41.4 inches) from the support
3) at the quarter point of the damage, 421 mm (20.4 inches) from the support
4) at the eighth point of the damage, 387 mm (14.24 inches) from the support
5) at the three-eights point of the damage, 644 mm (24.74 inches) from the support.

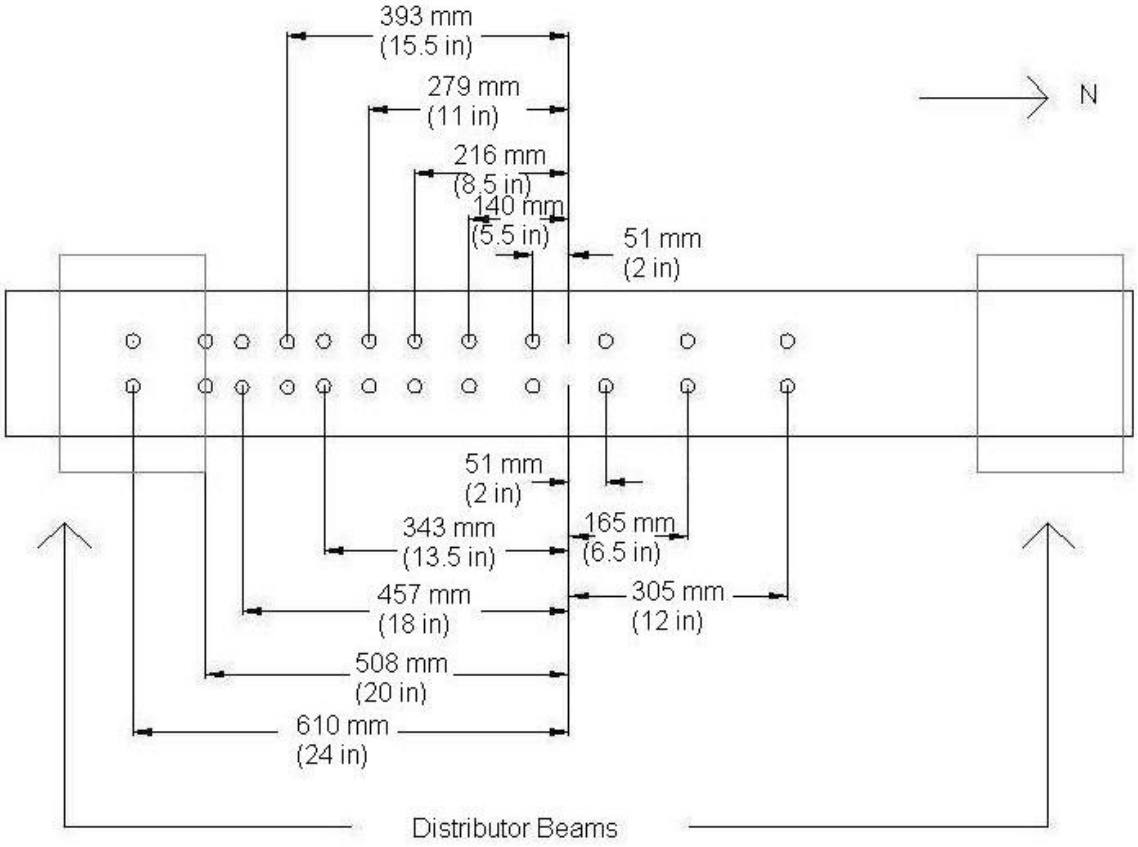

Figure 4.11: Z-spike center repair

The Z-spikes were added at the center of the damage first because that is the best location if only one were to be used. The second and third Z-spikes were added at the three-quarter and one-quarter points of the damage because these are the best locations if three were to be used. The fourth and the fifth spikes were added closer to the support because the rods are more effective closer to the support than to the load.

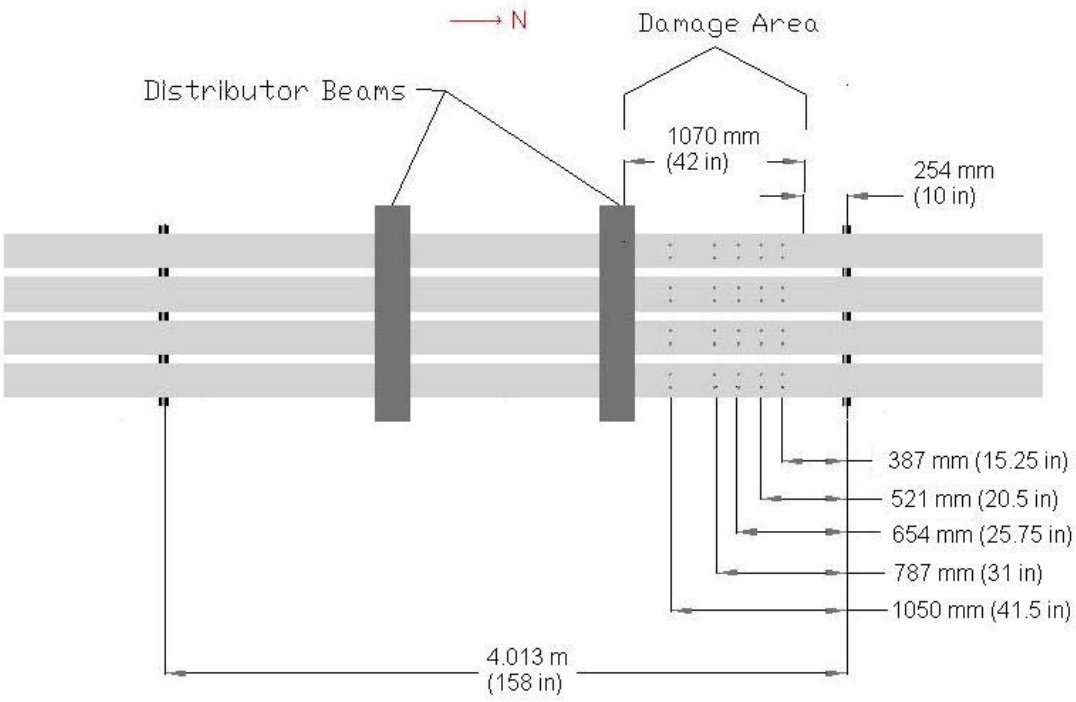

Figure 4.12: Plan view of Z-spike locations

The Z-spikes were inserted in a manner similar to that of Schilling et al. [41]. Holes were drilled at the intended location of each Z-spike. A sequence of three drilled holes was made as shown in Figure 4.13. First, a pilot hole was drilled to 330 mm (13 inches) with a 13 mm (1/2-inch) diameter bit (Figure 4.13a). Next, a 19 mm (3/4-inch) diameter auger bit was used to enlarge the hole to a depth of 394 mm (14.4 inches) (Figure 4.13b). The holes were drilled to approximately 13 mm (1/2-inch) less than the depth of the beam so that when the epoxy was placed, it would remain in the hole, causing a better bond than if it were allowed to flow out a through-hole. Finally, a 21 mm (13/16-inch) diameter bit was used to ream the upper 102 mm (4 inches) of the hole to increase the ease of installation (Figure 4.13c). It was the intent to use as few different bits as possible to make these holes in order to reduce the installation time.

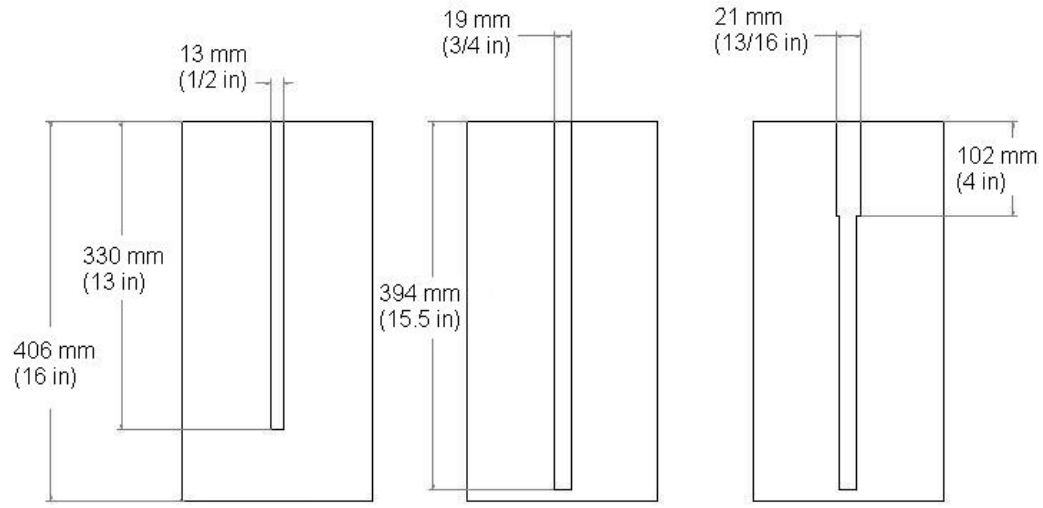

a) Pass 1 b) Pass 2 c) Pass 3

Figure 4.13: Drill depths

The epoxy used for bonding the FRP rods to the wood is a three-part mixture made from ingredients obtained from the supplier, West Systems. The 104-epoxy resin is mixed with the 206-hardener in a 4:1 resin to hardener ratio as shown in Figure 4.14. Silica thickener was added to increase the viscosity to approximately the consistency of baker's frosting as shown in Figure 4.15. This was done so the mixture would not all flow to the bottom of the holes during insertion. The exact amount of silica thickener was not measured as it was added in stages and the final consistency was determined by visual inspection.

The resin-hardener-silica combination has been proven to bond well to both the FRP and the wood. The pot life is 20-24 minutes with a solid state time of 10-14 hours. The maximum strength of the final cure is attained in 1-4 days. These times are highly dependent on the room temperature, with lower temperatures resulting in longer cure times. During application of the epoxy mixture in this research, the temperature was held near room temperature, within the 14-32º C (60-90º F) manufacturer specification.

Figure 4.14: Adding resin to epoxy mix

Figure 4.15: Adding silica to epoxy mix

Approximately 60 mL (2 fluid ounces) of epoxy was used for each Z-spike. The epoxy was poured into the hole and the Z-spike was pounded in with a wooden block, as shown in Figures 4.16 and 4.17. The wooden block was used instead of a hammer so that the Z-spike would not split, as would be the case if a hammer were used.

Figure 4.16: Pouring the epoxy

Figure 4.17: Installation of the Z-spikes

An entire row of Z-spikes was installed in one work day and the epoxy was allowed to cure for two days before the load testing was performed.

4.4 Loading

Two hydraulic actuators were used to apply point loads along the longitudinal centerline of the test specimen. Each actuator was attached to the center of an overhead frame located at the third points on the center span. The actuator was attached to the center of the overhead cross-beam frame, and could not be moved laterally to apply loads on individual stringers. Thus as shown in Figure 4.18, a lateral distributor beam made of steel was placed below each actuator cylinder. The distributor beam was 203 mm (8 inches) deep and 1.42 m (4 feet) long. It spanned all four stringers and was shimmed to distribute the load to each stringer.

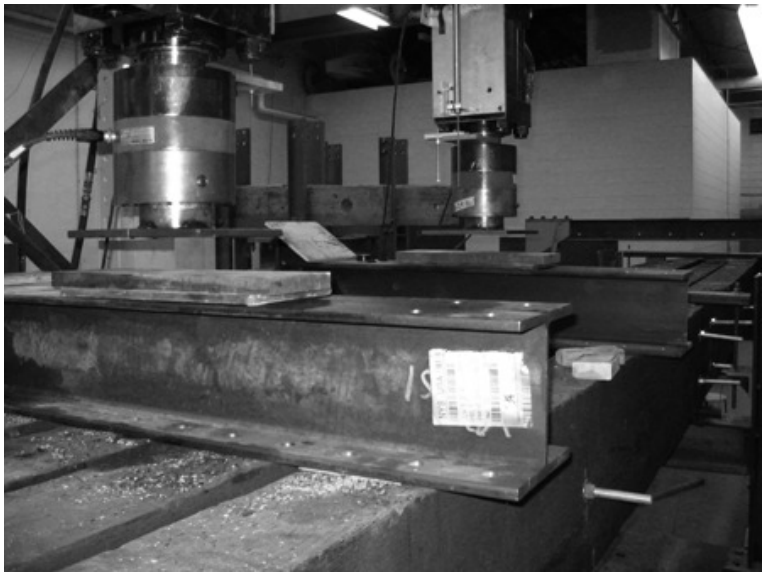

Figure 4.18: Actuators and distributor beams

Each actuator had a load capacity of 444 kN (100 kips), but the maximum load applied by an individual actuator was be 311 kN (70 kips), i.e. a total of 623 kN (140 kips). After the beam was

intentionally damaged, the maximum load applied to test the specimen was reduced. As mentioned previously, the load was applied to intentionally propagate the 41 mm (2 inches) on the width of the inner stringers that the chainsaw could not reach. During this loading, the remaining 41 mm (2 inches) of the inner two members was separated, but the loading also induced unexpected damage. After that event, the maximum load was reduced from 311 kN (70 kips) per actuator, i.e. 623 kN (140 kips) total to 146 kN (34 kips) per actuator, i.e. 311 kN (70 kips) total. After the north half of the center span was intentionally damaged using the chainsaw, the maximum load was reduced again. The maximum load was 111 kN (24 kips) per actuator, i.e. 222 kN (40 kips) total, but during the loading, a loud cracking noise was heard. After the cracking noise occurred, the specimen was loaded again and it was deduced that it had not been further damaged because the load-displacement curves from before and after the cracking noise matched. As an extra precaution to avoid unexpectedly damaging the specimen any further, the maximum load was reduced to 66.7 kN (14 kips) per actuator, i.e. a total of 133 kN (30 kips).

4.4 Deflection Measurements

Vertical deflections of the test specimen were measured using string potentiometers placed as shown in Figure 4.19. Potentiometers were attached to the underside of each stringer at the midspan of each span, in the center of the width of each stringer.

Figure 4.19: String potentiometer setup

4.6 Material Properties

As mentioned earlier, the timber members were available from the prior project completed in 1996. The stringers were solid sawn, creosote pressure-treated Douglas fir timbers. The beam configuration is shown in Figure 4.20 and the measured dimensions of each member are listed in Table 4.1.

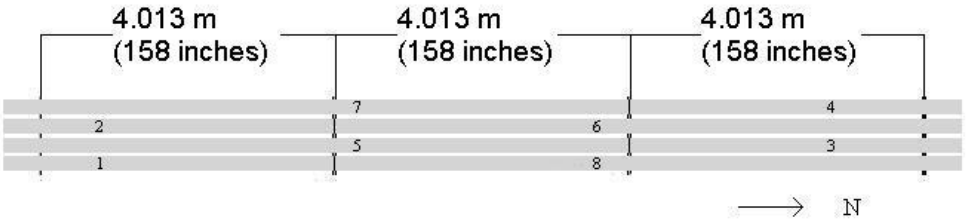

F**igure 4.20:** Plan view of specimen with labeled beam numbers

Table 4.1: Stringer dimensions

Beam	b (mm)	h (mm)	b (in)	h (in)
1	203	406	8.00	16.00
2	210	406	8.24	16.00
3	197	406	7.74	16.00
4	210	400	8.24	14.74
4	191	406	7.40	16.00
6	197	419	7.74	16.40
7	197	413	7.74	16.24
8	200	419	7.88	16.40

A Z-spike is a pultruded rod comprised of thin strands of fiberglass oriented in the longitudinal direction. These strands are bonded together with polyester resin. The rod is graded for general purpose use so the resin is effective up to 140º C (302º F). Based on manufacturer literature, the average ultimate tensile strength of the rods is 483 MPa (70 ksi) and the average (longitudinal) compressive strength is 276 MPa (40 ksi). The average transverse compressive strength is 138 MPa (20 ksi). The average flexural strength at room temperature is 483 MPa (70 ksi). The average flexural modulus of elasticity is 2.1 x 10^4 MPa (3.0 x 10^6 psi). The flexural modulus of elasticity and ultimate strengths decrease at high temperatures (1.4 x 10^4 MPa and 172 MPa at 100 ºC, 1.0 x 10^4 MPa and 103 MPa at 140ºC) (2.0 x 10^6 psi and 24 ksi, respectively, at 212 ºF, 1.4 x 10^6 psi and 14 ksi, respectively, at 302 ºF). Other technical data is included in Appendix A (Liberty Pultrusions [29]).

Four-point load tests were used to measure the modulus of elasticity (MOE) of each timber beam before the bridge chord specimen was created and the damage inflicted. Four-point loading is a standard way to eliminate shear deformation from a portion of the beam. Equal point loads were applied by hydraulic actuators at the third points of the 3.66 m (12 foot) span. Deflections were measured by string potentiometers at three locations: the center of the beam and directly below each point load. In the case of the two-span continuous members, approximately 2.74 m (9 feet) was overhanging each support of the 3.66 m (12 foot) span. This overhanging portion of the beam causes deflection in the center span due to its dead weight. But this is insignificant because the deflections were taken relative to the equilibrium position of the unloaded beam; in other words, after its dead weight had been applied. The applied actuator load and corresponding deflection was measured incrementally from 0 kN (0 kips) to the maximum load applied by each actuator (which ranged between 22.2 and 28.9 kN (between 4 and 6.4 kips)), staying well within the elastic region of material behavior.

The middle third of the beam (the portion between the two point loads) experiences no shear deformation due to the applied load because the shear is zero in that segment. Analytically, this segment was treated as a 1.22 m (4 foot) beam with concentrated point moments applied at its supports using Figure 4.21.

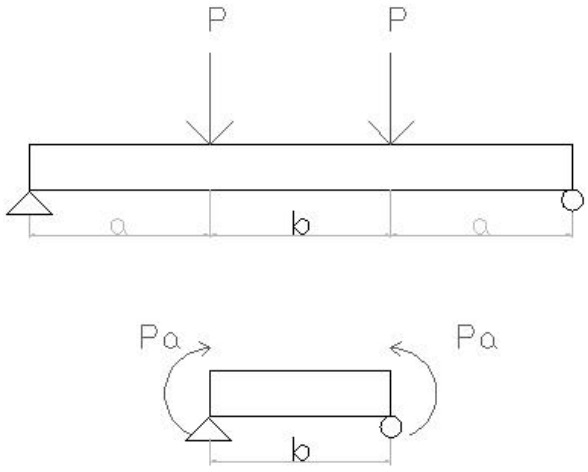

Figure 4.21: Analytical beam diagram

In the figure, the upper beam is the 3.68 m (12 foot) beam and the lower beam is the 1.22 m (4 foot) analytical beam used to calculate MOE. In the beam diagram, each segment is approximately one third of the length of the beam [(a = 1140 mm and b = 1220 mm) (a = 44 inches and b = 48 inches)]. The difference from equal thirds is negligible in calculating the MOE. "Δ" is the deflection at the center of the beam. In the computation, this deflection of the 1.22 m (4 foot) beam was taken relative to the average value of the deflections measured under the point loads. The modulus of elasticity was determined using equation 4.1 and the slope (δP/δΔ) of the linear regression line fitted to the load-deflection data, exemplified in Figure 4.22, neglecting the first few non-linear data points as the beam settled on the supports.

$$MOE = \left(\frac{\delta P}{\delta \Delta}\right)\left(\frac{1}{8I}\right)\left(a^2 * b\right) \qquad \text{(Equation 4.1)}$$

As an example, for Beam 8, Figure 4.22 shows slope (δP/δΔ). δP/δΔ = 42.4 kN/mm (300 kips/inch), I = 1.23 x 10^9 mm^4 (2940 $inch^4$), a = 1220 mm (48 inches), and b = 1220 mm (48 inches). Using these values in equation 4.1 results in

$$MOE_8 = \left(52.5\frac{kN}{mm}\right)\left(\frac{1}{8 * 1.23\ x\ 10^9\ mm^4}\right)\left(1220^2\ mm^2 * 1220\ mm\right)$$

MOE_8 = 9.70 x 10^3 MPa (1.41 x 10^6 psi)

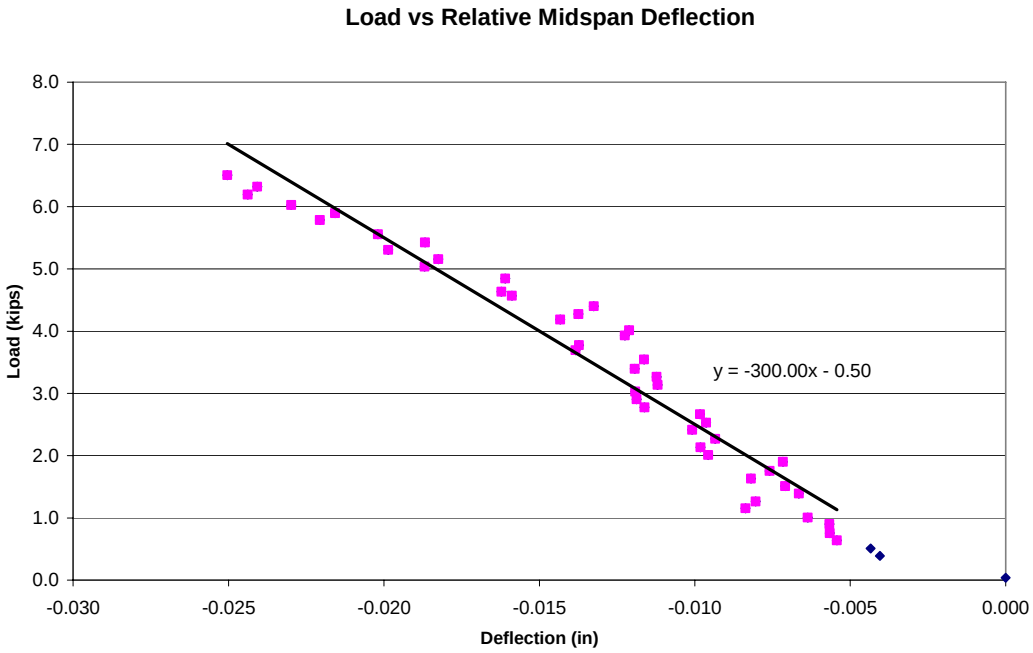

Figure 4.22: Beam 8 load – deflection curve

The resulting modulus of elasticity values were determined in a similar manner. The load-deflection data for Beams 1 through 7 (labeled previously in Figure 4.20) are included in Appendix B. The calculated MOE values are shown in Table 4.2.

Table 4.2: Calculated MOE

Beam	MOE (MPa)	MOE (psi)
1	1.30E+04	1.88E+06
2	1.43E+04	2.07E+06
3	8.60E+03	1.24E+06
4	1.06E+04	1.43E+06
4	9.90E+03	1.44E+06
6	7.38E+03	1.07E+06
7	9.91E+03	1.44E+06
8	9.70E+03	1.41E+06

5. RESULTS

5.1 Evaluation Methodology

Load testing was performed to determine the effective stiffness of each member in the center span. The effective stiffness (ST) in kN-m^2 (kip-in^2) was calculated by substituting the measured span length (l) in meters (inches) and the slope ($\delta P/\delta\Delta$) of the corresponding measured load-deflection plot in kN/m (kip/in) into equation 5.1. The equation was derived for a two-span continuous beam with the equal loads (P) applied at the third points of one span. At midspan, deflection can be seen as expressed in equation 5.1. The constant 1/4 is used because the load used in the slope ($\delta P/\delta\Delta$) is the total load applied to the four stringers.

$$ST = \frac{1}{4}\left(\frac{\delta P}{\delta \Delta}\right)\left(\frac{l^3}{2692/65}\right) \qquad \text{(Equation 5.1)}$$

The efficiency of the Z-spikes is given by Equation 5.2, as discussed by Pault [34].

$$Efficiency\ of\ repair_j = \frac{ST_j - ST_i}{ST_k - ST_i} \times 100\ \% \qquad \text{(Equation 5.2)}$$

where the three states ST_j, ST_i, and ST_k are chosen to investigate various conditions relative to chosen states. A common use of this equation would assign ST_i to the minimum measured effective stiffness (e.g. the original full damage state), ST_k to be the maximum measured effective stiffness (e.g. the fully repaird state), and ST_j to be an intermediate effective stiffness (e.g. a partially repaired state). Equation 5.2 defines the efficiency of the intermediate ST (ST_j) relative to the minimum (ST_i) and maximum (ST_k) ST.

Using the center span of the west stringer as an example, the undamaged north half had a ST of 1.03 x 10^4 kN-m^2 (3.60 x 10^6 kip-in^2) (ST_k) the completely damaged ST was 8.44 x 10^3 kN-m^2 (2.98 x 10^6 kip-in^2) (ST_i) and the ST when five sets of Z-spikes were added was 1.02 x 10^4 kN-m^2 (3.44 x 10^6 kip-in^2) (ST_j). Substituting these values into equation 5.2, the efficiency of the five sets of Z-spikes relative to the minimum and maximum ST values is 89.4 percent:

$$\frac{10.2 - 8.54}{10.3 - 8.54} \times 100\ \% \quad = 89.5\ \%$$

In other words, five sets of Z-spikes recovered 89.4 percent of the stiffness lost due to the original full damage state.

In each of the three spans, each of the four stringers was given a set of labels for various segments of the bridge chord specimen, as shown in Figure 5.1. The label definitions are as follows:
C—center span
S—south span
N—north span

E—east stringer
ME—middle east stringer
MW—middle west stringer
W—west stringer

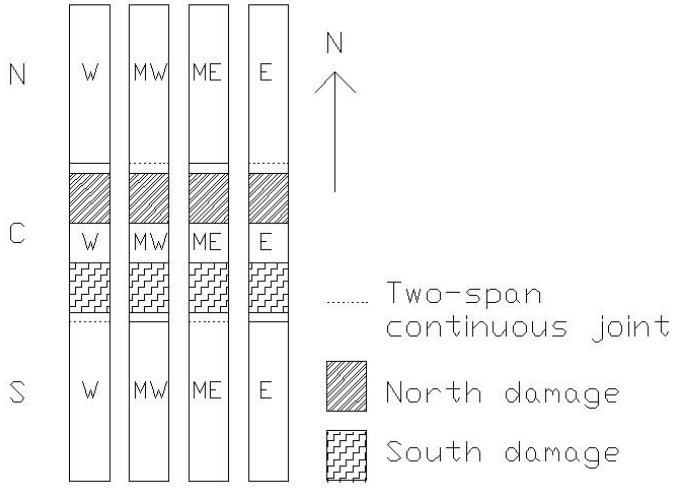

Figure 5.1: Stringer labels

5.2 Damage/Repair to South End

For the damage/repair in the south half of the beam, the data was incomplete. Load tests were not done to determine how much ST changed either becaue of the cut or because of the unexpected damage (cracking of the beam). The effective stiffness and efficiency was calculated at 11 increments given as described in Chapter 4.

The patterns of changing measured ST of the center span because of the south end damage/repair are listed in Table 5.1 (SI units) and Table 5.2 (US customary units) and shown graphically in Figures 5.2 and 5.3 respectively. The load-deflection data used to calculate the effective stiffness for the south end damage/repair is found in Appendix C.

Table 5.1: Effective stiffness values of the center span due to south end damage/repair (SI)

Stringer Condition	Stiffness (kN-m^2)				
	C-W	C-MW	C-ME	C-E	C Avg
no damage	1.44E+04	1.28E+04	1.23E+04	1.19E+04	1.31E+04
8" cut (before crack)	1.32E+04	1.29E+04	1.11E+04	1.17E+04	1.22E+04
8" cut (after crack)	1.09E+04	1.09E+04	8.97E+03	9.24E+03	1.00E+04
full cut completed	8.46E+03	7.97E+03	4.42E+03	6.74E+03	7.20E+03
Z-spikes in end	8.27E+03	8.97E+03	4.89E+03	8.46E+03	7.92E+03
repaired center beams (south)	9.40E+03	1.04E+04	8.80E+03	9.74E+03	9.61E+03
repaired center beams (north)	9.32E+03	9.90E+03	8.84E+03	9.26E+03	9.33E+03
1st set of Z-spikes	9.73E+03	1.01E+04	9.34E+03	9.63E+03	9.71E+03
2nd set of Z-spikes	9.61E+03	1.04E+04	9.81E+03	9.69E+03	9.87E+03
3rd set of Z-spikes	1.04E+04	1.10E+04	1.01E+04	9.84E+03	1.03E+04
repaired center beams (south2)	1.01E+04	9.44E+03	9.63E+03	9.06E+03	9.47E+03

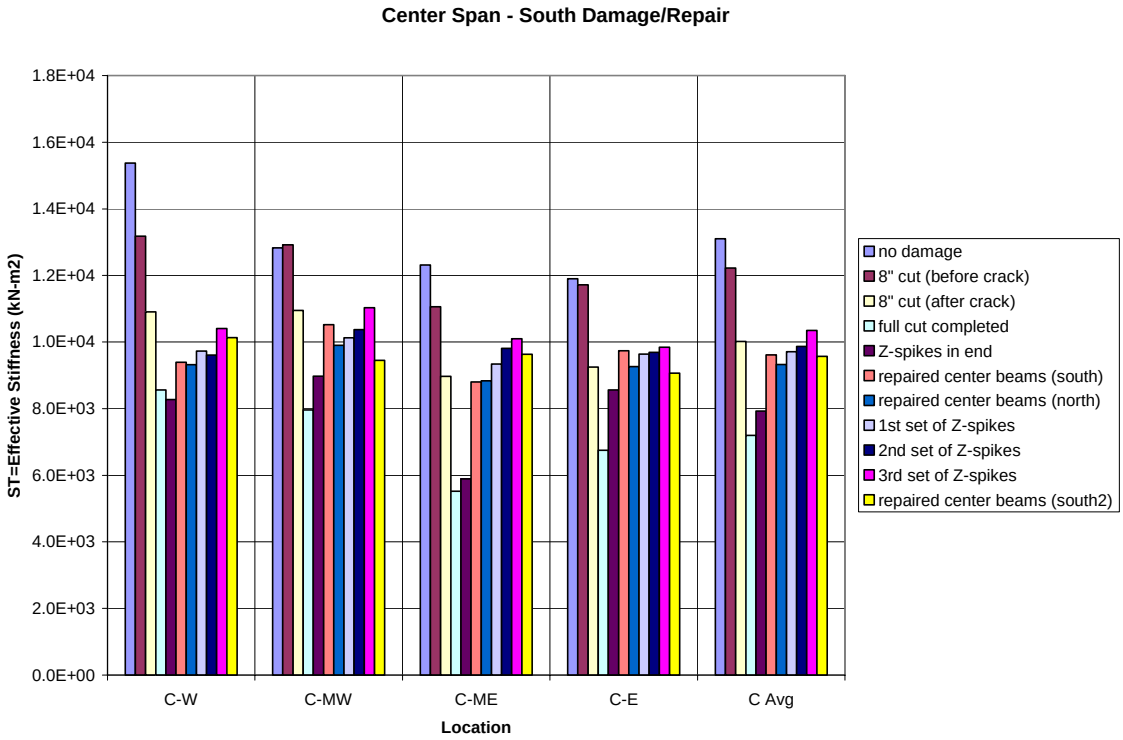

Figure 5.2: Effective stiffness of the center span due to south damage/repair (SI)

Table 5.2: Effective stiffness values of the center span due to south end damage/repair (US customary)

Stringer Condition	Stiffness (kip-in^2)				
	C-W	C-MW	C-ME	C-E	C Avg
no damage	4.36E+06	4.47E+06	4.29E+06	4.14E+06	4.47E+06
8" cut (before crack)	4.49E+06	4.40E+06	3.86E+06	4.08E+06	4.26E+06
8" cut (after crack)	3.80E+06	3.81E+06	3.13E+06	3.22E+06	3.49E+06
full cut completed	2.98E+06	2.78E+06	1.92E+06	2.34E+06	2.41E+06
Z-spikes in end	2.88E+06	3.13E+06	2.04E+06	2.98E+06	2.76E+06
repaired center beams (south)	3.27E+06	3.67E+06	3.07E+06	3.39E+06	3.34E+06
repaired center beams (north)	3.24E+06	3.44E+06	3.08E+06	3.23E+06	3.24E+06
1st set of Z-spikes	3.39E+06	3.43E+06	3.24E+06	3.36E+06	3.38E+06
2nd set of Z-spikes	3.34E+06	3.61E+06	3.42E+06	3.38E+06	3.44E+06
3rd set of Z-spikes	3.63E+06	3.84E+06	3.42E+06	3.43E+06	3.60E+06
repaired center beams (south2)	3.43E+06	3.29E+06	3.36E+06	3.16E+06	3.33E+06

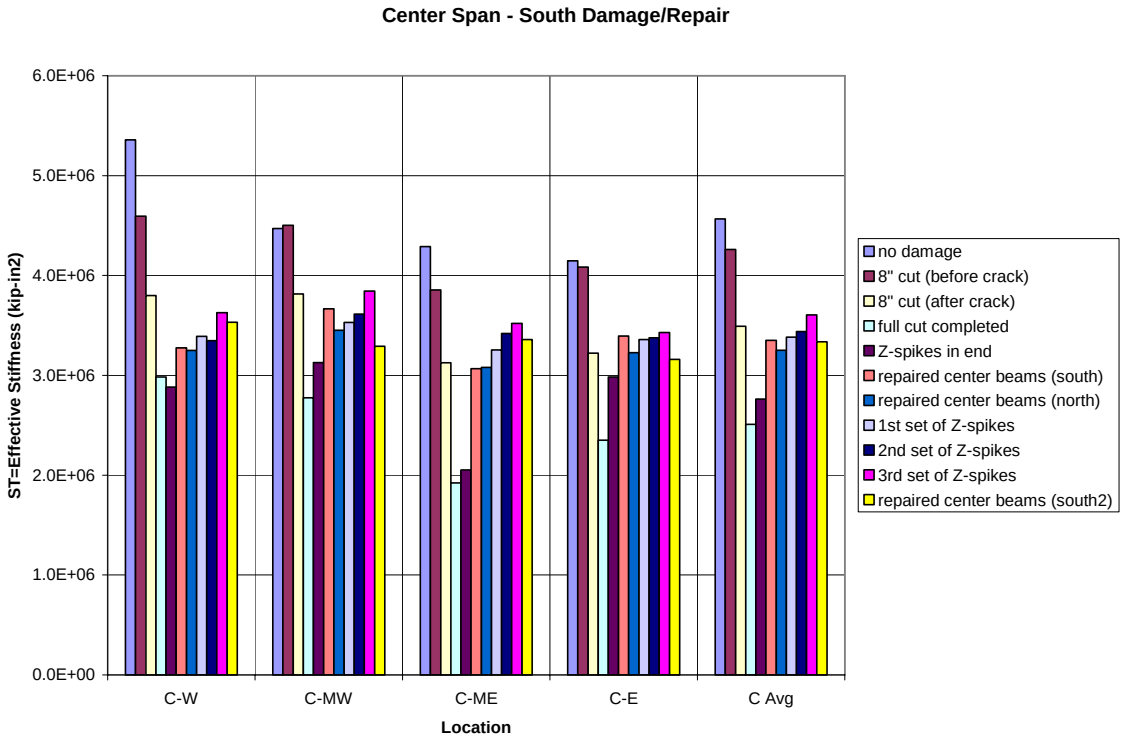

Figure 5.3: Effective stiffness of the center span due to south end damage/repair (US)

Table 5.3 is a listing of the decreases in efficiency caused by the progression of damage and these are graphically shown in Figure 5.4. The "no damage" state is used as ST_k and the "full cut completed" state is used as ST_i in calculating efficiency from Equation 5.2. The efficiency equation and states ST_i, ST_j, and ST_k are used, but the definition of efficiency does not hold, because the data shown is for progression of damage and not repair. Instead these data show how

the effective stiffness decreases with increasing damage. It is evident that the cut reduced the effective stiffness of each stringer.

Table 5.3: Efficiency values of the center span due to south end damage
(ST_i = "full cut completed" and ST_k = "no damage")

Stringer Condition	Efficiency (%)				
	C-W	C-MW	C-ME	C-E	C Avg
no damage	100.0	100.0	100.0	100.0	100.0
8" cut (before crack)	67.8	101.9	81.6	96.4	84.1
8" cut (after crack)	34.3	61.4	40.8	48.4	47.7
full cut completed	0.0	0.0	0.0	0.0	0.0

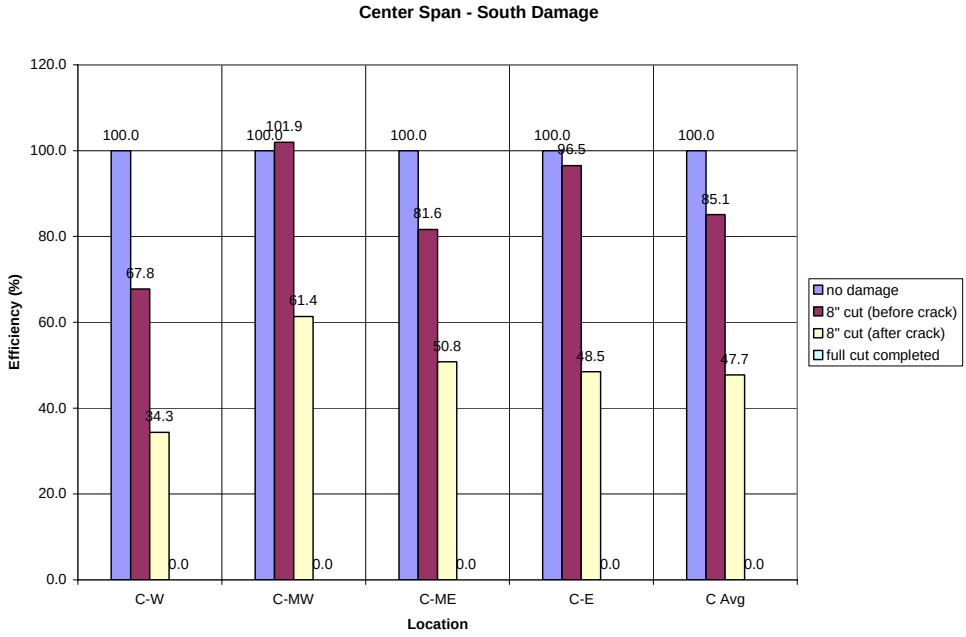

Figure 5.4: Efficiencies of the center span due to south end damage

The efficiencies associated with the progression of the center repair are listed in Table 5.4 and shown in Figure 5.4. The "repaired center beams (north)" state is used as ST_k and the "full cut completed" state is used as ST_i in calculating efficiency from Equation 5.2.

Table 5.4: Efficiency values of the center span due to south end center repair
(ST_i = "full cut completed" and ST_k = "repaired center beams (north)")

Stringer Condition	Efficiency (%)				
	C-W	C-MW	C-ME	C-E	C Avg
full cut completed	0.0	0.0	0.0	0.0	0.0
Z-spikes in end	-38.6	42.0	11.2	72.2	34.0
repaired center beams (south)	110.1	131.8	99.0	119.1	113.4
repaired center beams (north)	100.0	100.0	100.0	100.0	100.0

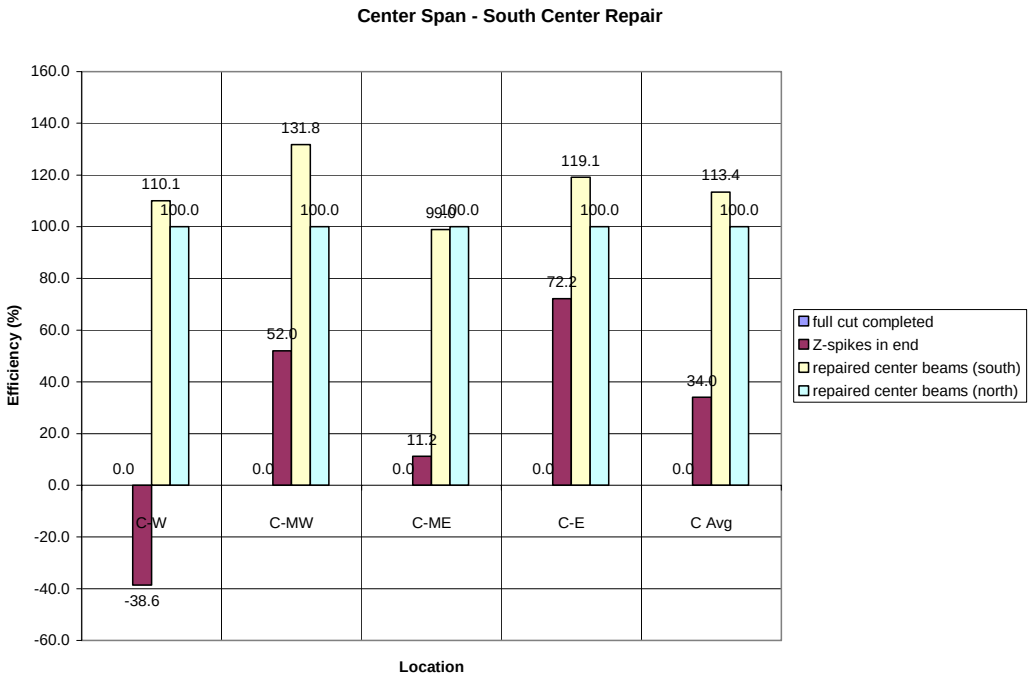

Figure 5.5: Efficiencies of the center span due to south end center repair

It is evident from the data that the installation of Z-spikes in the middle of the center span increased the effective stiffness. The effective stiffness was higher after the south half the center of the span was repaired than when both the south and the north halves were repaired. A possible explanation for this could be that the loss of the "sound" timber due to the drilling of the holes for the Z-spikes had more of a negative effect than the positive effect of the insertion of the Z-spikes. Note that in the west stringer, the efficiency decreased with the addition of the shear spikes near the end of the damage. This interesting phenomenon was also observed by both Radford et al. [38] and Schilling et al. [41].

The efficiencies associated with the progression of Z-spike insertion progression are listed in Table 5.5 and shown in Figure 5.6. The "no damage" state is used as ST_k and the "full cut completed" state is used as ST_i in calculating efficiency from Equation 5.2.

Table 5.5: Efficiency values of the center span due to south end Z-spike repair (ST_i = "repaired center beams (north)" and ST_k = "3rd set of Z-spikes")

Stringer Condition	Efficiency (%)				
	C-W	C-MW	C-ME	C-E	C Avg
repaired center beams (north)	0.0	0.0	0.0	0.0	0.0
1st set of Z-spikes	37.7	20.0	40.0	64.4	37.3
2nd set of Z-spikes	26.4	41.2	77.4	74.1	43.2
3rd set of Z-spikes	100.0	100.0	100.0	100.0	100.0

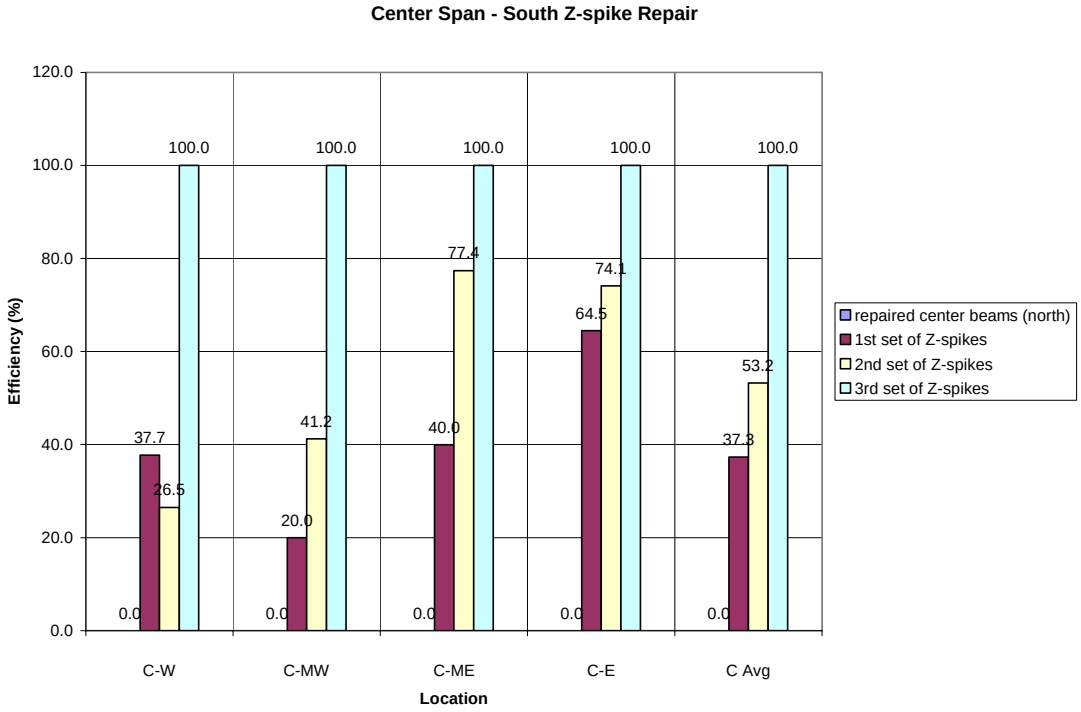

Figure 5.6: Efficiencies of the center span due to south end Z-spike repair

From the data in Table 5.6 and Figure 5.6, it is evident that the installation of Z-spikes to repair the cut increased the effective stiffness. On average, the last set of Z-spikes (inserted at the quarter point of the damage) had more effect than either of the other two sets. On average, the second set (inserted at the three-quarters point of the damage) had less effect than the other two sets.

The efficiencies of the combination of the center repair and the Z-spike repair are listed in Table 5.6 and graphically shown in Figure 5.7. The "3rd set of Z-spikes" state is used as ST_k and the "full cut completed" state is used as ST_i in calculating efficiency from Equation 5.2. The "State" number listed on the left column of Table 5.6 corresponds to "State j" in Figure 5.7.

Table 5.6: Efficiency values of the center span due to south end repair
(ST_i = "full cut completed" and ST_k = "3rd set of Z-spikes")

State	Stringer Condition	Efficiency (%)				
		C-W	C-MW	C-ME	C-E	C Avg
0	full cut completed	0.0	0.0	0.0	0.0	0.0
1	Z-spikes in end	-14.8	32.9	8.1	48.6	23.0
2	repaired center beams (south)	44.2	83.4	71.7	96.7	76.8
3	repaired center beams (north)	41.0	63.3	72.4	81.2	67.8
4	1st set of Z-spikes	63.3	70.6	83.4	93.3	79.8
4	2nd set of Z-spikes	46.7	78.4	93.8	94.1	84.9
6	3rd set of Z-spikes	100.0	100.0	100.0	100.0	100.0

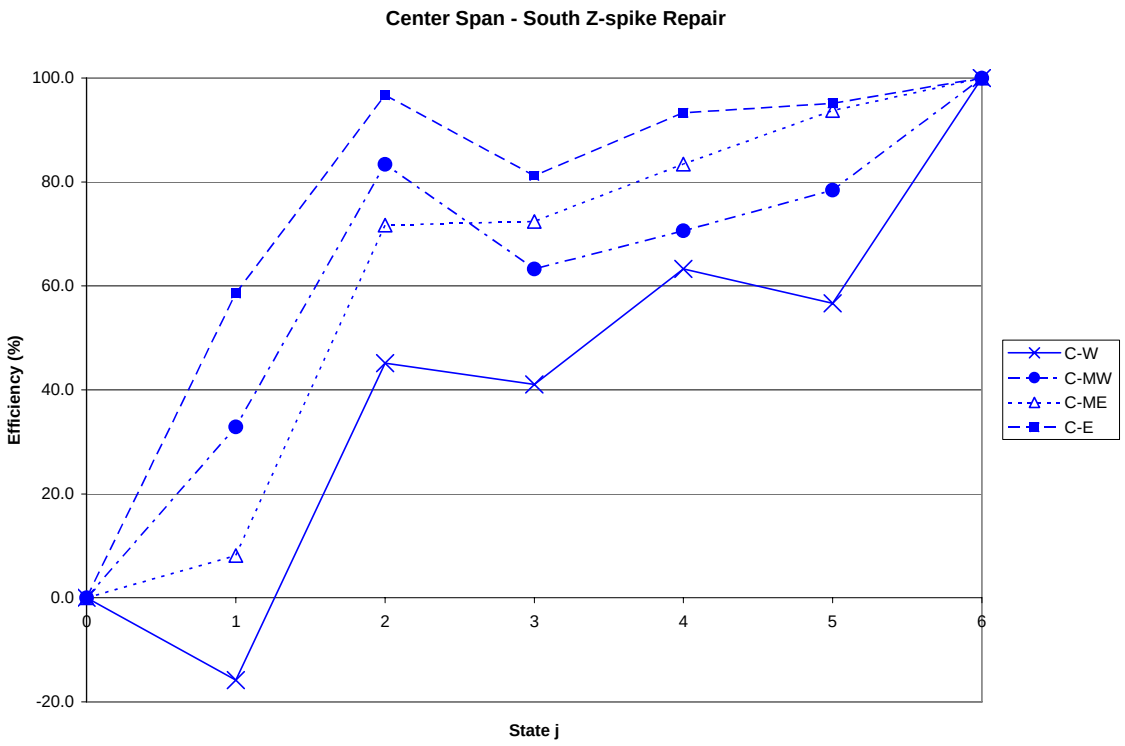

Figure 5.7: Efficiencies of the center span due to south end repair

From the data in Table 5.6 and Figure 5.7, it is evident that each of the four stringers follows approximately the same behavior from state to state. The efficiencies of all four stringers increase in the first and second states, then decrease or stay approximately the same in the third state, then increase again in the fourth, fifth, and sixth states. As mentioned earlier, a possible explanation for the decrease between the second and third states could be because the holes drilled for the Z-spikes caused a more negative effect on stiffness by removing sound wood than the positive effect of the addition of the Z-spikes.

5.3 Damage/Repair to North End

For the damage/repair in the north half of the center span of the beams, the stiffness and efficiency for each member in the center span were calculated before the damage, after the damage, and with each incremental addition of the five sets of Z-spikes, as described earlier in Chapter 4. The patterns of changing measured ST of the center span because of the repair of the inflicted damage in the north end are listed in Tables 5.7 (SI units) and 5.8 (US units) and shown graphically in Figures 5.8 and 5.9. The load-deflection data used to calculate the effective stiffness for the north end damage/repair can be found in Appendix D.

Table 5.7: Effective stiffness values of the center span due to north end damage/repair (SI)

Stringer Condition	Stiffness (kN-m^2)				
	C-W	C-MW	C-ME	C-E	C Avg
no damage	1.03E+04	1.00E+04	1.01E+04	9.22E+03	9.91E+03
full damage	8.44E+03	8.64E+03	8.44E+03	8.43E+03	8.44E+03
one set of Z-spikes	8.99E+03	8.68E+03	8.70E+03	8.42E+03	8.72E+03
two sets of Z-spikes	9.26E+03	8.87E+03	9.03E+03	8.79E+03	8.99E+03
three sets of Z-spikes	9.64E+03	9.24E+03	9.33E+03	9.06E+03	9.32E+03
four sets of Z-spikes	9.84E+03	9.44E+03	9.70E+03	9.31E+03	9.47E+03
five sets of Z-spikes	1.02E+04	9.62E+03	9.94E+03	9.46E+03	9.80E+03

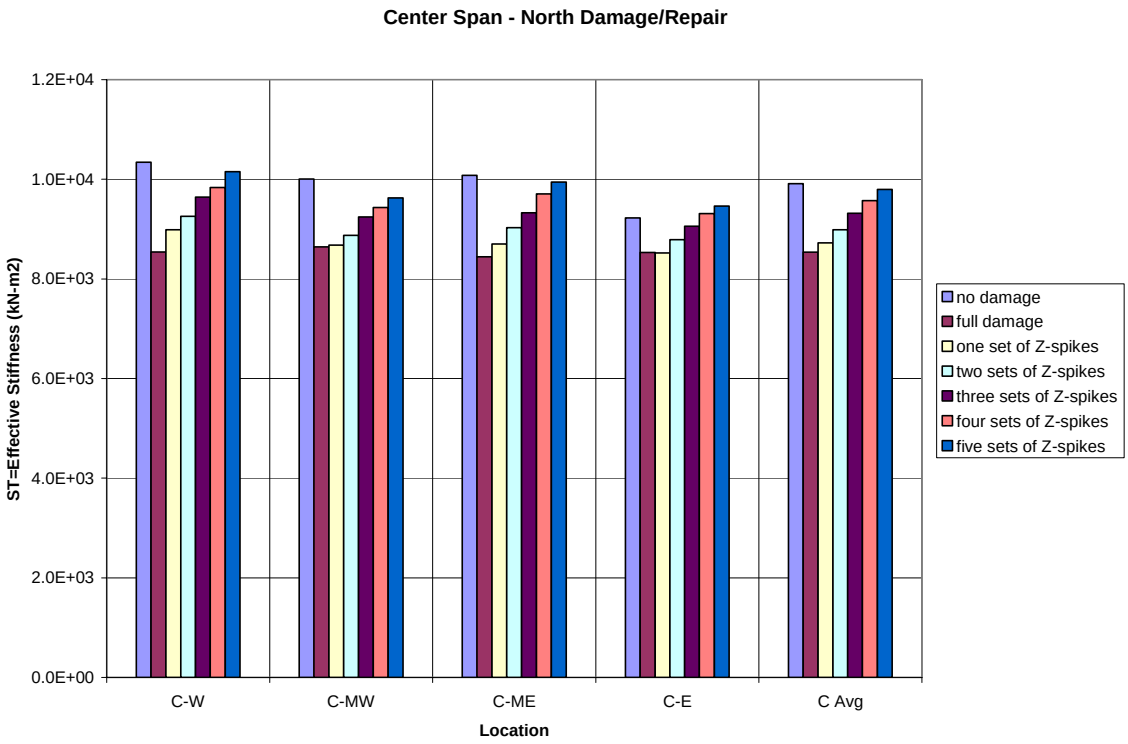

Figure 5.8: Effective stiffness of the center span due to north end damage/repair (SI)

Table 5.8: Effective stiffness values of the center span due to north end damage/repair (US)

Stringer Condition	Stiffness (kip-in^2)				
	C-W	C-MW	C-ME	C-E	C Avg
no damage	3.60E+06	3.49E+06	3.41E+06	3.21E+06	3.44E+06
full damage	2.98E+06	3.01E+06	2.94E+06	2.97E+06	2.98E+06
one set of Z-spikes	3.13E+06	3.02E+06	3.03E+06	2.97E+06	3.04E+06
two sets of Z-spikes	3.23E+06	3.09E+06	3.14E+06	3.06E+06	3.13E+06
three sets of Z-spikes	3.36E+06	3.22E+06	3.24E+06	3.16E+06	3.24E+06
four sets of Z-spikes	3.43E+06	3.29E+06	3.38E+06	3.24E+06	3.34E+06
five sets of Z-spikes	3.44E+06	3.34E+06	3.47E+06	3.30E+06	3.41E+06

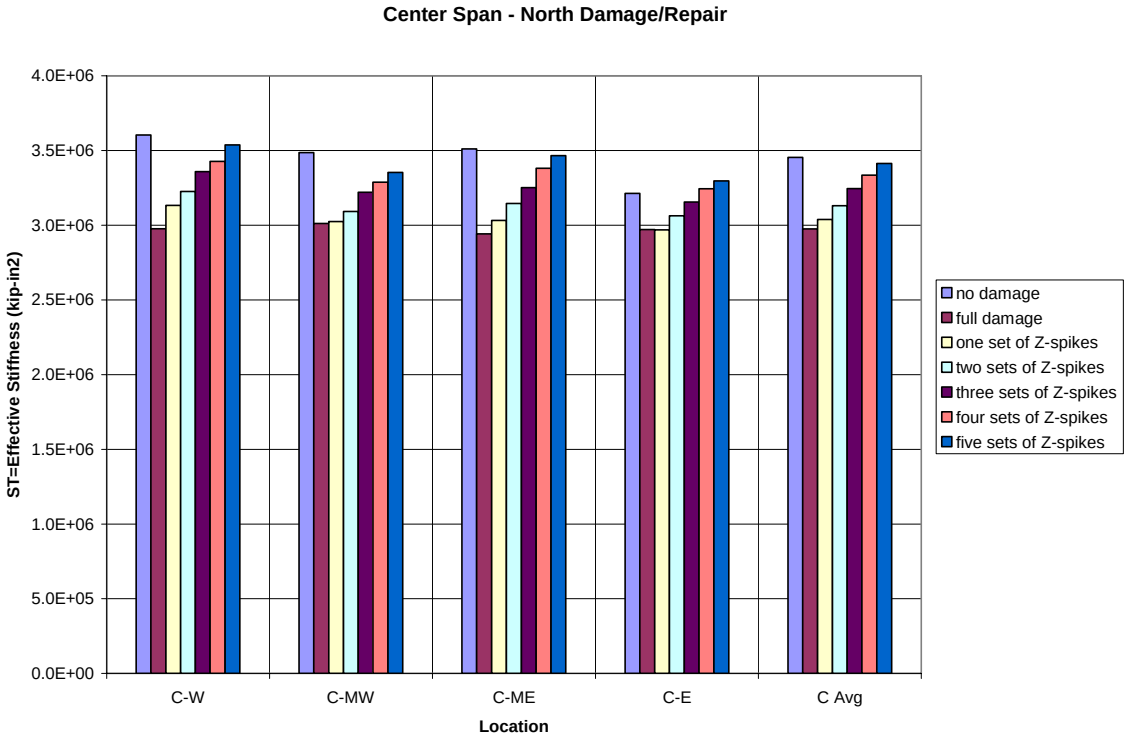

Figure 5.9: Effective stiffness of the center span due to north end damage/repair (US)

From the data in Tables 5.7 and 5.8 and Figures 5.8 and 5.9, it is evident that the installation of Z-spikes increases the effective stiffness of the members in the center span.

For the four stringers in the center span, the average effective stiffness is 8.72 x 10^3 kN-m^2 (3.04 x 10^6 kip-in^2) for the first set of Z-spikes, 8.99 x 10^3 kN-m^2 (3.13 x 10^6 kip-in^2) after adding the second set, 9.32 x 10^3 kN-m^2 (3.24 x 10^6 kip-in^2) after adding the third set, 9.47 x 10^3 kN-m^2 (3.34 x 10^6 kip-in^2) after adding the fourth set, and 9.80 x 10^3 kN-m^2 (3.41 x 10^6 kip-in^2) after adding the fifth set.

The effective stiffness increase for each of the four members varied throughout the testing. For example, after the installation of the first set of Z-spikes, the effective stiffness values were 8.99 x 10^3 kN-m^2, 8.68 x 10^3 kN-m^2, 8.70 x 10^3 kN-m^2, and 8.42 x 10^3 kN-m^2 (3.13 x 10^6 kip-in^2, 3.02 x 10^6 kip-in^2, 3.03 x 10^6 kip-in^2, and 2.97 x 10^6 kip-in^2) for the west, middle west, middle east, and east stringers, respectively. After the installation of the fifth set, the corresponding effective stiffness values were 10.2 x 10^3 kN-m^2, 9.62 x 10^3 kN-m^2, 9.94 x 10^3 kN-m^2, and 9.46 x 10^3 kN-m^2 (3.44 x 10^6 kip-in^2, 3.34 x 10^6 kip-in^2, 3.47 x 10^6 kip-in^2, and 3.30 x 10^6 kip-in^2), respectively.

The efficiencies associated with of the Z-spike repair are listed in Table 5.9 and shown graphically in Figure 5.10. The "no damage" state is used as ST_k and the "full damage" state is used as ST_i in calculating efficiency from Equation 5.2. The "State" number listed on the left column of Table 5.9 corresponds to "State j" in Figure 5.10.

Table 5.9: Efficiency values of the center span due to north end damage/repair (ST_i = "full cut completed" and ST_k = "no damage")

State	Stringer Condition	Efficiency (%)				
		C-W	C-MW	C-ME	C-E	C Avg
X	no damage	100.0	100.0	100.0	100.0	100.0
0	full damage	0.0	0.0	0.0	0.0	0.0
1	one set of Z-spikes	24.8	2.7	14.8	-1.2	13.4
2	two sets of Z-spikes	39.7	16.8	34.7	37.7	32.6
3	three sets of Z-spikes	61.0	44.0	44.2	74.8	46.7
4	four sets of Z-spikes	71.9	48.2	77.2	112.9	74.3
4	five sets of Z-spikes	89.4	72.1	92.0	134.4	91.6

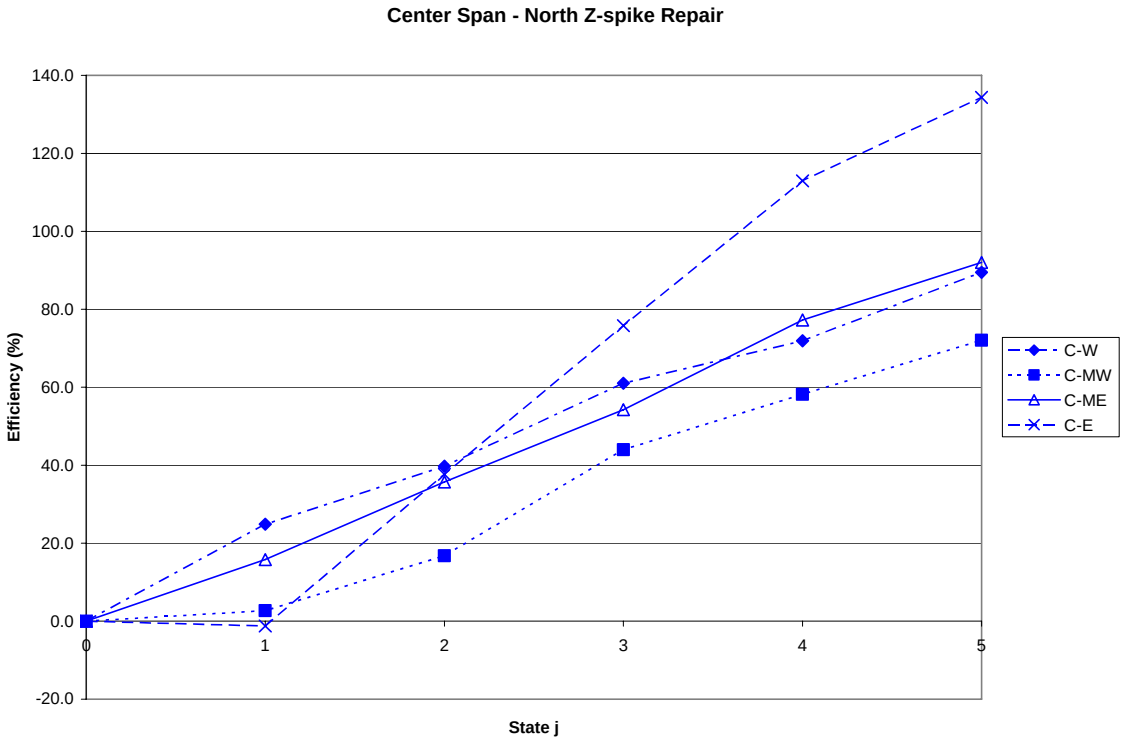

Figure 5.10: Efficiency of the center span due to north end damage/repair

From the data in Table 5.9 and Figure 5.10, it is evident that the installation of Z-spikes increases the efficiency of the members in the center span. For the four stringers in the center span, the average efficiency is 13.4 percent for the first set of Z-spikes, 32.6 percent after adding the second set, 46.7 percent after adding the third set, 74.3 percent after adding the fourth set, and 91.6 percent after adding the fifth set. After five sets of Z-spikes, the average efficiency is nearly to the magnitude of the members before they experienced damage because of the cut. One value (C-E) actually exceeded the original effective stiffness, that is, the efficiency was 134 percent. The unexpected damage was the most severe in this member, thus it is believed that the effective stiffness exceeded the original effective stiffness because the addition of Z-spikes was repairing the cut made in the north half plus part of the unexpected damage that occurred in the south half.

The increase in effective stiffness of the four members varied throughout the testing. For example, after the installation of the first set of Z-spikes, the effective stiffness values were 24.8 percent, 2.7 percent, 14.8 percent, and -1.2 percent, for the west, middle west, middle east, and east stringers, respectively. After the installation of the fifth set, the corresponding effective stiffness values were 89.4 percent, 72.1 percent, 92.0 percent, and 134.4 percent, respectively.

6. OBSERVATIONS, CONCLUSIONS, AND RECOMMENDATIONS

6.1 Observations

- Each of the four stringers in the loaded span exhibited linear load-deflection behavior up to the load level used before and after the insertion of Z-spikes.

- By not drilling a hole through the complete depth of the stringers, no epoxy was pushed out the bottom and all was used. It was visually observed on the outside stringers that beads of epoxy had penetrated from the drilled hole through the wood fibers. It is concluded that the epoxy is entering the voids in the wood fibers, which is contributing to the strengthening of the stringer.

6.2 Conclusions

- The results of this study show that the use of vertically-oriented Z-spikes significantly improves the effective stiffness of full-scale timber stringers in a bridge chord specimen. The use of five sets of Z-spikes in the north half of the center span averaged 91.6 percent recovery of the effective stiffness lost because of intentional damage from a cut at mid-depth. The highest and lowest effective stiffness recoveries were 134.4 percent and 72.1 percent.

- The results of this large-scale testing were similar to that measured by Radford et al. [38] and Schilling et al. [41] at smaller scales. As each set of shear spikes was inserted in the laboratory specimen, the effective stiffness increased just as Schilling et al. measured stiffness increases in the testing of the crossties. The 91.6 percent average effective stiffness recovery because of the use of shear spikes to repair the north end damage is comparable to the effective 100 percent repair measured by Radford et al. when the 2x4s were split and repaired.

- The Z-spikes developed significant interlayer shear transfer between the top and bottom layers in the intentionally damaged area.

- The dense use of Z-spikes in the center third of the center span to repair the region of unexpected damage (cracking under load) increased the effective stiffness for each of the four stringers. But since there was not enough data to determine how much the effective stiffness changed due to the unexpected damage, it is not possible to quantify to what degree this unexpected damage was repaired.

6.3 Recommendations

- The effect of Z-spikes on the effective stiffness was not investigated in the end spans. If it were to be studied in the unloaded spans, crossties should be used to connect the four stringers rather than relying on solely the tie rods.

- The effect of Z-spikes on a full-scale bridge specimen should be studied using damage representative of deterioration from decay in an in situ bridge specimen.

- A study of the effects of the addition of Z-spikes to an in situ bridge is the next rational step in this ongoing research. It is recommended that the Z-spikes be implemented to rehabilitate a degraded bridge.

- If good-quality materials are used to enable controlled damage, damage should be inflicted on members before the assembly of the test specimen.

- A finite element computer model could be developed to analyze the test specimen behavior. This would be feasible and effective if the amount of intentional damage was known and no unknown, unintentional damage was inflicted.

- A method for identifying the maximum level of degradation at which the Z-spikes are effective should be considered. If the timber is in good condition, the shear spikes will not add much stiffness and, thus, their use is not recommended in that situation. As a result, the quantification of "good condition" should be attempted, possibly based on the sorting methodology used by Schilling et al. [41].

- A fixture should be created so that installation of the shear spikes can be done with a metal hammer rather than using a wood block to impact the spikes. This fixture could have a hole with a slightly larger diameter than the shear spike. The Z-spike could then fit in this hole and a rubber cushion could be used on the fixture-shear spike interface. It is necessary that this fixture would not cause the Z-spike to split during the installation process.

- The ultimate bending strength of stringers reinforced with Z-spikes should be investigated on members of reasonably large sizes.

7. REFERENCES

1. American Railway Engineering and Maintenance of Way Association (1994). *Manual for Railway Engineering, vol. 2 structures.* Chapter 7: Timber Structures.

2. Anon (1996). Wood and Wood Composites Reinforced with High-Strength Plastic: Innovative, cost effective, Structural Materials. *Materials Technology*, *11*, 84-87.

3. Avent, R. R. (1986). Design Criteria for Epoxy Repair of Timber Structures. *Journal of Structural Engineering*, *112*, 222-240.

4. Baker, A.J (1974). Degradation of Wood by Products of Metal Corrosion. U.S. Department of Agriculture, Forest Products Laboratory, Madison WI. Research Paper FPL 229.

5. Barbero, E; Davalos, J. & Munipalle, U. (1994). Bond strength of FRP-Wood Interface. *Journal of Reinforced Plastics and Composites*, *13*, 834-844.

6. Bohannan, B. (1962). Prestressing wood members. *Forest Products Journal, 12 (12)*. 496-602.

7. Bulleit, W.M. (1984). Reinforcement of Wood Materials: A Review. *Wood and Fiber Science*, *16 (3)*, 391-397.

8. Cox, B.N. (1999). Mechanisms and Models for Delamination in the Presence of Through Thickness Reinforcement. Proceeding ICCM-12, Paris, July 1999.

9. Davalos, J.F., P. Qiao, and B.S. Trimble. (2000). Fiber-Reinforced Composite and Wood Bonded Interfaces: Part 1. Durability and Shear Strength. *Journal of Composite Technology and Research*, *22*, 224-231.

10. Davalos, J.F., P. Qiao, and B.S. Trimble. (2000). Fiber-Reinforced Composite and Wood Bonded Interfaces: Part 2. Fracture. *Journal of CompositeTechnology and Research*, *22*, 232-240.

11. Davalos, J.F., M.G. Zipfel, and P. Qiao. (1999). Feasibility Study of Prototype GFRP Reinforced Wood Railroad Crosstie. *Journal of Composites for Construction*, *3*, 92-99.

12. Doyle, K.R., R.M. Gutkowski, M.E. Criswell, P.J. Pellicane and J. Balogh. (2000). Laboratory Tests and Analysis of Full-Scale Open-Deck Timber Trestle Railroad Bridge Chords. Structural Research Report No. 82, Colorado State University.

13. GangaRao, H.V.S and P.V. Vijay (1998). Bending Behavior of Concrete Beams Wrapped with Carbon Fabric. *Journal of Structural Engineering*, *124*, 3-10.

14. GangaRao, H.V.S, S.S. Sonti, and M.C. Superfesky (1996). Static Response of Wood Crossties Reinforced with Composite Fabrics. International Society of the Advancement of Materials and Process Engineering Symposium and Exhibition. Volume 41, 1291-1303.

15. Gardner, D.J., J.F. Davalos, and U.M. Munipalle (1994). Adhesive Bonding of Pultruded Fiber Reinforced Plastic to Wood. *Forest Products Journal, 44,* 62-66.

16. Gentile, C., D. Svecova, and F. Rizkalla (2002). Timber Beams Strengthened with GFRP Bars: Development and Applications. *Journal of Composites for Construction*, *6*, 11-20.

17. Gilfillan, J.R., S.G. Gilbert, and G.R.H. Patrick (2003). The Use of FRP Composites in Enhancing the Structural Behavior of Timber Beams. *Journal of ReinforcedPlastics and Composites*, *22,* 1373-1388.

18. Gutkowski, R.M., J. Balogh, and A.M.T. Shigidi. Tests and Analysis of a Full-Scale Timber Trestle Bridge Chord. Proceedings, Innovative Wooden Structures and Bridges, IABSE, Lahti, Finland.

19. Gutkowski, R.M. and J. Balogh (2001). Refined Load Tests and Analysis of a Timber Trestle Railroad Bridge Specimen. Proceedings 9th International Conference and Exhibition in Structural Faults and Repair—2001, ASCE, London, UK.

20. Gutkowski, R.M., K.R. Doyle, and J. Balogh (2000). Laboratory Tests of a Timber Trestle Bridge Chord. Presented at and written in Proceedings of the World Conference on Timber Engineering—2000. Whistler Resort, B.C., Canada. Department of Civil Engineering, Department of Wood Science; School of Architecture, University of British Columbia, Vancouver, Canada.

21. Gutkowski, R.M., K.R. Doyle, and J. Balogh (2002). Full-Scale Laboratory Testing of a Timber Trestle Railroad Bridge Chord (Phase 1). Mountain Plains Consortium, Report No. 02-139.

22. Gutkowski, R.M., M. Peterson, G.C. Robinson, U. Uppal, D. Oliva-Maal, and D. Otter (1999). Field Studies of Timber Railroad Bridges. Association of American Railroads, Transportation Technology Center, Inc. Report No. R-933.

23. Gutkowski, R.M., A.S. Shigidi, A.V. Tran, U. Uppal, and D.E. Otter (2002). Field Study of a Strengthened Timber Railroad Bridge. Association of American Railroads, Transportation Technology Center, Inc. Report No. R-946.

24. Gutkowski, R.M., A.M.T. Shigidi, A.V. Tran, and M. Peterson (2001). Field Studies of a Strengthened Timber Railway Bridge. Presented and written in Transportation Research Record No. 1770 Design of Structures 2001. *Journal of the Transportation Research Board*, National Research Council, Washington D.C.

25. Gutkowski, R.M., A.V. Tran, and M. Peterson (2000). Field Tests of a Strengthened Timber Trestle Railway Bridge. Presented at and written in Proceedings of the World Conference on Timber Engineering—2000. Whistler Resort, B.C., Canada. Department of Civil Engineering, Department of Wood Science; School of Architecture, University of British Columbia, Vancouver, Canada.

26. InterCad Kft, Axis VM Version 7 User's Manual. Budapest Hungary (2003).

27. Johns, K.C. and S. Lacroix (2000). Composite Reinforcement of Timber in Bending. *Canadian Journal of Civil Engineering*, *27*, 899-906.

28. Lantos, G. (1964). Reinforced and Post-tensioned Glue-laminated Beams under Development at TRADA Labs. *Civil Engineering and Public Works Review*, London *49*, 690.

29. Liberty Pultrusions. Pultruded Rod Technical Data, 2004.

30. Moody, R.C., R.L. Tuomi, W.E. Eslyn, and F.W. Muchmore (1979). Strength of Log Bridge Stringers after Several Year's Use in Southeast Alaska. U.S. Department of Agriculture, Forest Products Laboratory, Madison WI. Research Paper FPL 346.

31. Muchmore, F.W. (1984). Techniques to Bring New Life to Timber Bridges. *Journal of Structural Engineering*, *110*, 1832-1846.

32. Oomen, G. and R.A.P. Sweeney (1996). Application of Modern Technologies in Railway Bridge Infrastructure Management and Decision Making. NATO ASI Series, Partnership Sub Series 2, Environment. Volume 4, 339-346.

33. Peterson, J.L. (1964). Wood Beams Prestressed with Bonded Tension Elements. *ASCE Journal Structural Division 91(ST1)*, 103-119.

34. Peterson, S.T., D.I. McLean, and D.G. Pollock (2003). Application of Dynamic System Identification to Timber Bridges. *Journal of Structural Engineering, 129,*116-124.

35. Pault, J.D. (1977). Composite Action in Glulam Timber Bridge Systems. Master Science Thesis: Colorado State University, Fort Collins, Colorado.

36. Powers, P.S. (1996). Timber Carries Pennsylvania Roads. *Roads & Bridges*, *34*, 48-60.

37. Radford, D., R. Gutkowski, D. Van Goethem, and M. Peterson (2003). Pultruded composite shear spike for repair of timber members. STREMAH 2003, Eighth International Conference on Structural Studies, Repairs and Maintenance of Heritage Architecture, Halkidiki, Greece, Essex Institute of Technology, UK, 737-740.

38. Radford, D.W., M.L. Peterson, and D. VanGoethem, Composite Repair of Timber Structures. Mountain Plains Consortium, Report No. 00-112, June 2000.

39. Radford, D., D. Van Goethem, R.M. Gutkowski, and M.L. Peterson (2001). Composite repair of Timber Bridges. Proceedings 9th International Conference and Exhibition in Structural Faults and Repair—2001, ASCE, London, UK.

40. Radford, D., D. Van Goethem, R.M. Gutkowski, and M.L. Peterson (2002). Composite repair of timber structures. *Construction and Building Materials*, Elsevier Publications, *16*, 417-424.

41. Schilling, T.J., R.M. Gutkowski, and D. Radford (2004). Composite Repair of Railroad Crossties through the Process of Shear Spiking. Mountain Plains Consortium, Report No. 04-163.

42. Seigel, M. and L. Cerny (1981). Study of Timber Trestles on Columbus and Greenville Railway, *AREA Bulletin 683*, vol. 82.

43. Singh, J. and N. White (1997). Timber Decay in Buildings: Pathology and Control. *Journal of Performance of Constructed Facilities, 11*, 3-12.

44. Sliker, A. (1962). Reinforced Wood Laminated Beams. *Forest Products Journal, 12 (2)*, 91-96.

45. Steves, C.A. and N.A. Fleck (1999). In-Plance Properties of CFRP Laminates Containing Through-Thickness Reinforcing Rods (Z-pins). Proceeding ICCM-12, Paris, July 1999.

46. Triantafillou, T.C. (1997). Shear Reinforcement of Wood Using FRP Materials. *Journal of Materials in Civil Engineering*, *9*, 64-69.

47. Uppal, U. and D.E. Otter (1998). Methodologies for Strengthening and Extending Life of Timber Railroad Bridges. Association of American Railroads, Transportation Technology Center, Inc. Report No. R-922.

48. van de Kuilen, J.W.G. (1991). Theoretical and Experimental Research on Glass Fibre Reinforced Laminated Timber Beams. *Proceedings of the International Timber Engineering Conference*, 3.226-3.233. London, England.

49. Wipf, T.J., D. Wood, D. Otter, P. Rogers, and A.S. Uppal (1997). Field Testing of Two Open Deck Timber Railroad Bridges. AAR Report R-913. Association of American Railroads.

8. APPENDICES

Appendix A: Liberty Pultrusions Technical Data

Table A.1: Liberty Pultrusions Technical Data [29]

Property	Test Method	Condition	Units	Value
Ultimate tensile strength	ASTM D-638	RT	Mpa (ksi)	483 (70)
Flexural strength	ASTM D-790	RT 100°C (212°F) 140°C (302°F)	Mpa (ksi) Mpa (ksi) Mpa (ksi)	483 (70) 172 (24) 103 (14)
Flexural modulus of elasticity	ASTM D-790	RT 100°C (212°F) 140°C (302°F)	Mpa (psi) Mpa (psi) Mpa (psi)	2.07×10^4 (3.0×10^6) 1.38×10^4 (2.0×10^6) 1.03×10^4 (1.4×10^6)
Impact strength	ASTM D-246	RT	kN-m/m notch (ft-lb/in notch)	1.6 (30)
Compressive strength	ASTM D-694			
Flatwise		RT	Mpa (ksi)	138 (20)
Lengthwise		RT	Mpa (ksi)	276 (40)
Thermal coefficient of expansion	ASTM D-696		mm/mm/°C (in/in/°F)	1.67×10^{-6} (3×10^{-6})
Thermal conductivity			$W/m^2/°C$ ($BTU/hr/ft^2/in/°F$)	0.2 (4)
Specific gravity	ASTM D-792			1.94
Water absorption	ASTM D-349	24 hrs	%	0.3

Appendix B: MOE Load-Deflection Data

(1 kip = 4.448 kN) (1 kN = 0.2248 kips)
(1 inch = 24.4 mm) (1 mm = 0.03937 inches)

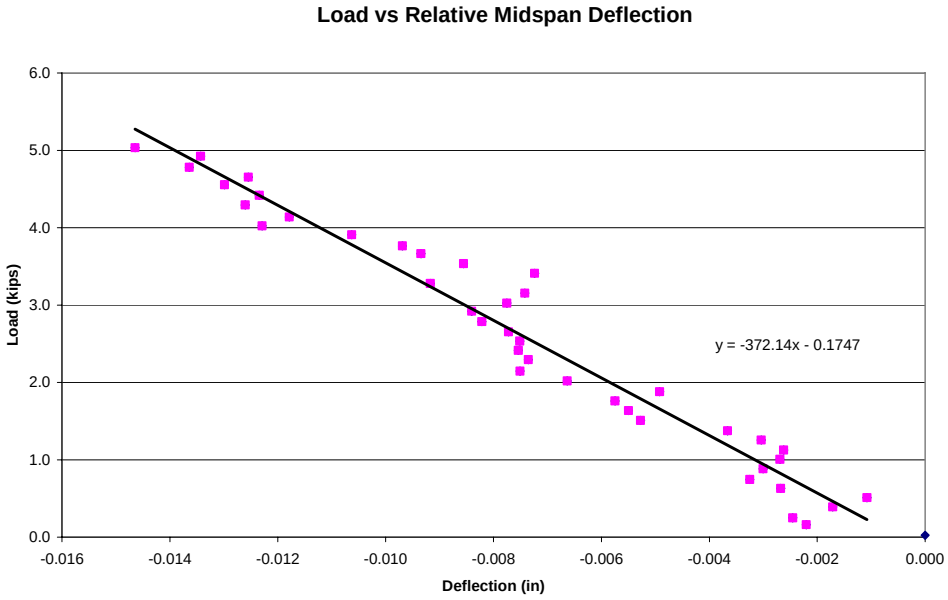

Figure B.1: Beam 1 Load-Deflection

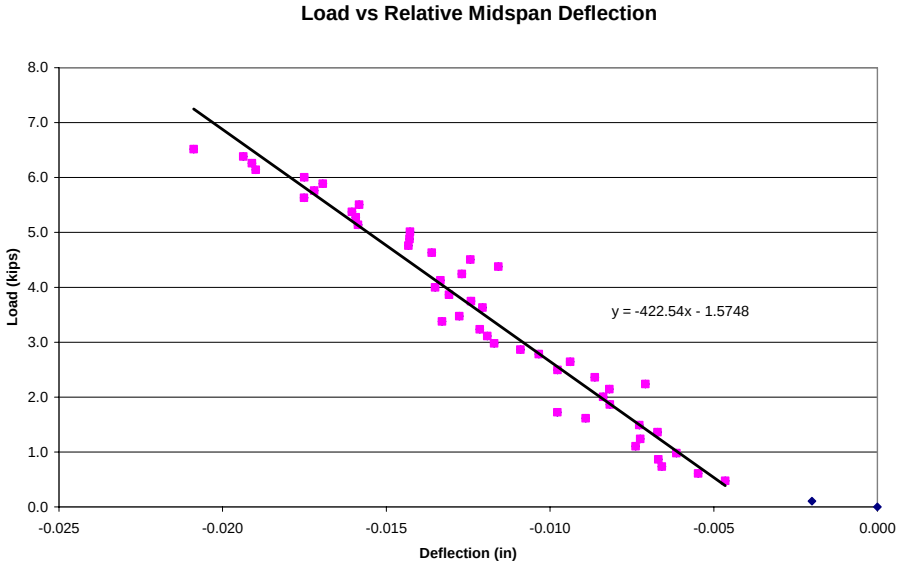

Figure B.2: Beam 2 Load-Deflection

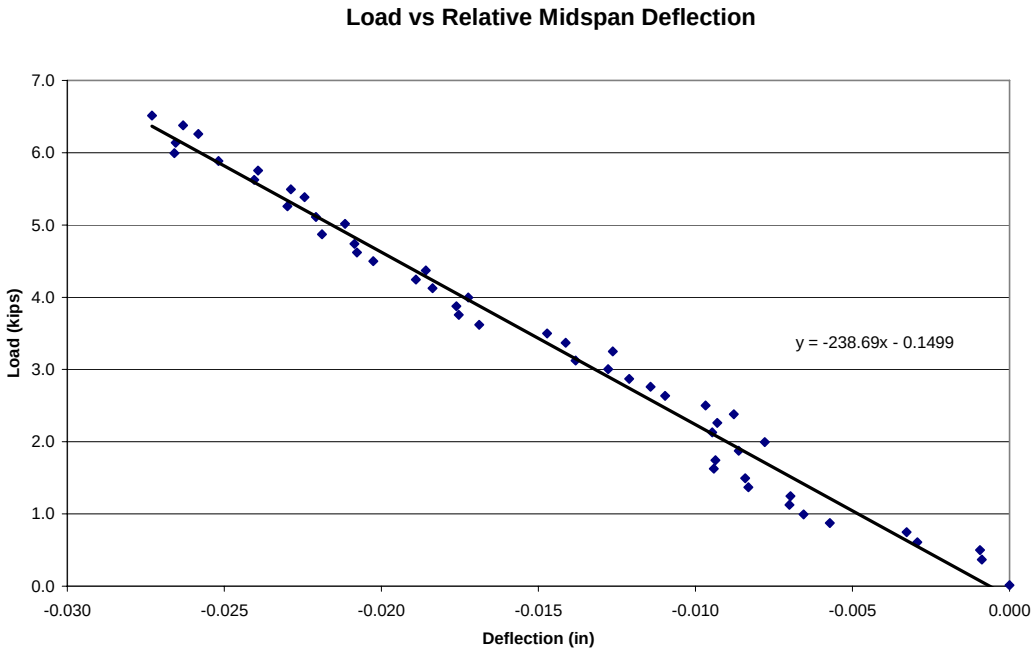

Figure B.3: Beam 3 Load-Deflection

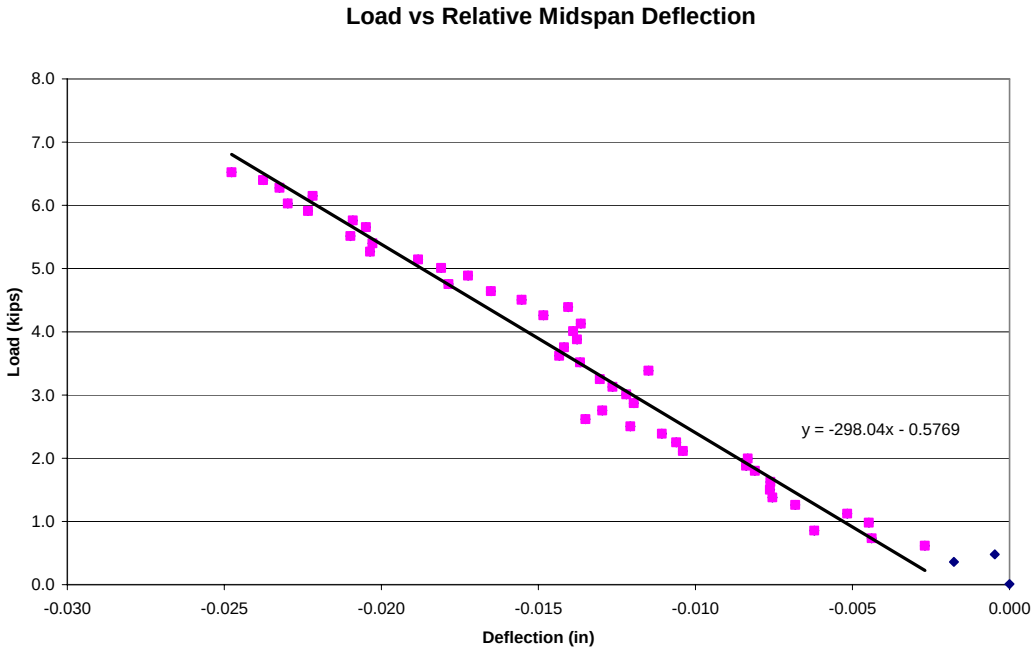

Figure B.4: Beam 4 Load-Deflection

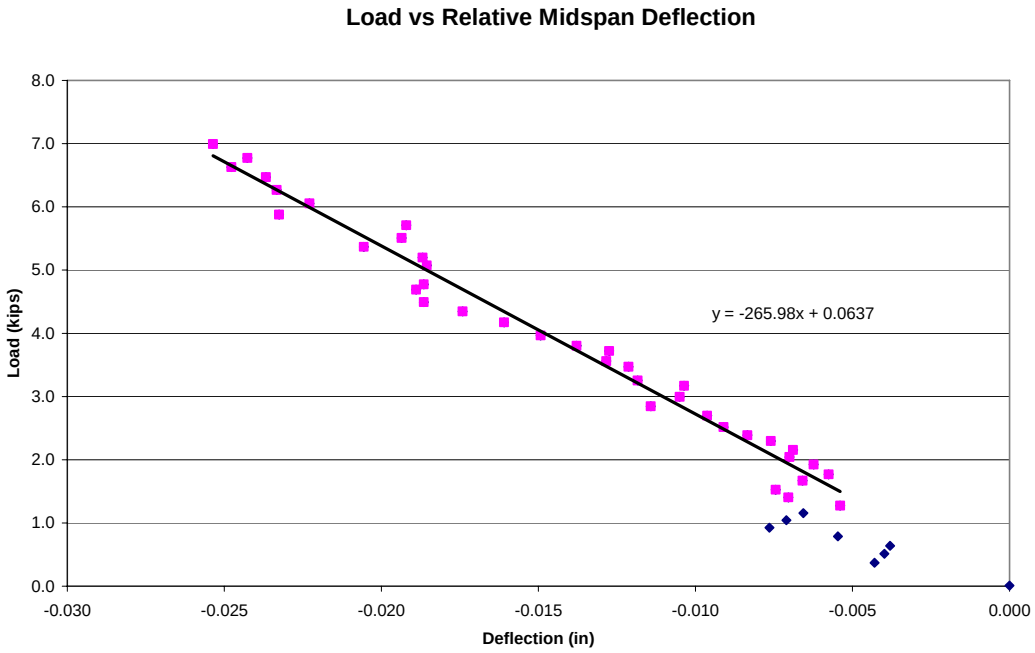

Figure B.5: Beam 4 Load-Deflection

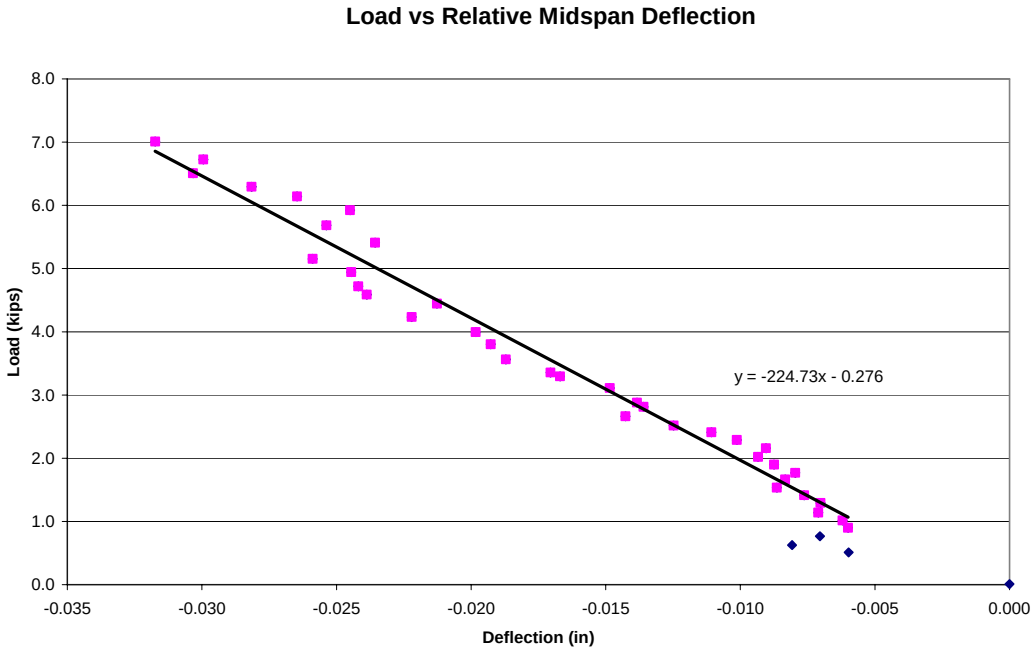

Figure B.6: Beam 6 Load-Deflection

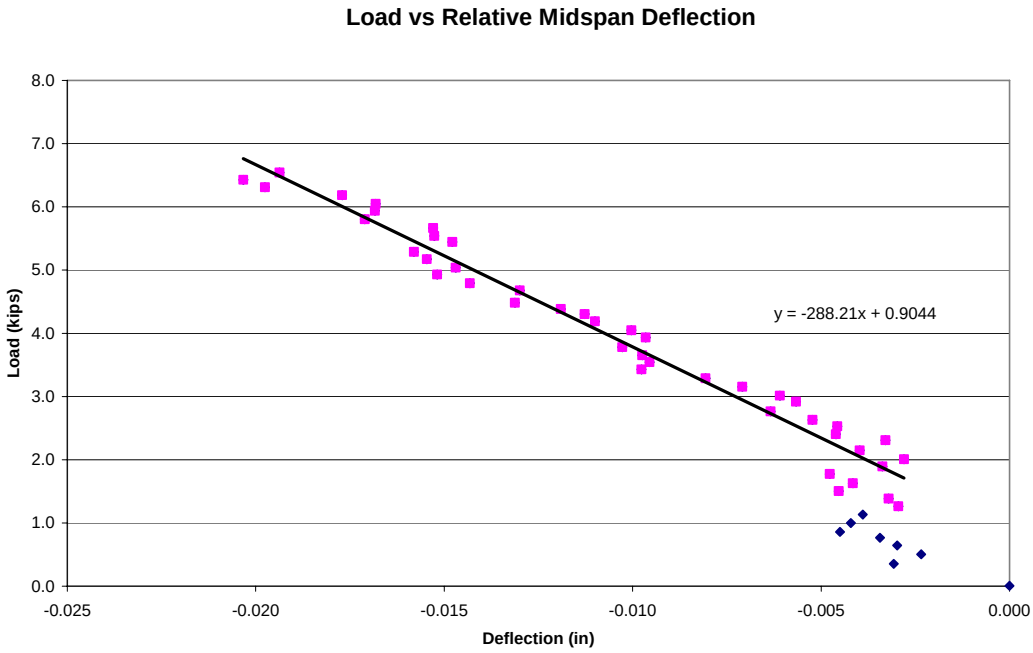

Figure B.7: Beam 7 Load-Deflection

Appendix C: South Damage Load-Deflection

(1 kip = 4.448 kN) (1 kN = 0.2248 kips)
(1 inch = 24.4 mm) (1 mm = 0.03937 inches)

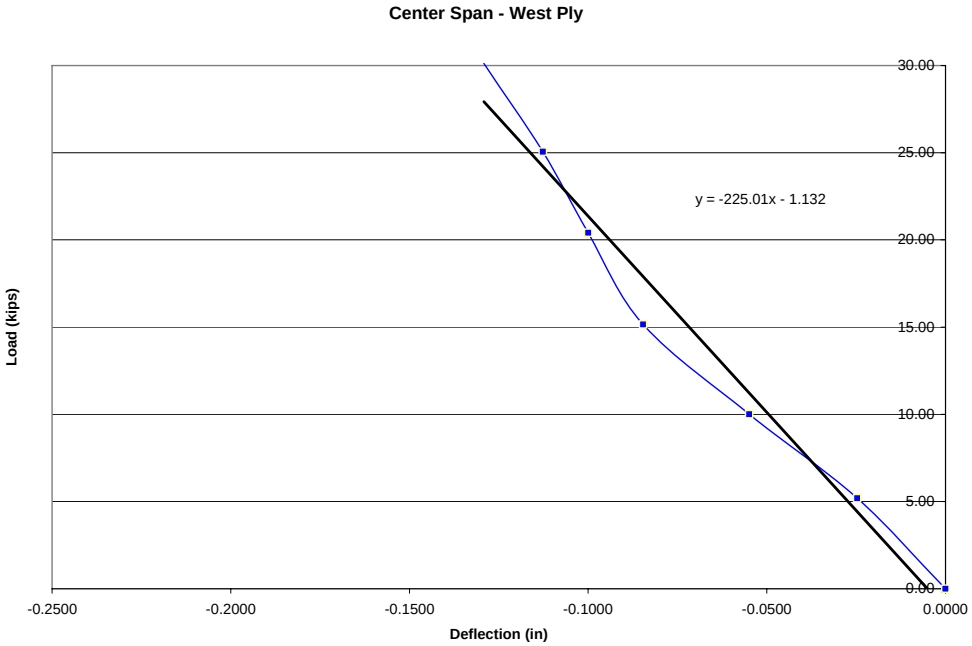

Figure C.1: C-W no damage

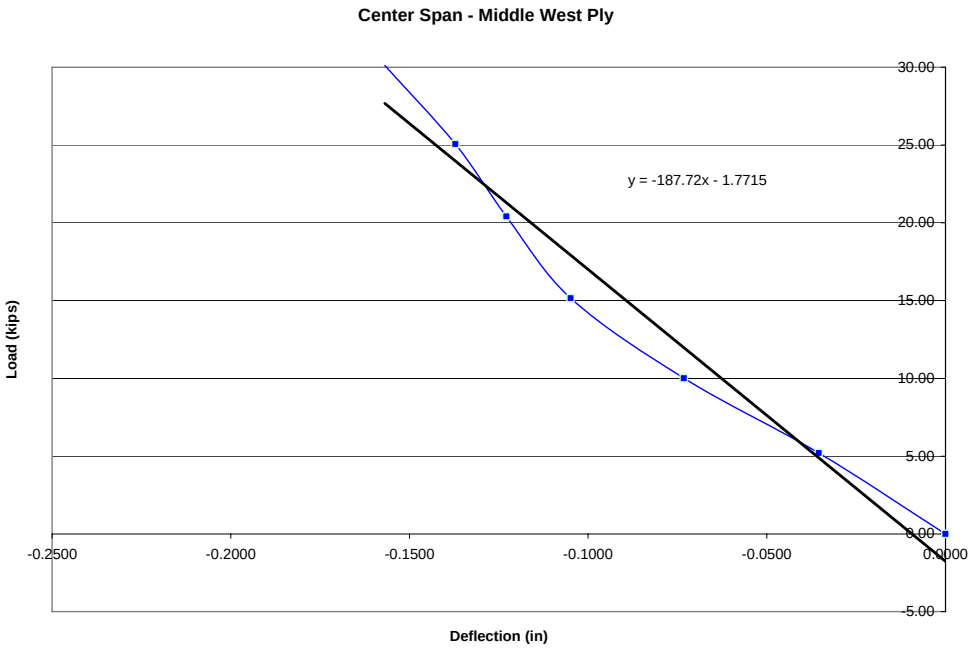

Figure C.2: C-MW no damage

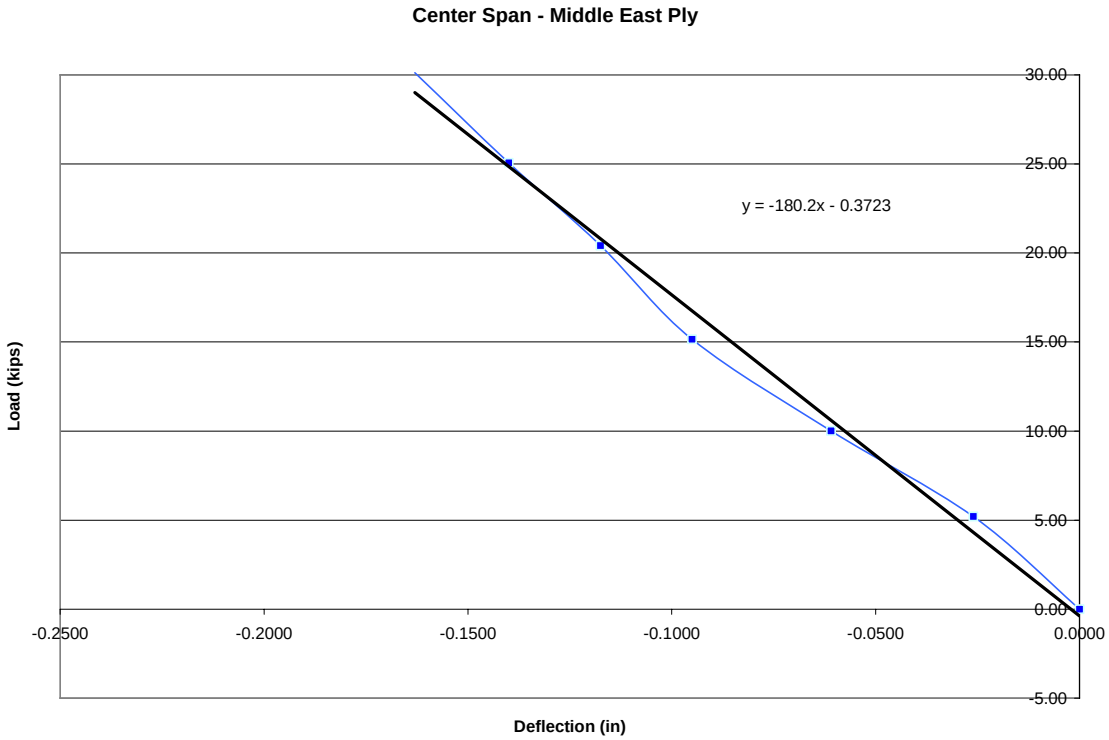

Figure C.3: C-ME no damage

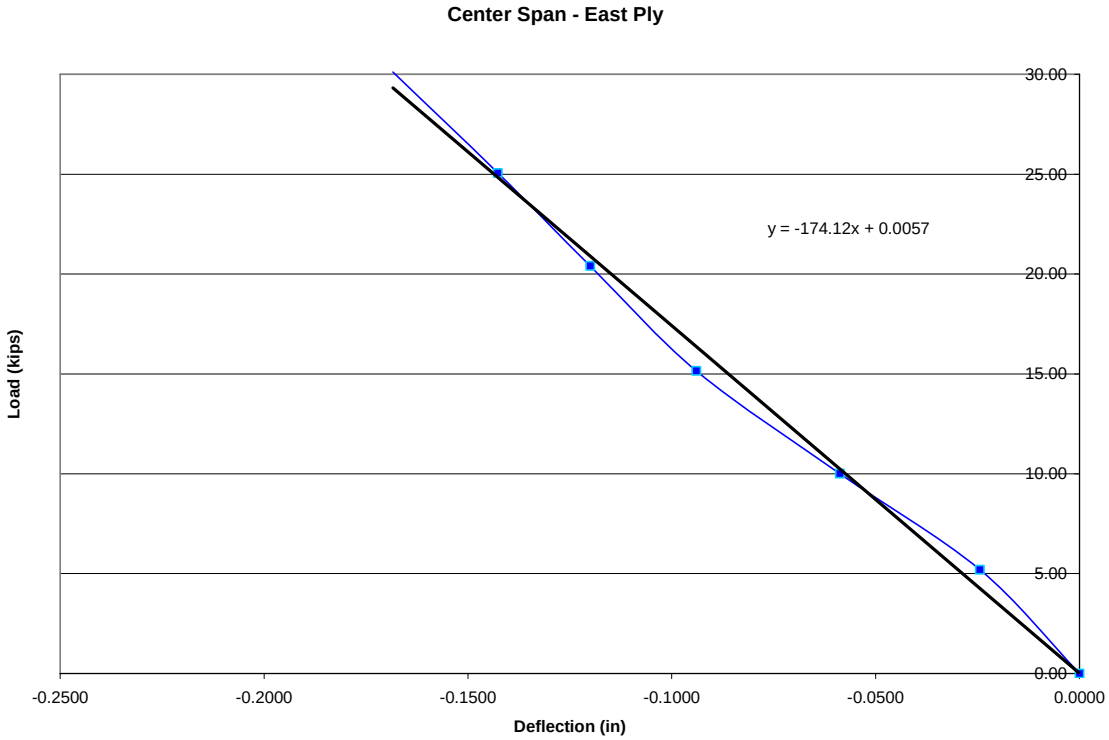

Figure C.4: C-E no damage

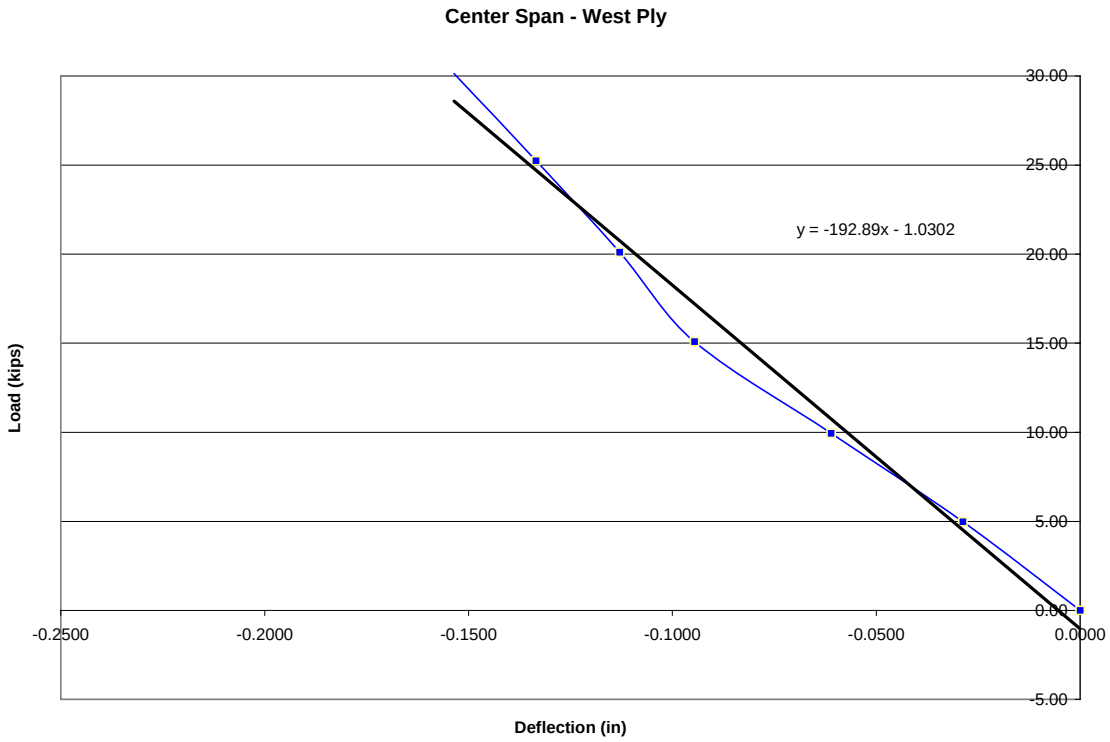

Figure C.5: C-W 8 inch cut (before crack)

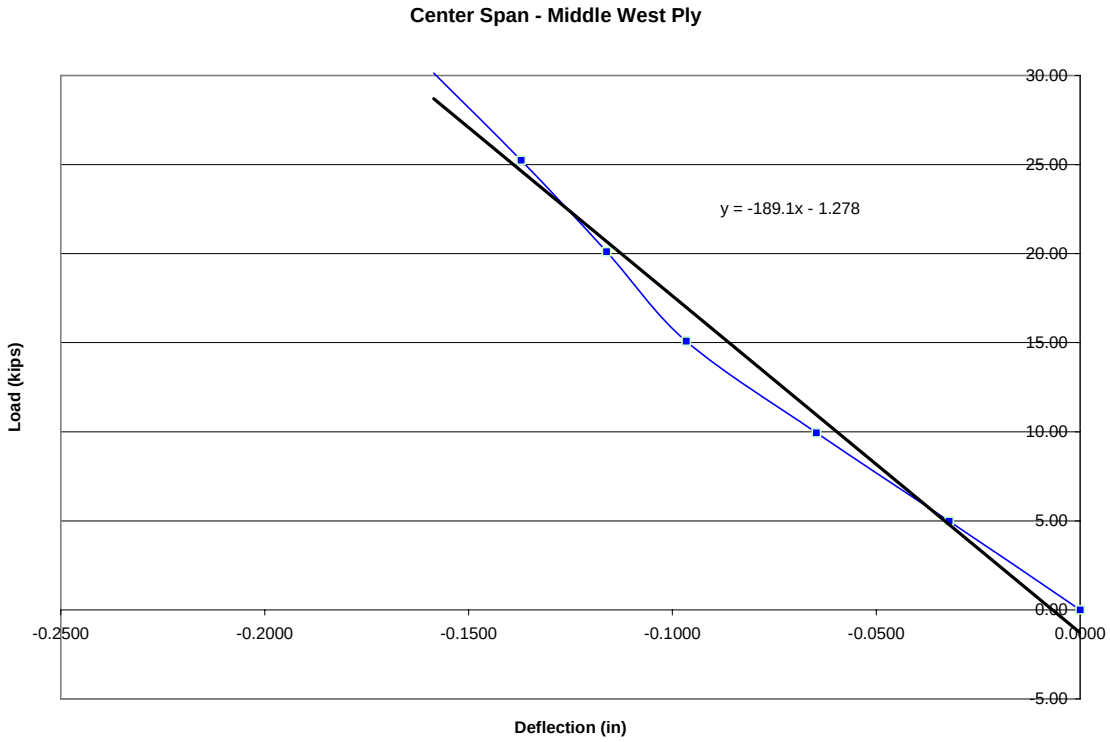

Figure C.6: C-MW 8 inch cut (before crack)

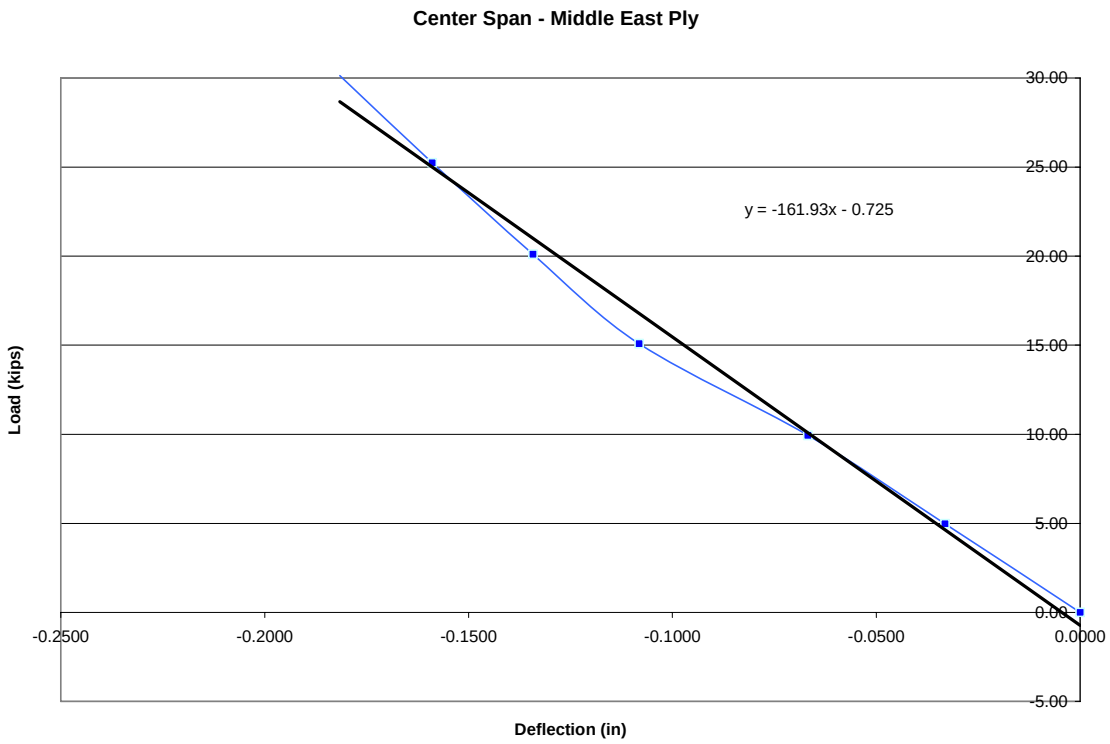

Figure C.7: C-ME 8 inch cut (before crack)

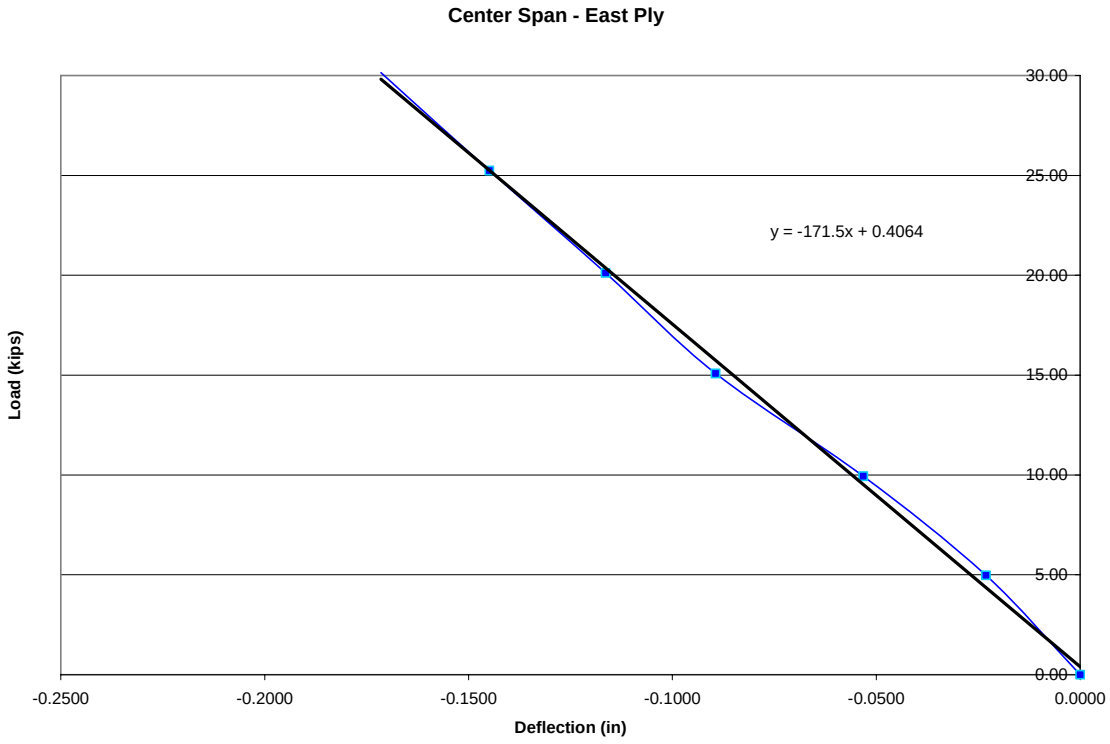

Figure C.8: C-E 8 inch cut (before crack)

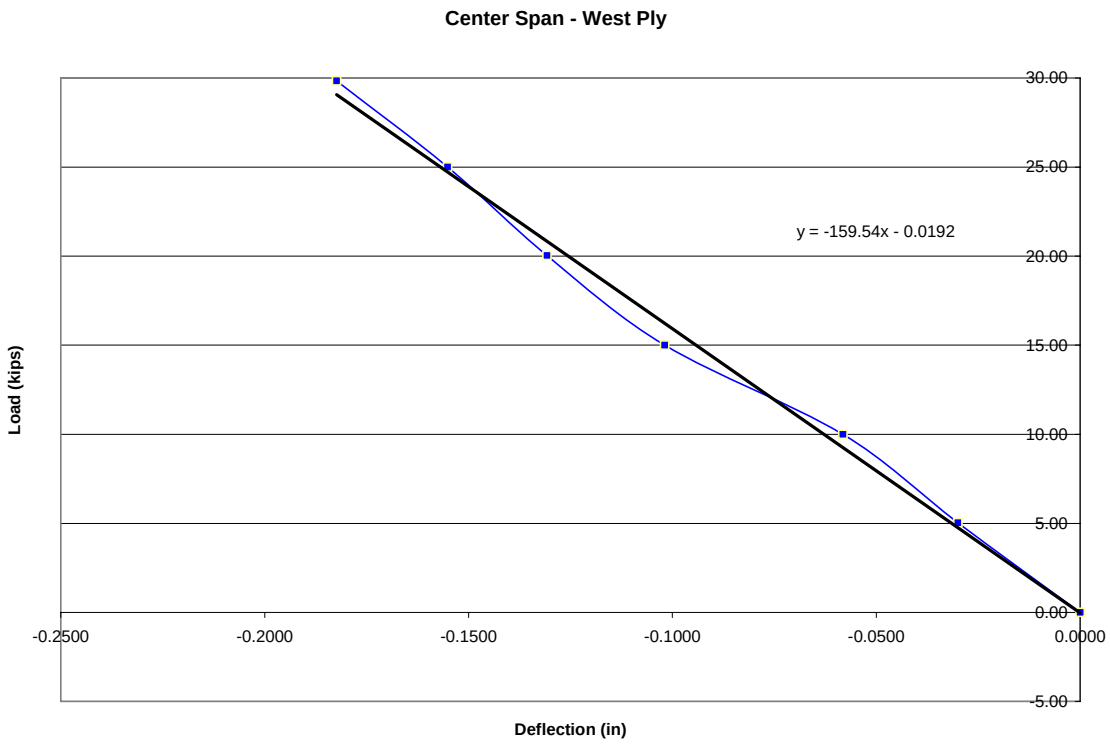

Figure C.9: C-W 8 inch cut (after crack)

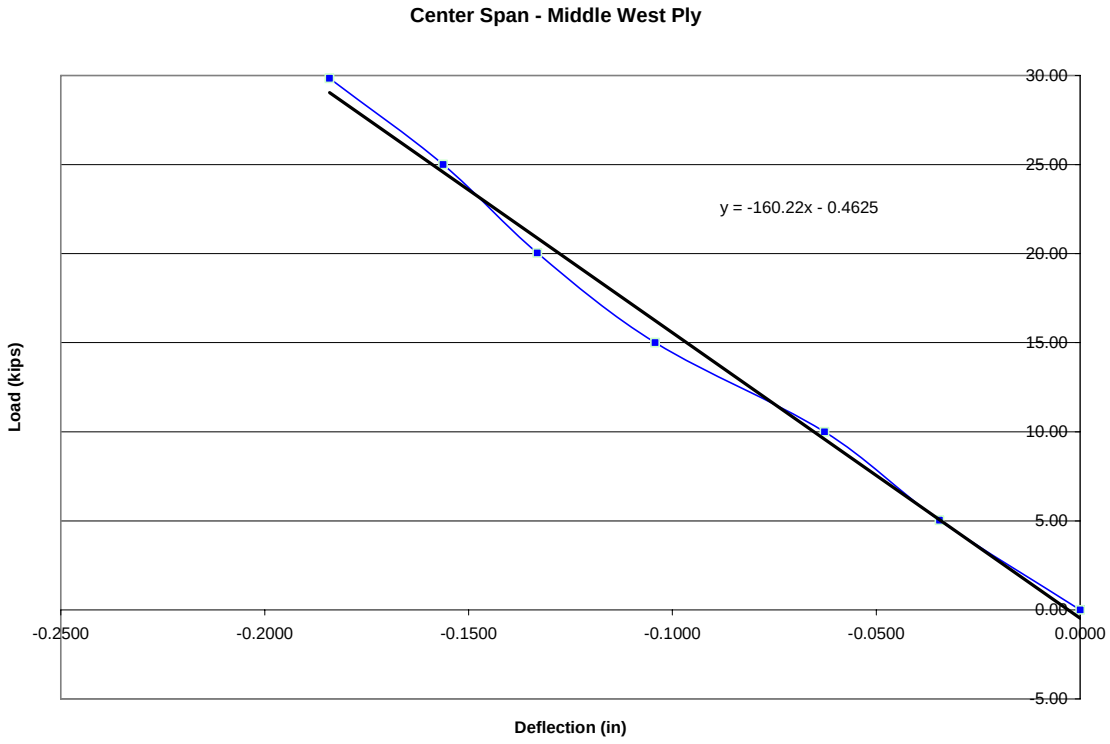

Figure C.10: C-MW 8 inch cut (after crack)

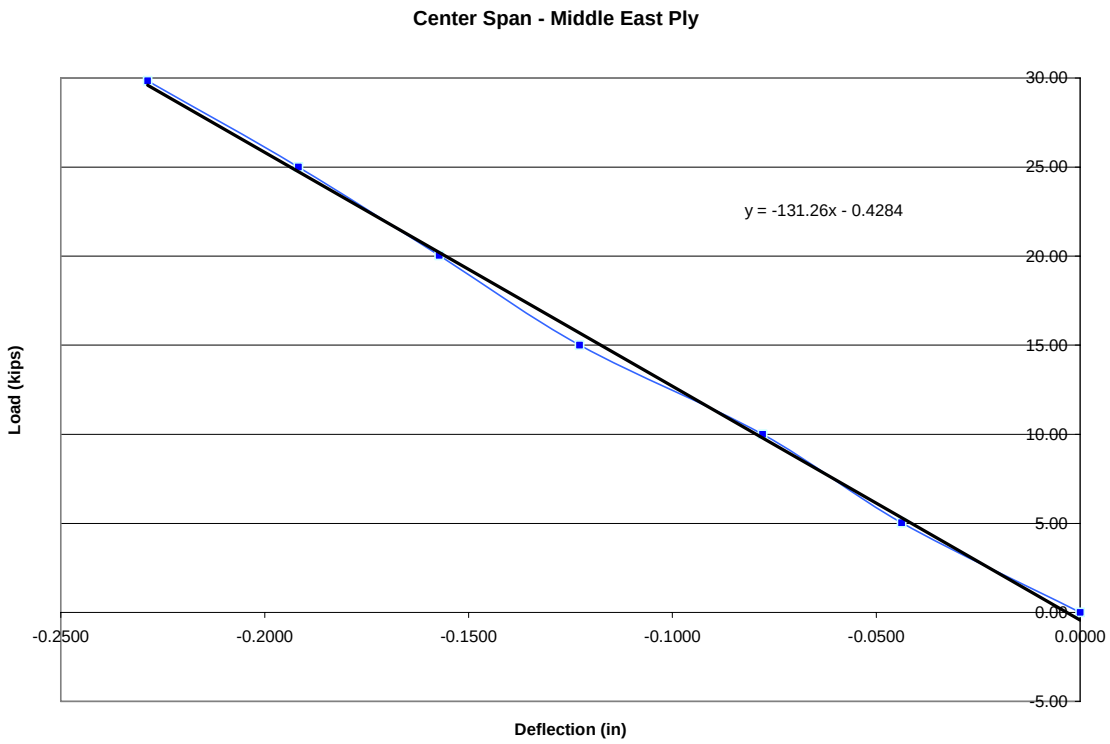

Figure C.11: C-ME 8 inch cut (after crack)

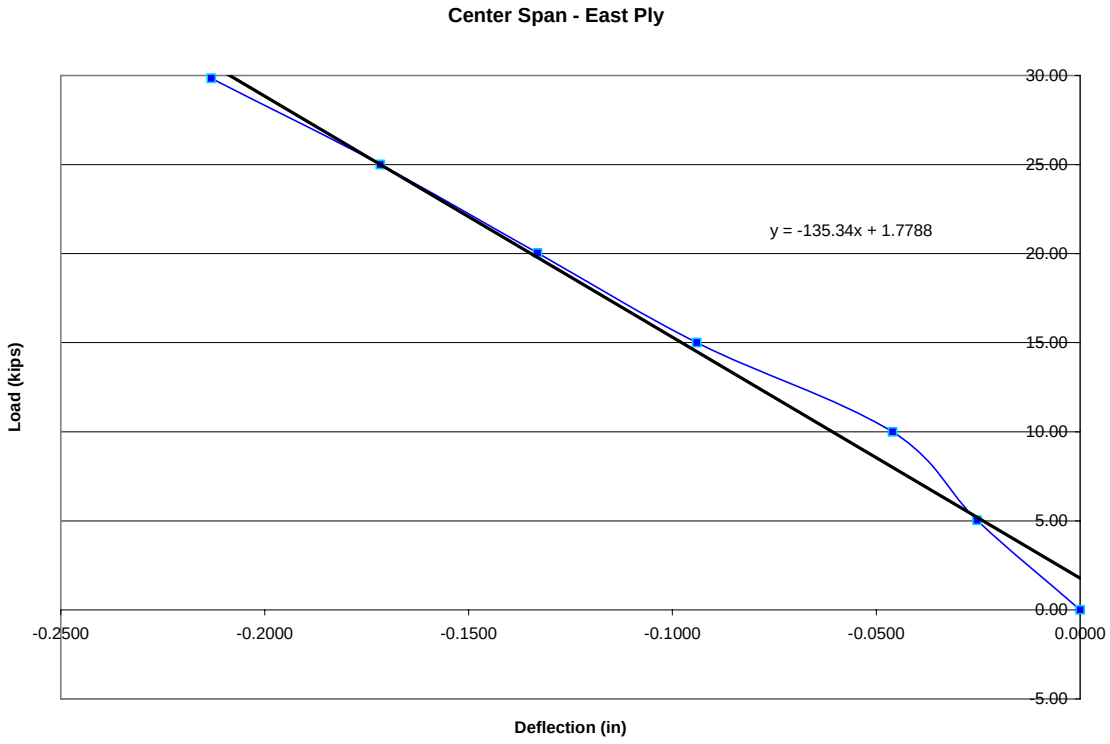

Figure C.12: C-E 8 inch cut (after crack)

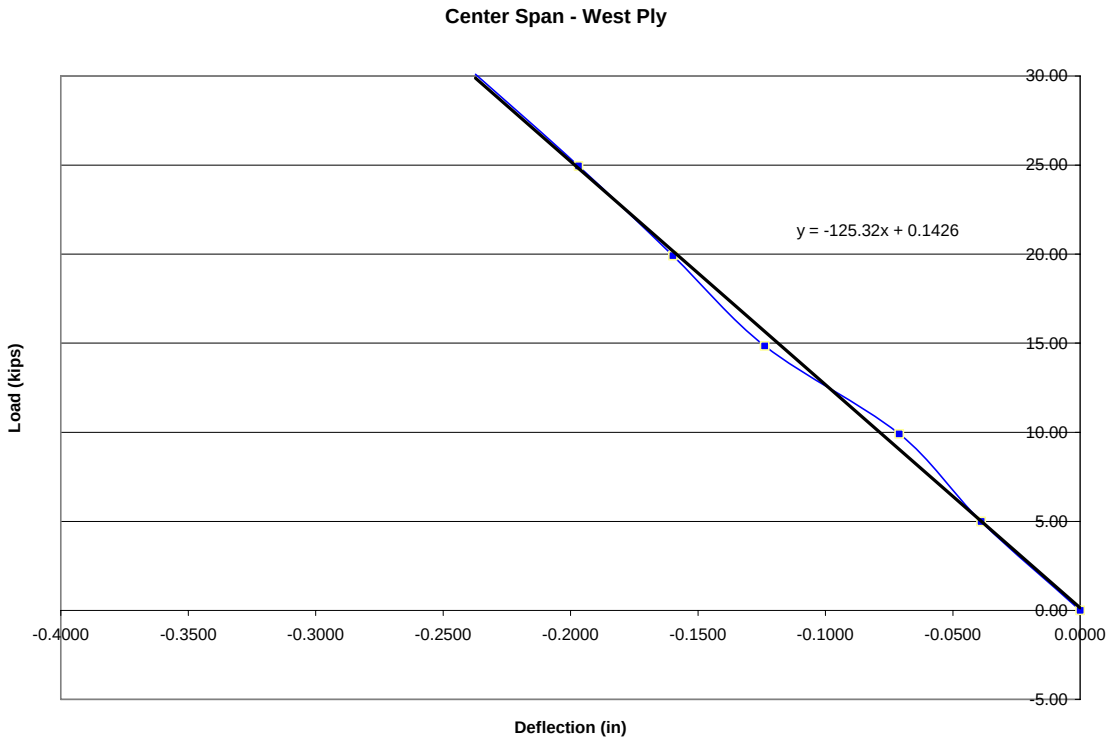

Figure C.13: C-W full cut completed (south damage/repair)

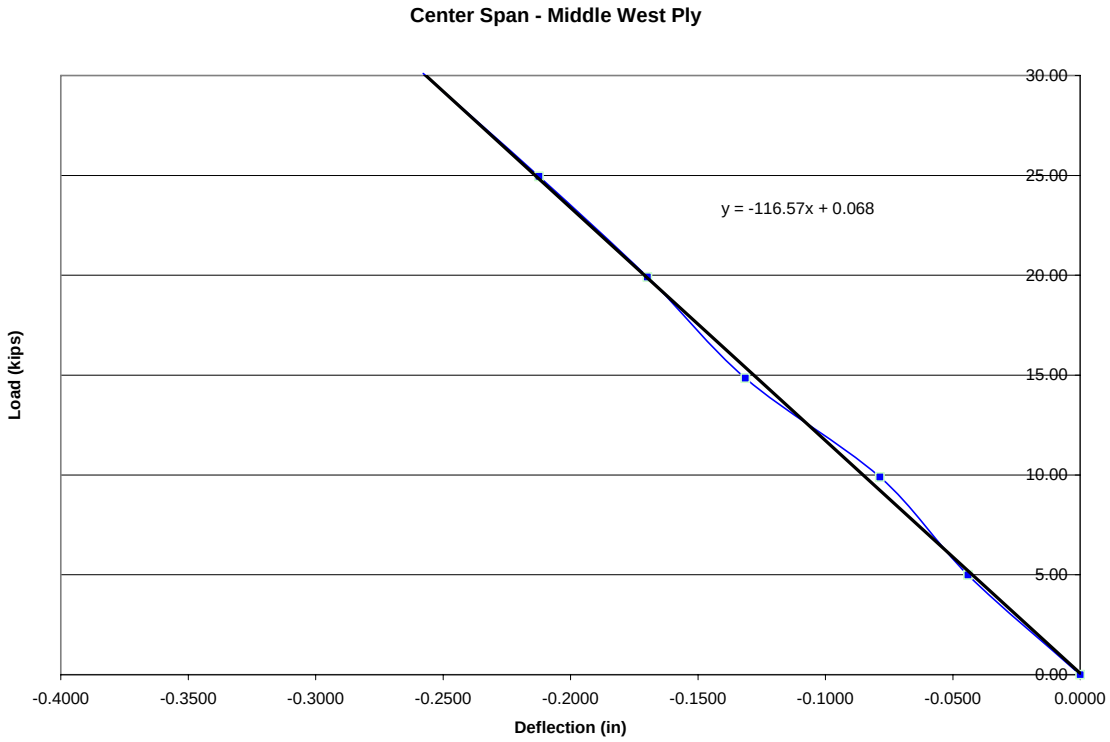

Figure C.14: C-MW full cut completed (south damage/repair)

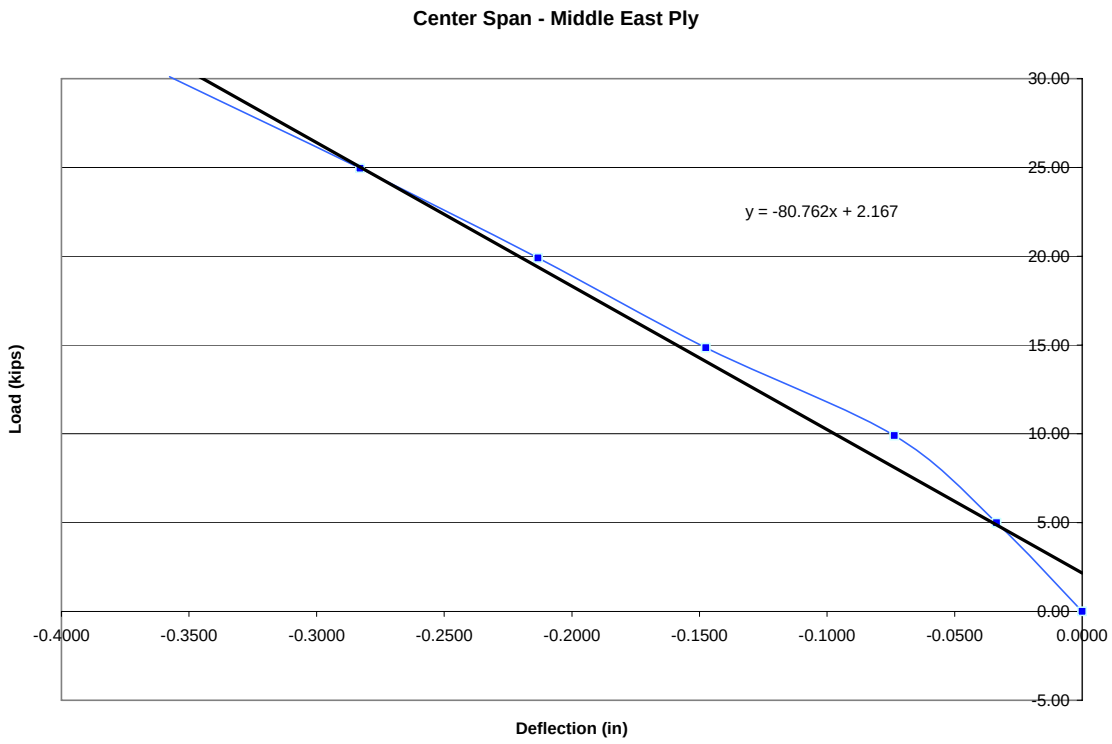

Figure C.15: C-ME full cut completed (south damage/repair)

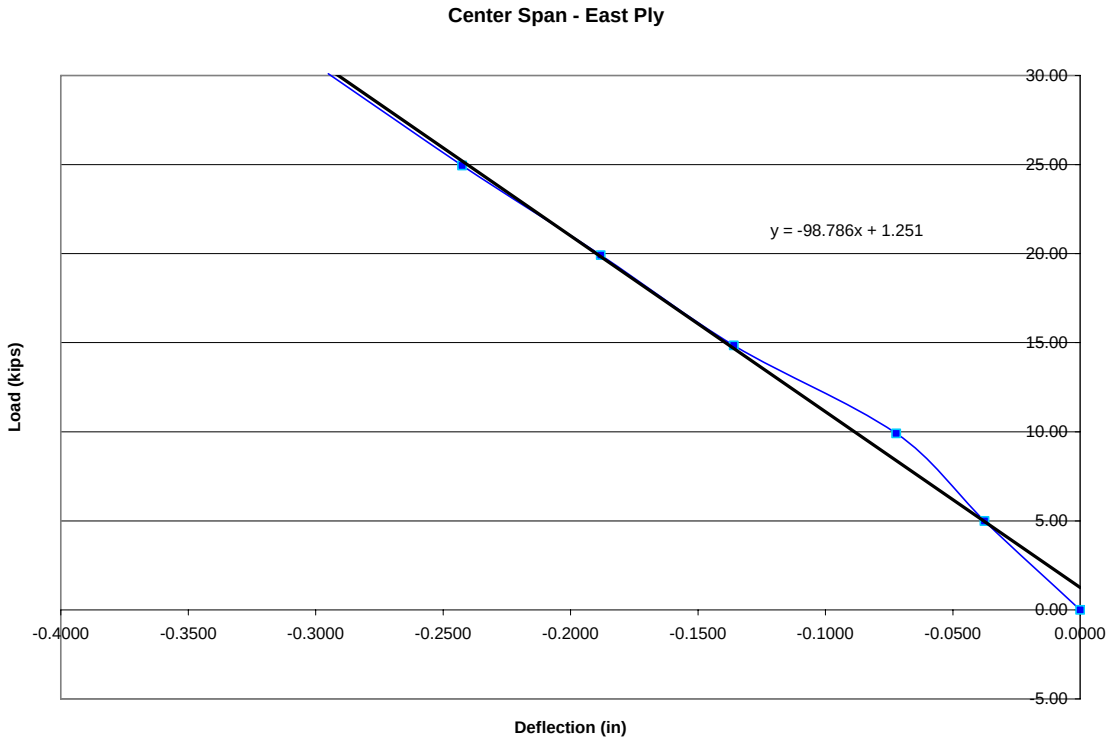

Figure C.16: C-E full cut completed (south damage/repair)

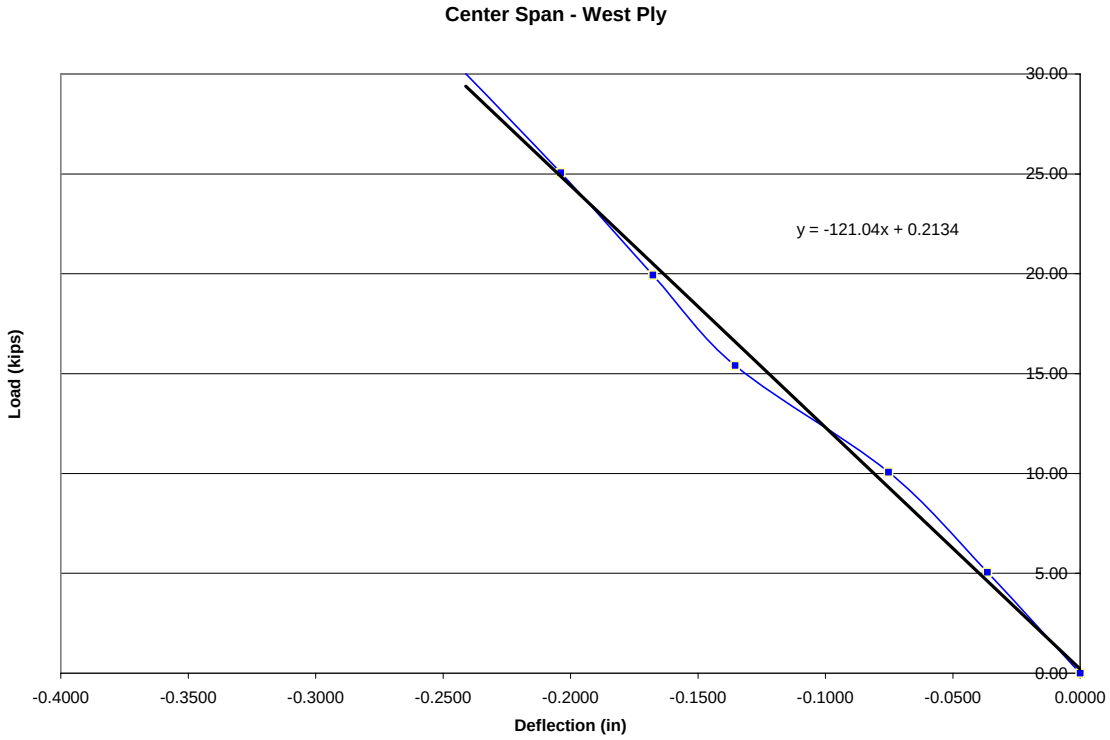

Figure C.17: C-W Z-spikes in end (south damage/repair)

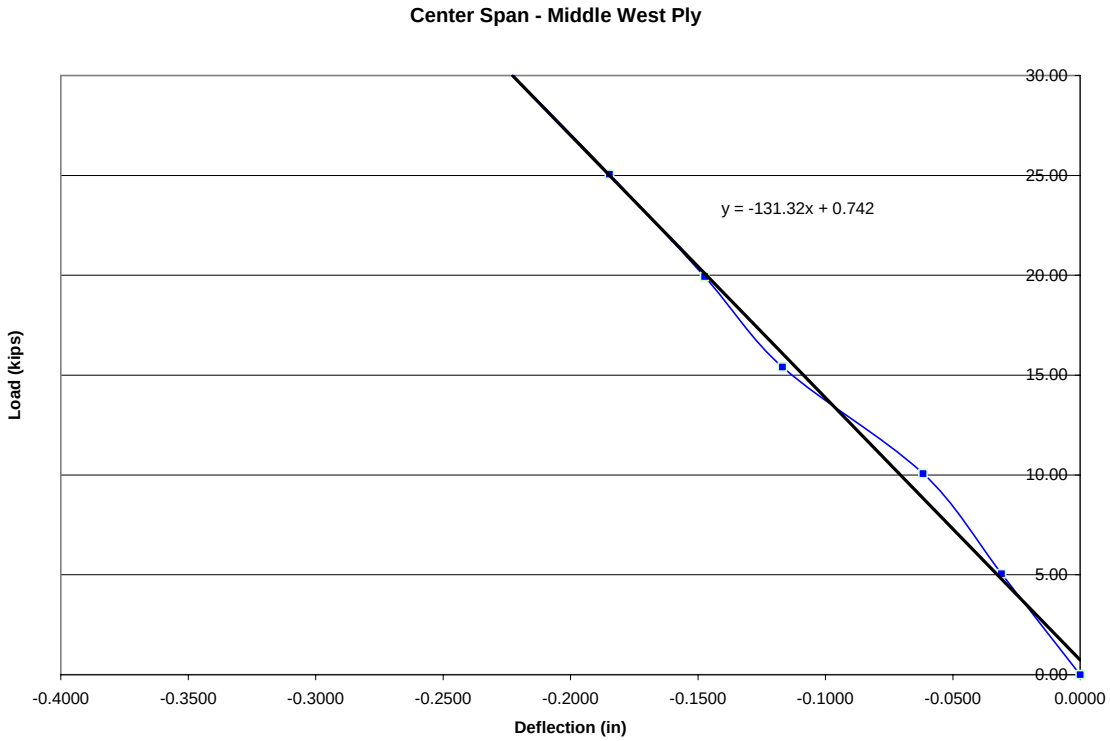

Figure C.18: C-MW Z-spikes in end (south damage/repair)

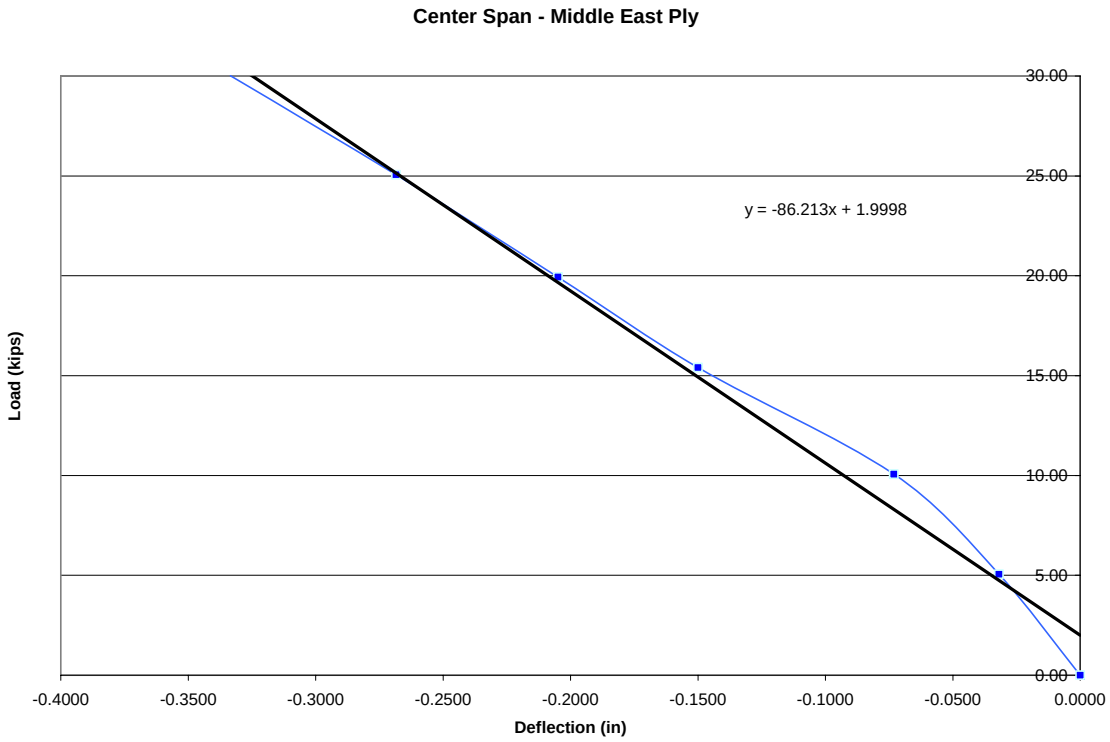

Figure C.19: C-ME Z-spikes in end (south damage/repair)

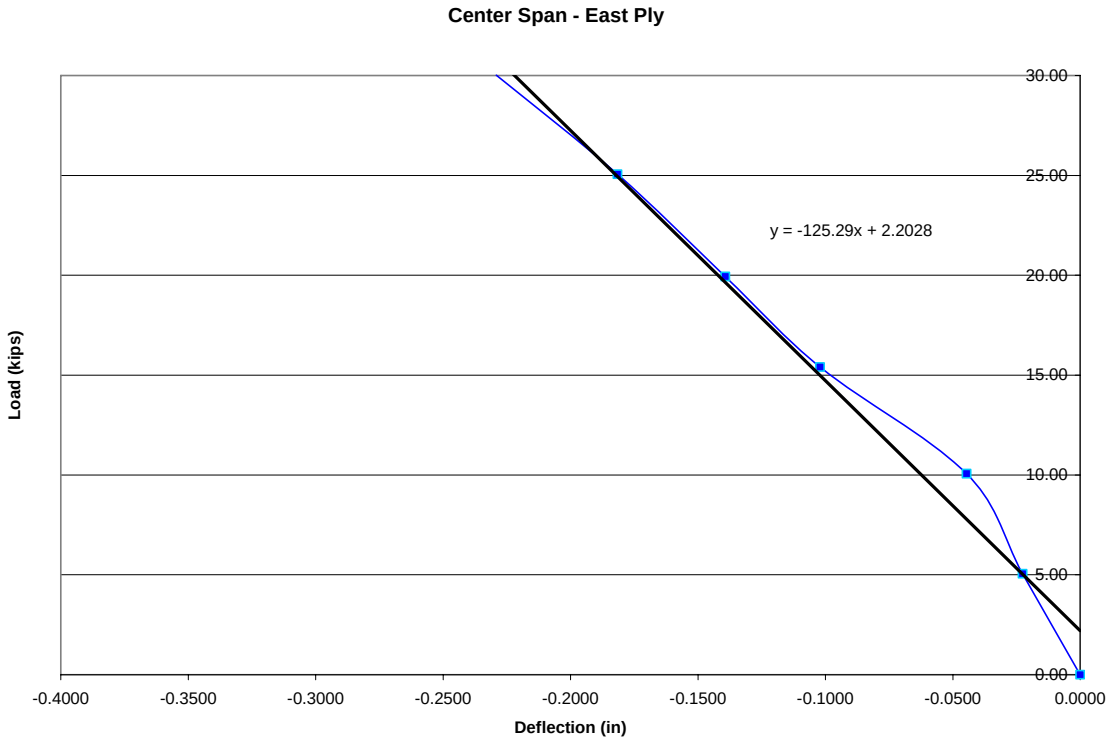

Figure C.20: C-E Z-spikes in end (south damage/repair)

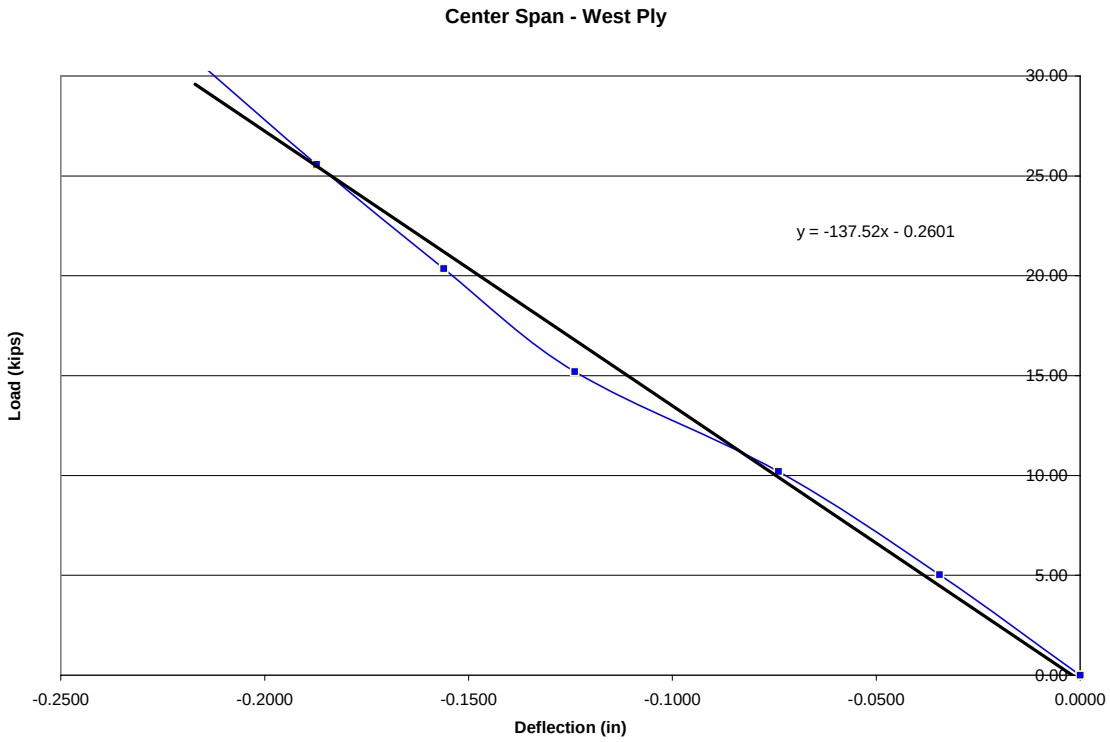

Figure C.21: C-W repaired center beams (south) (south damage/repair)

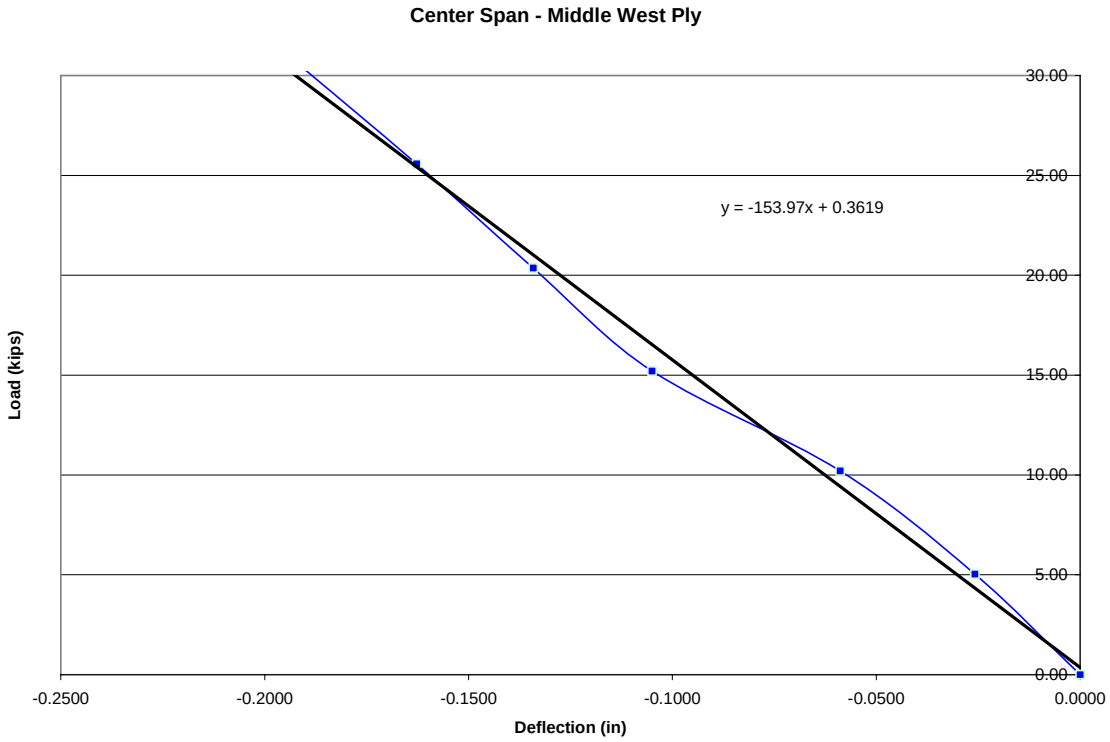

Figure C.22: C-MW repaired center beams (south) (south damage/repair)

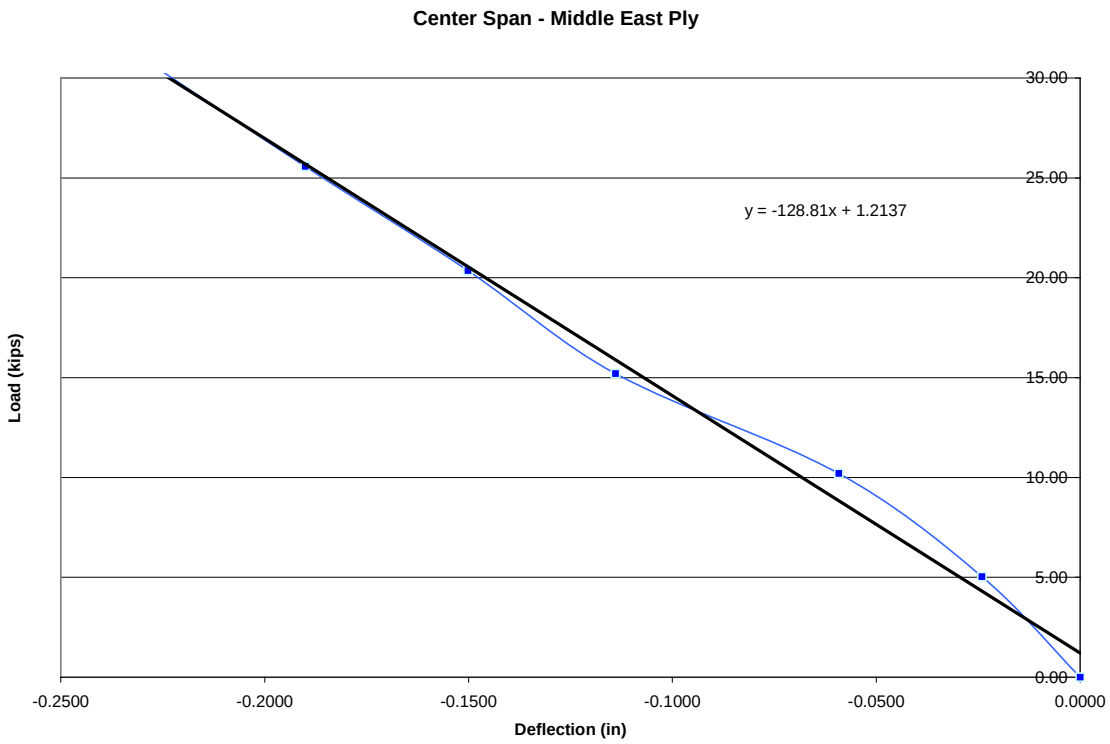

Figure C.23: C-ME repaired center beams (south) (south damage/repair)

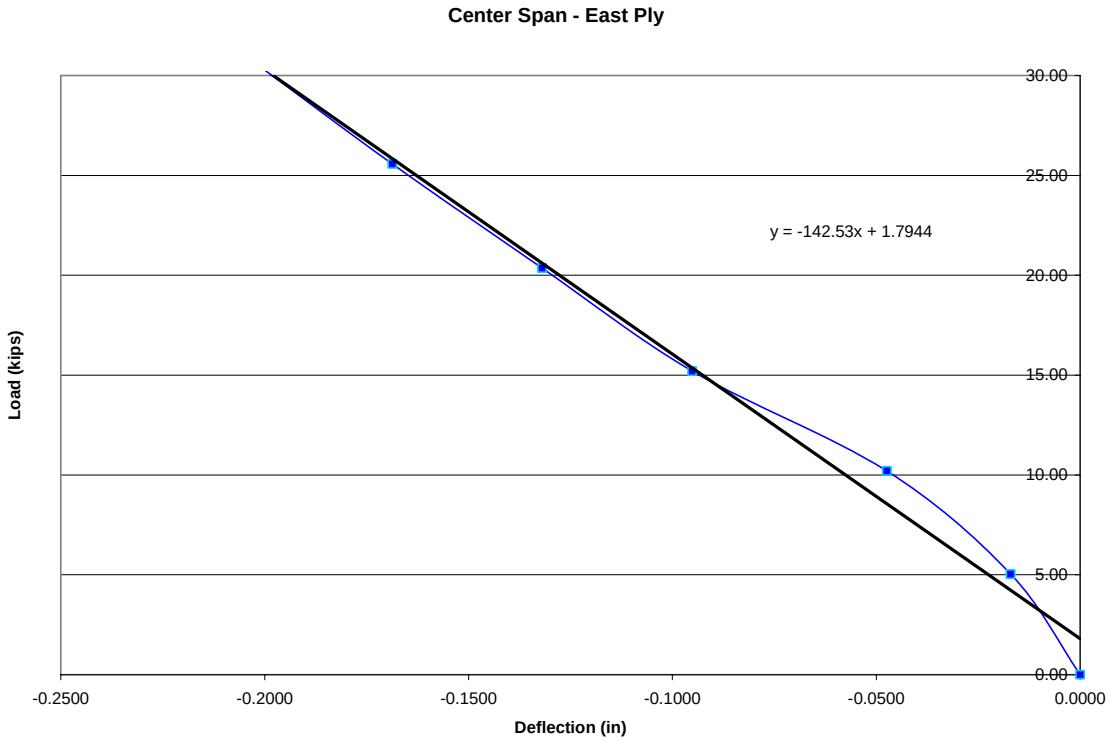

Figure C.24: C-E repaired center beams (south) (south damage/repair)

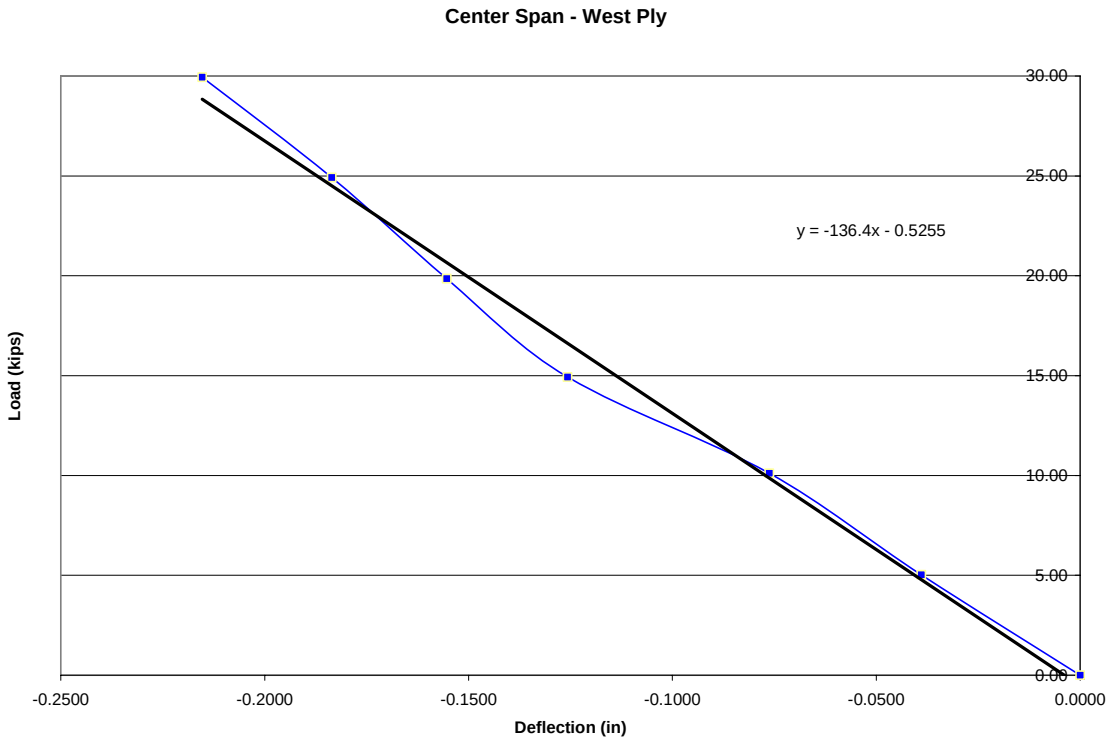

Figure C.25: C-W repaired center beams (north) (south damage/repair)

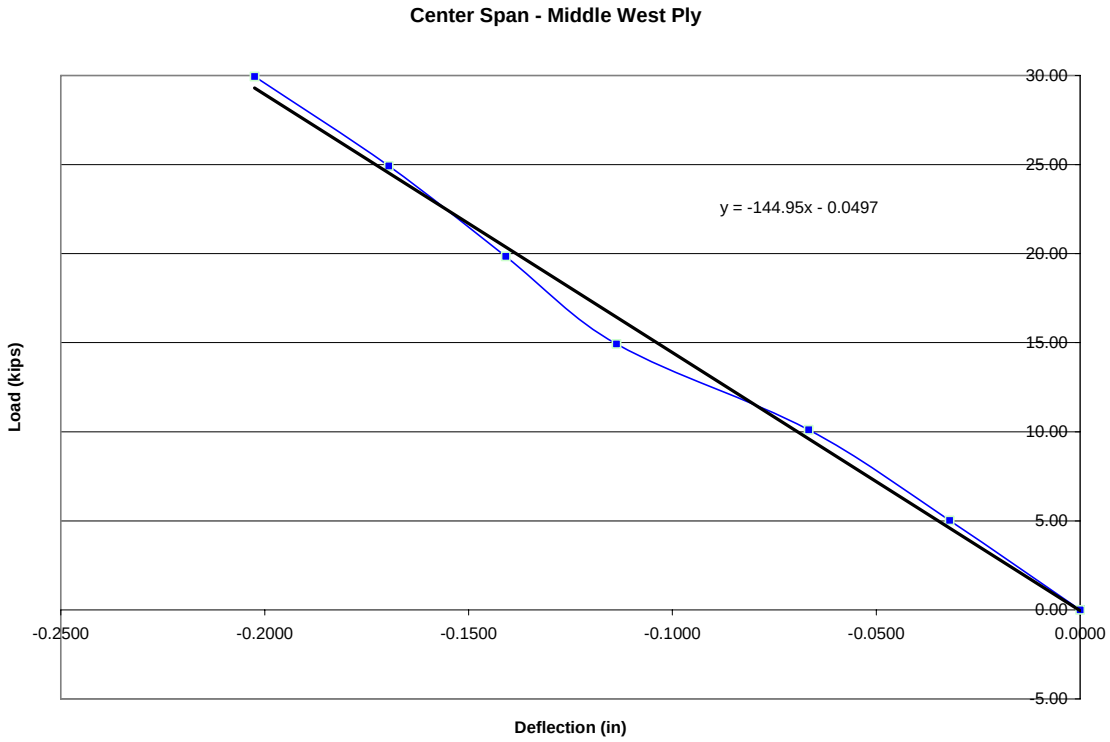

Figure C.26: C-MW repaired center beams (north) (south damage/repair)

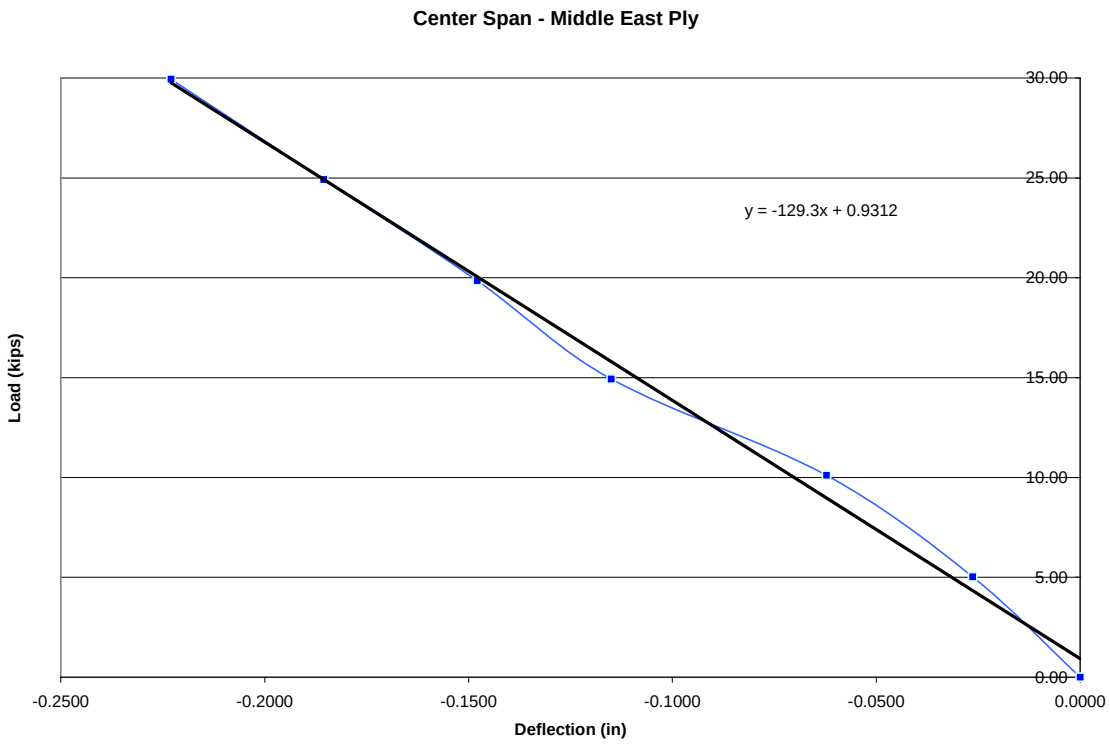

Figure C.27: C-ME repaired center beams (north) (south damage/repair)

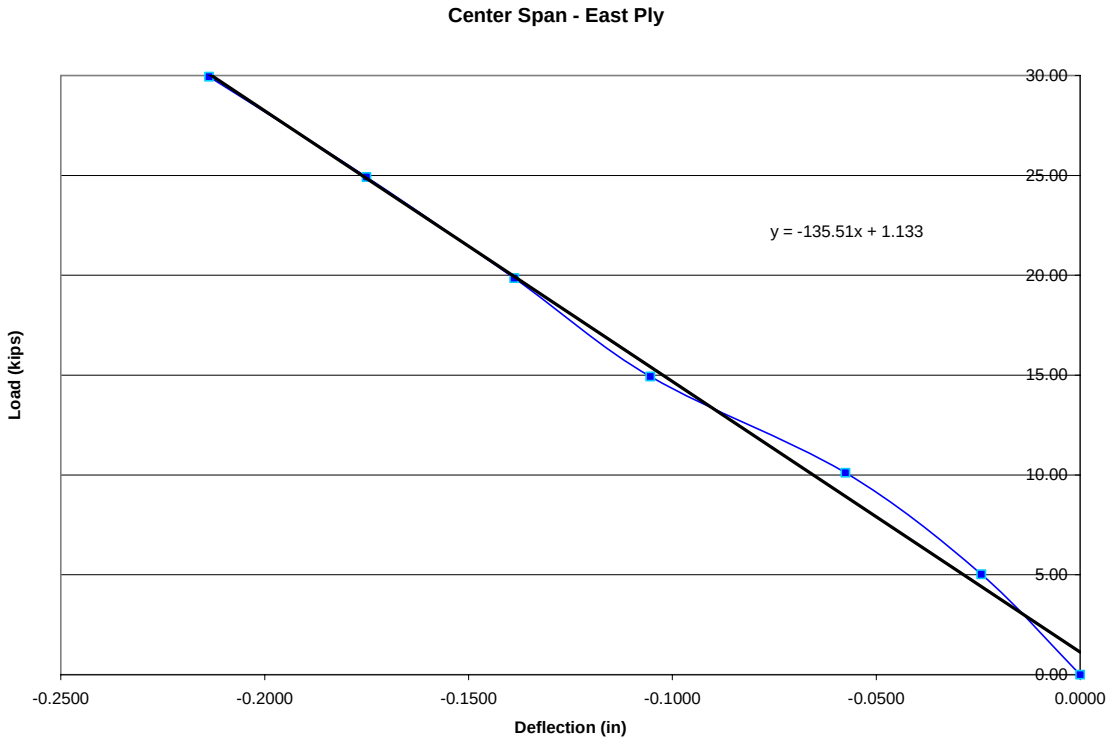

Figure C.28: C-E repaired center beams (north) (south damage/repair)

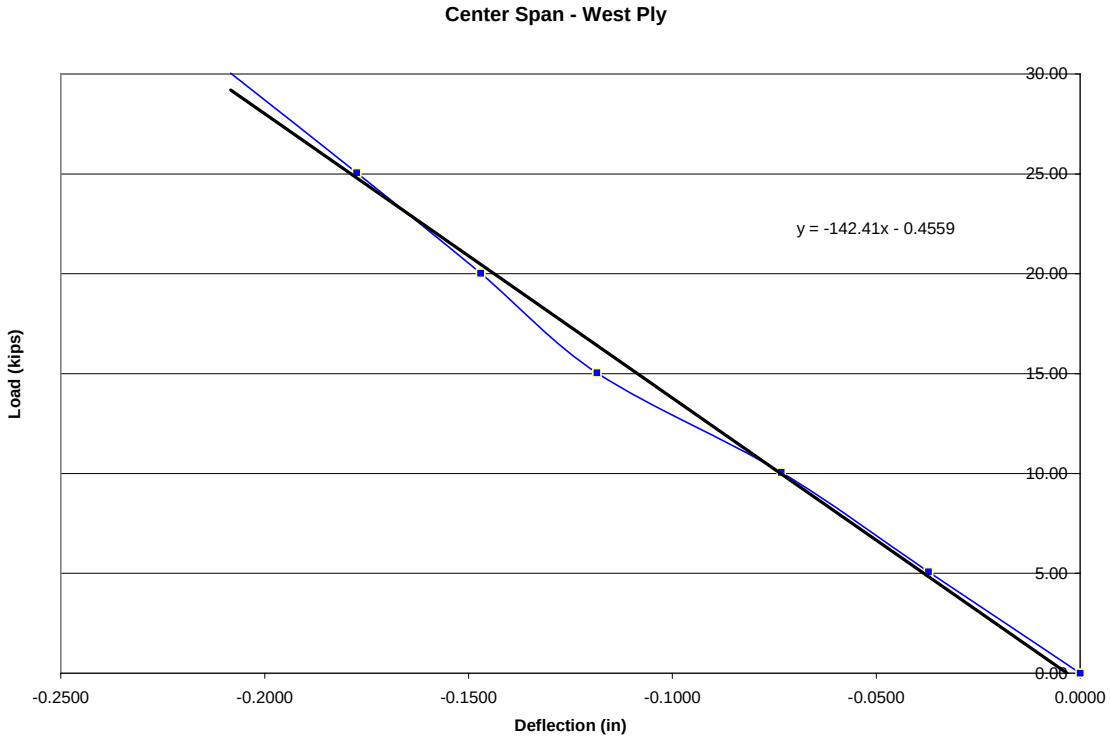

Figure C.29: C-W 1st set of Z-spikes

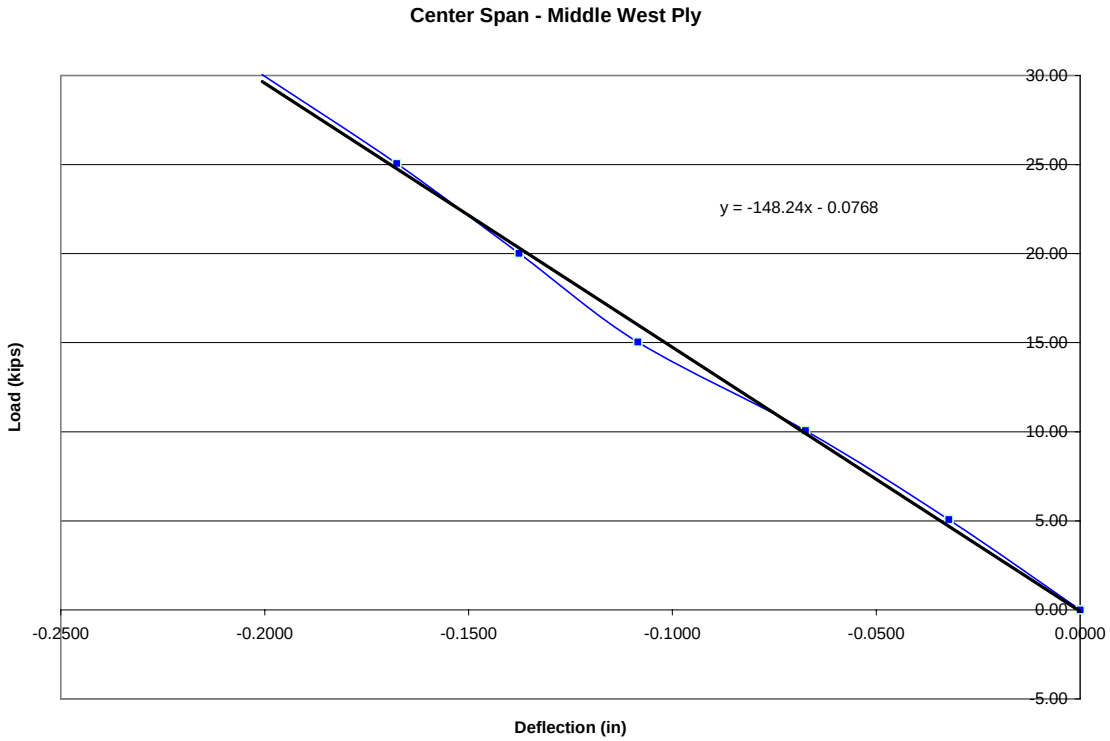

Figure C.30: C-MW 1st set of Z-spikes

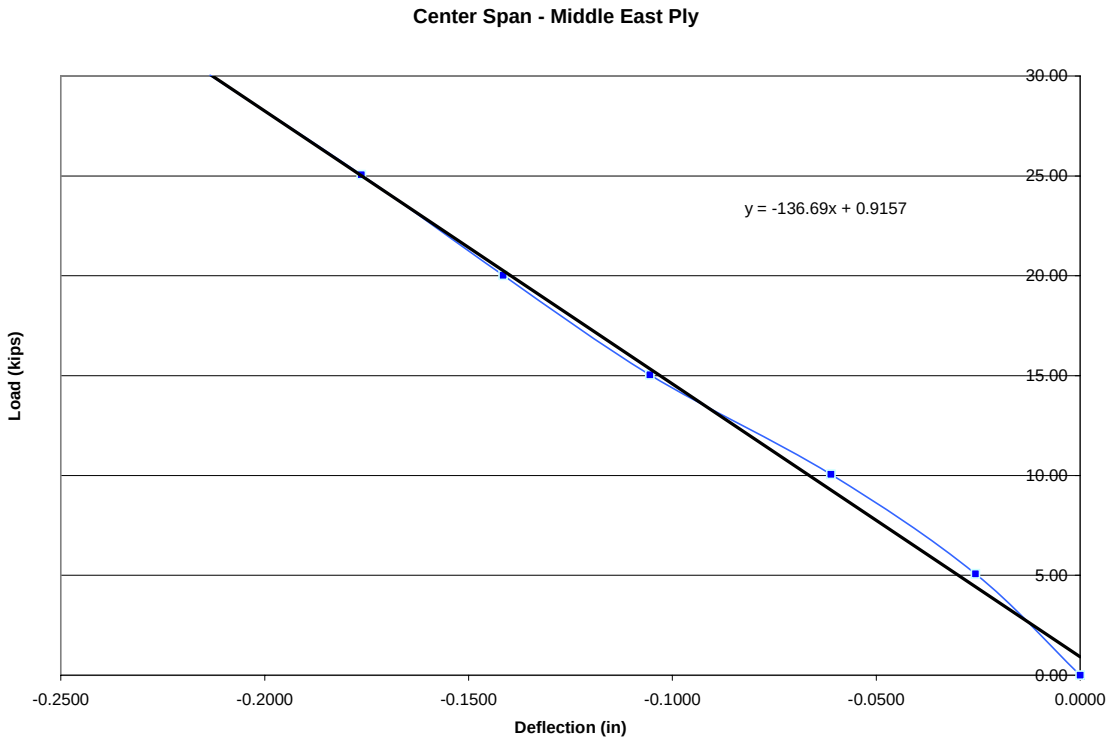

Figure C.31: C-ME 1st set of Z-spikes

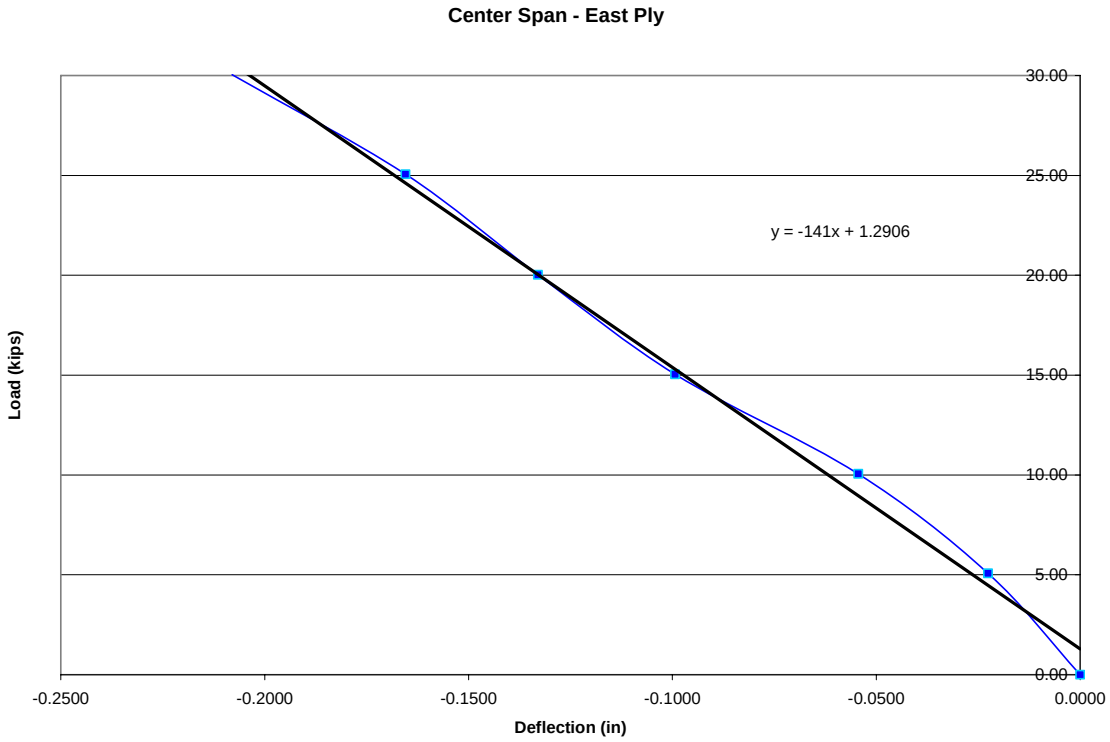

Figure C.32: C-E 1st set of Z-spikes

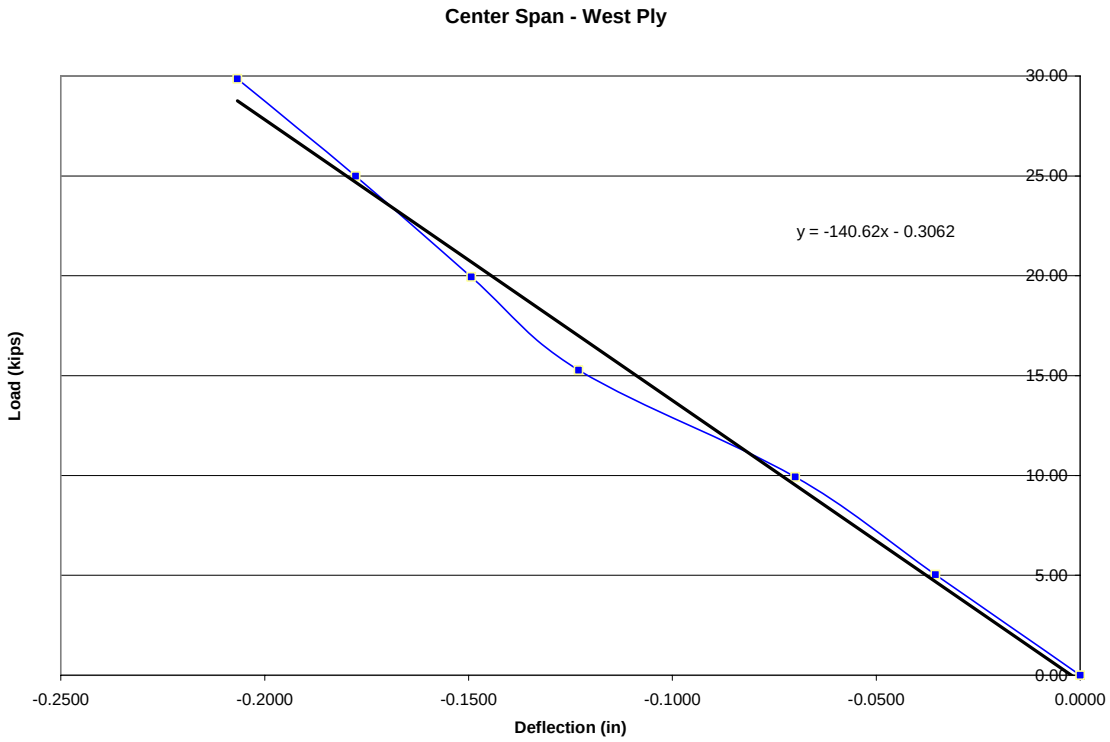

Figure C.33: C-W 2nd set of Z-spikes

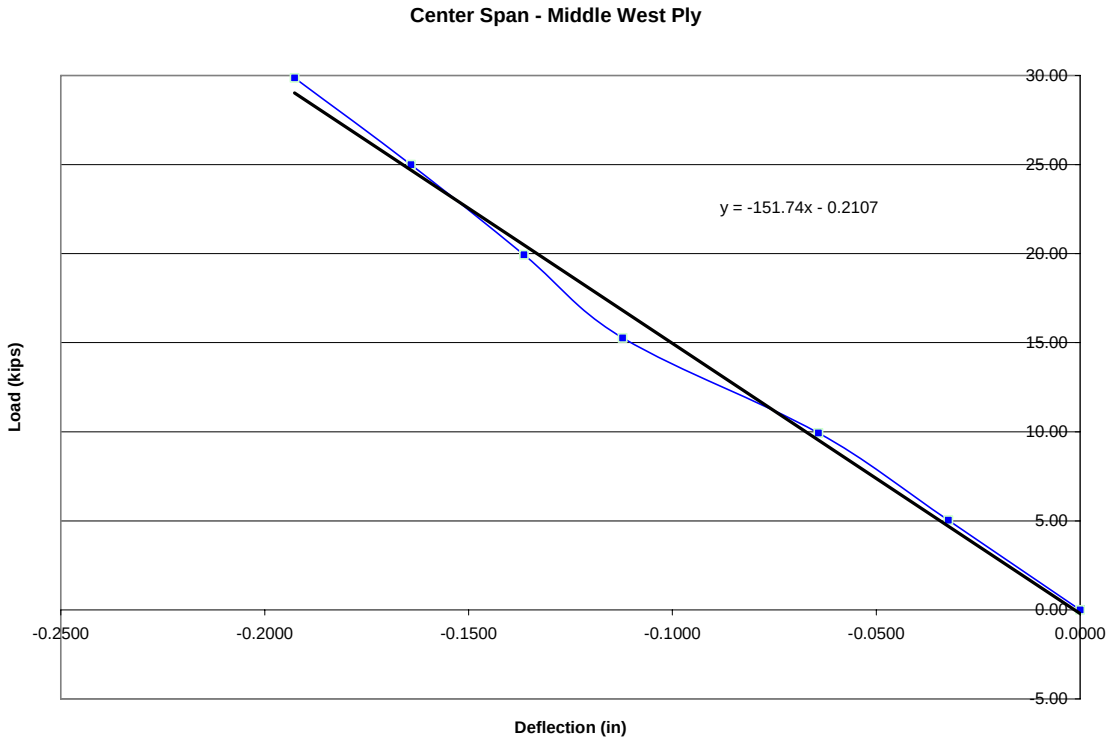

Figure C.34: C-MW 2nd set of Z-spikes

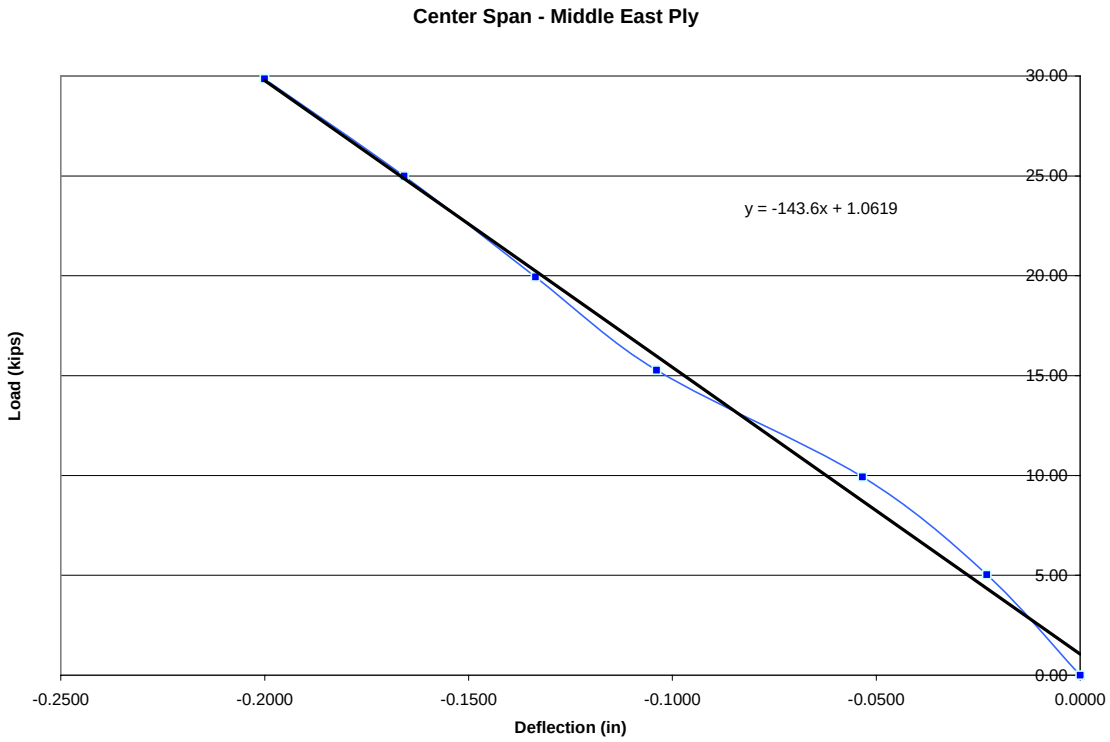

Figure C.35: C-ME 2nd set of Z-spikes

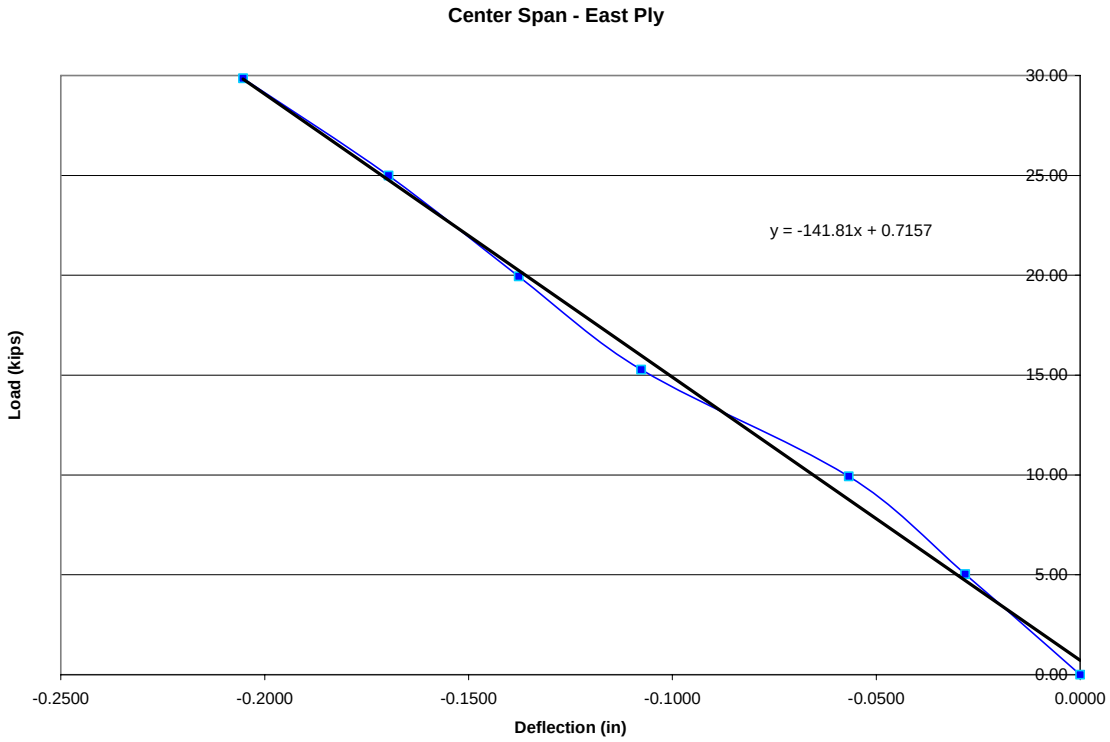

Figure C.36: C-E 2nd set of Z-spikes

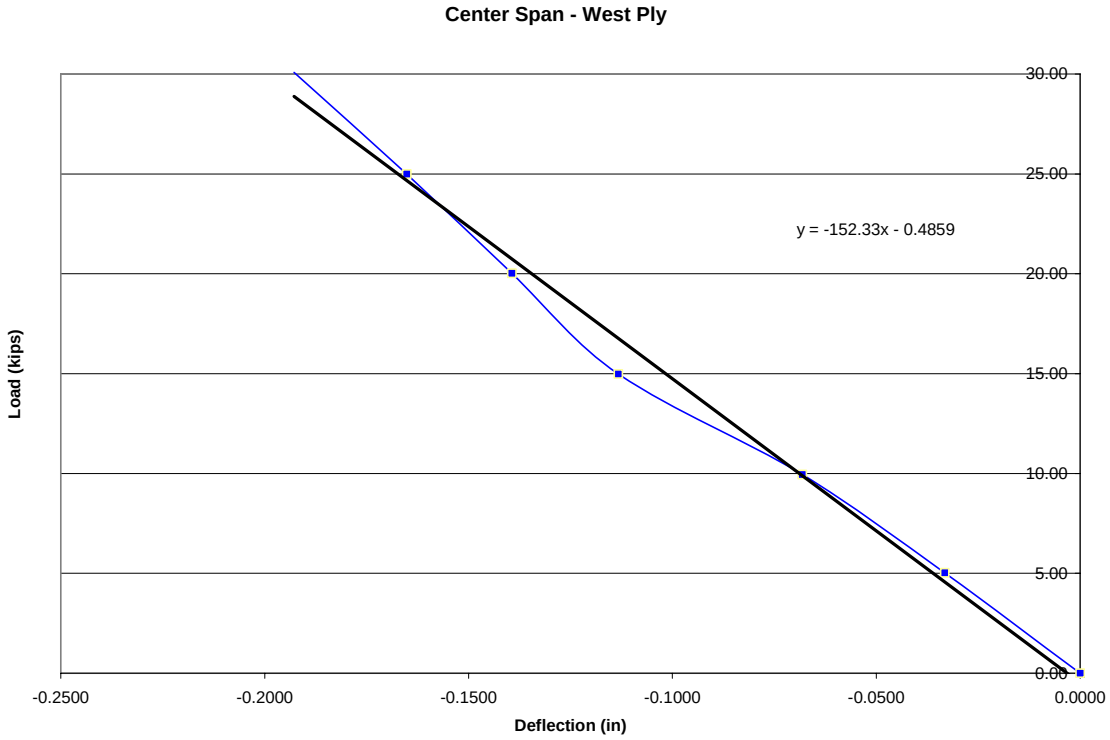

Figure C.37: C-W 3rd set of Z-spikes

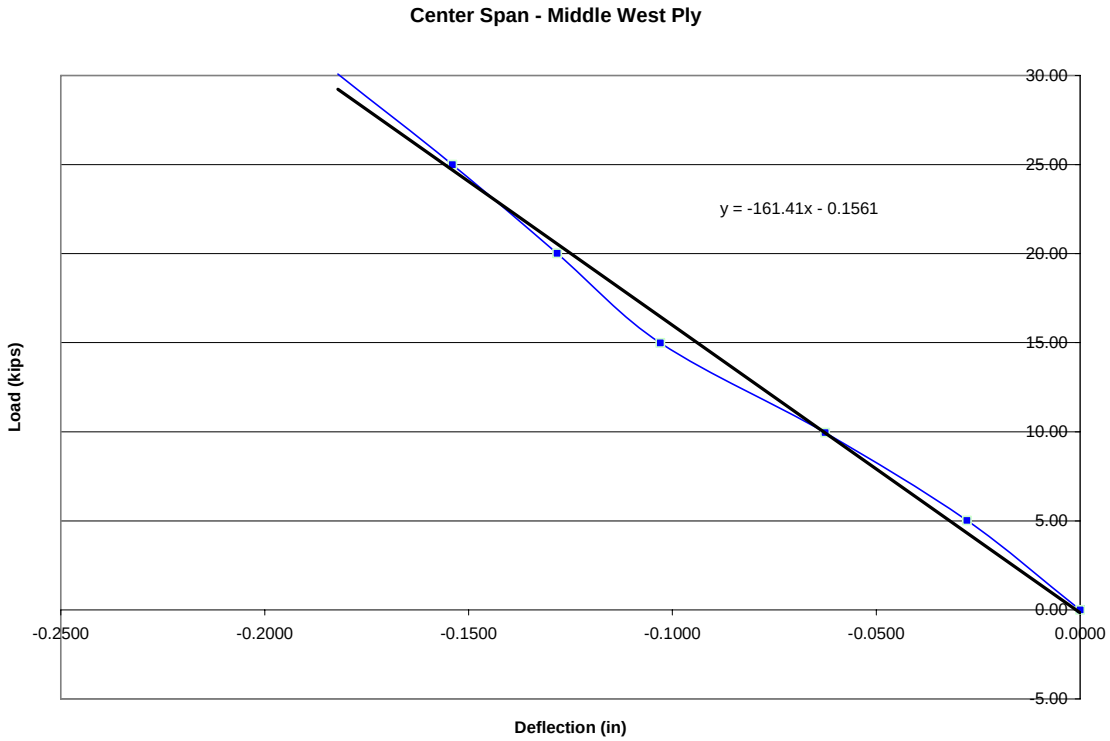

Figure C.38: C-MW 3rd set of Z-spikes

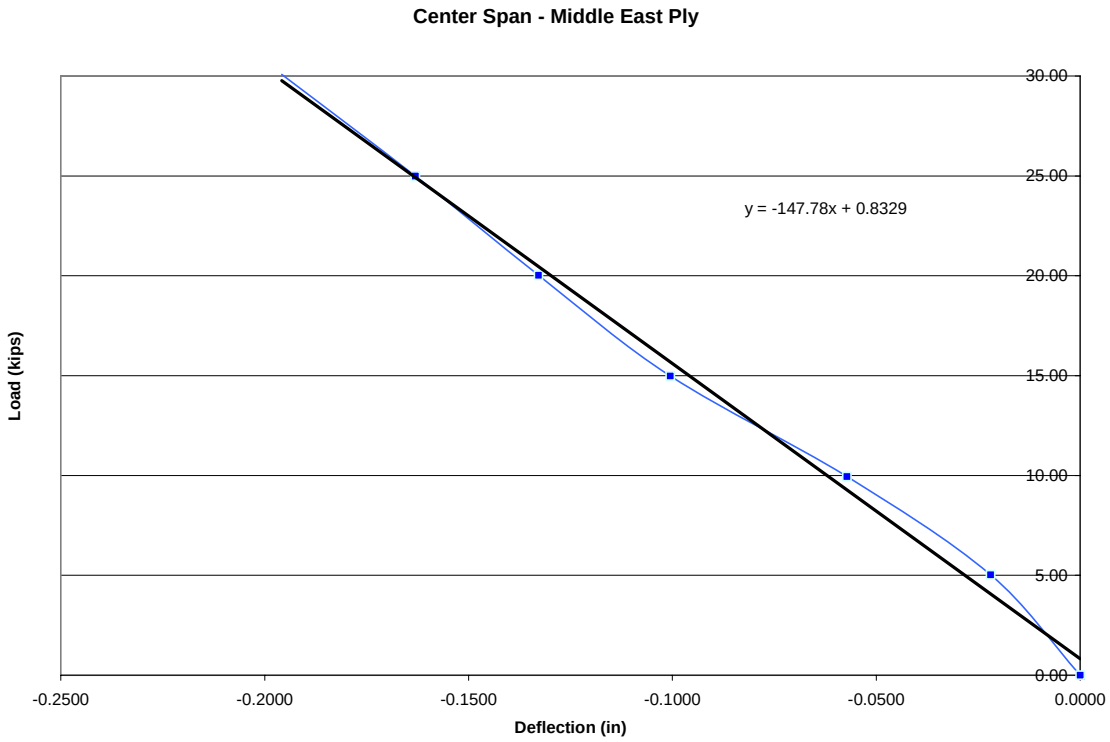

Figure C.39: C-ME 3rd set of Z-spikes

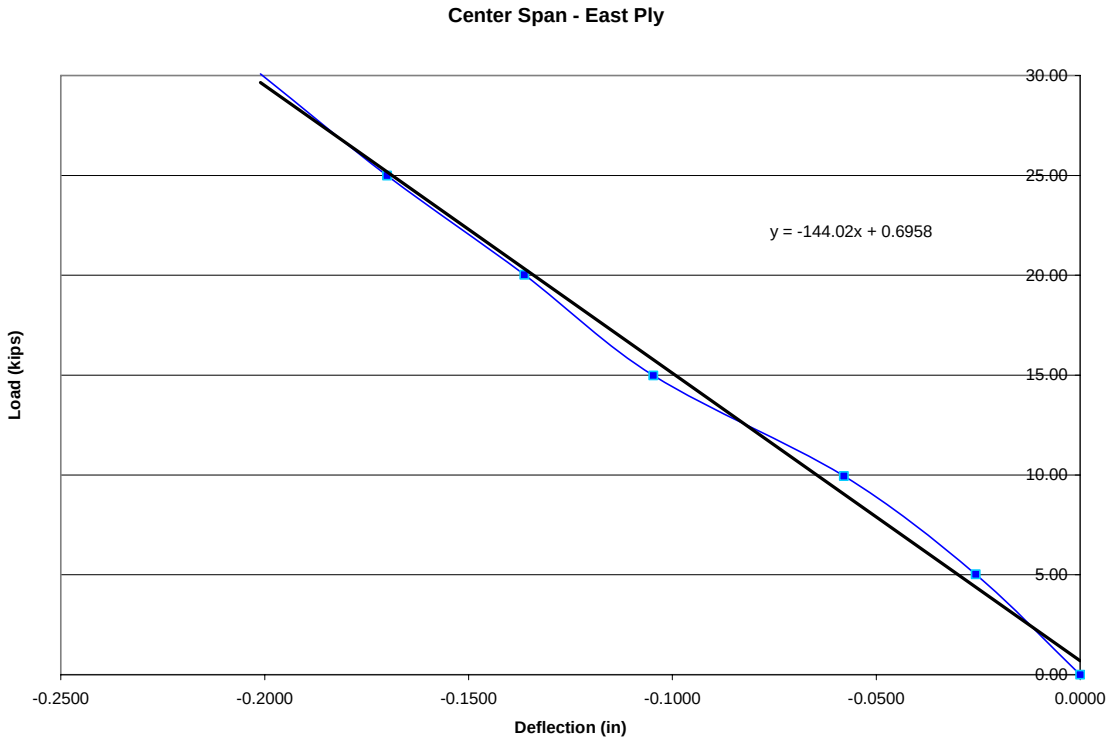

Figure C.40: C-E 3rd set of Z-spikes

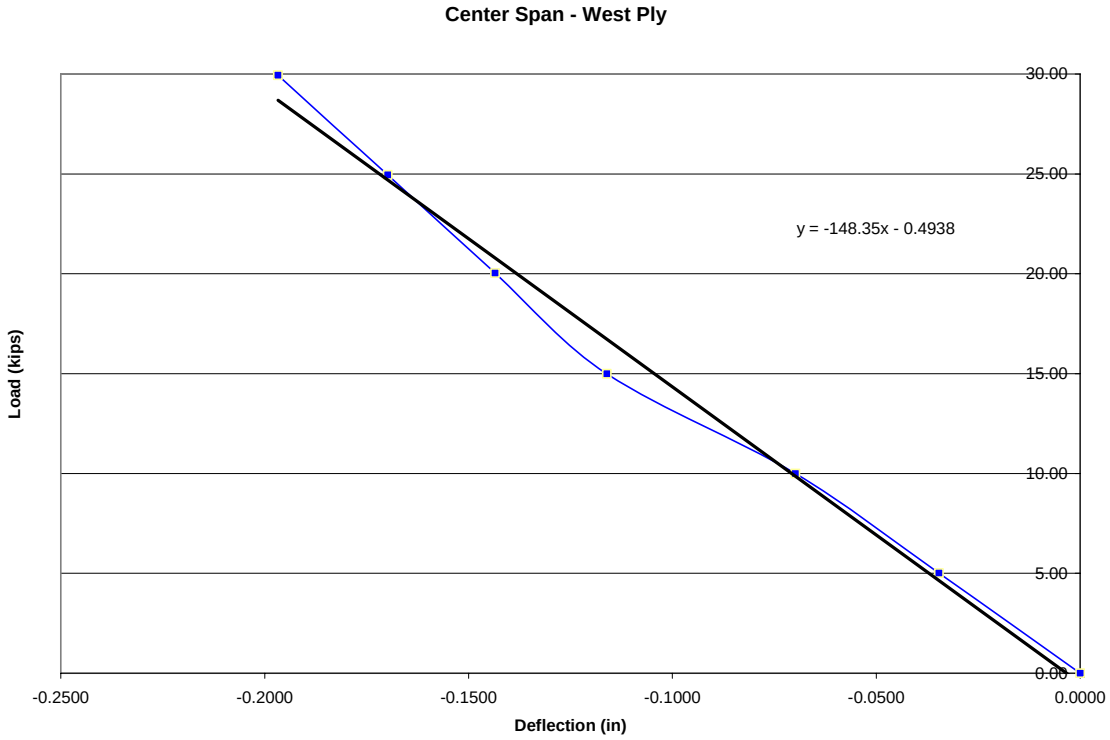

Figure C.41: C-W repaired center beams (south2)

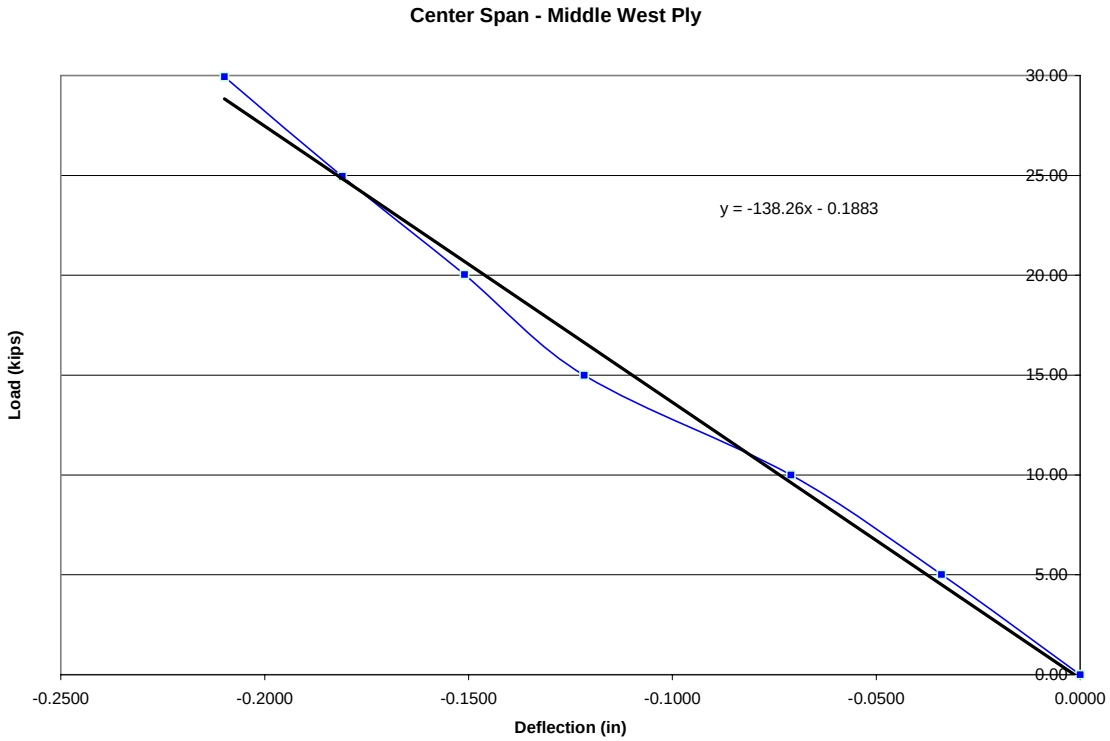

Figure C.42: C-MW repaired center beams (south2)

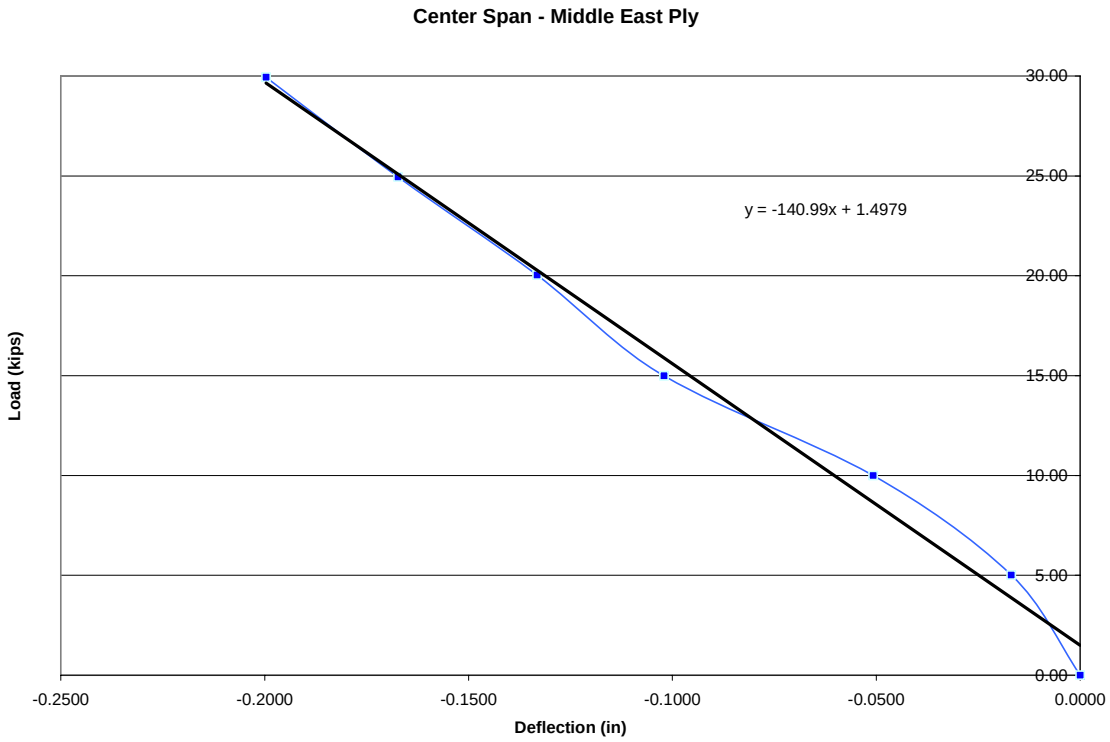

Figure C.43: C-ME repaired center beams (south2)

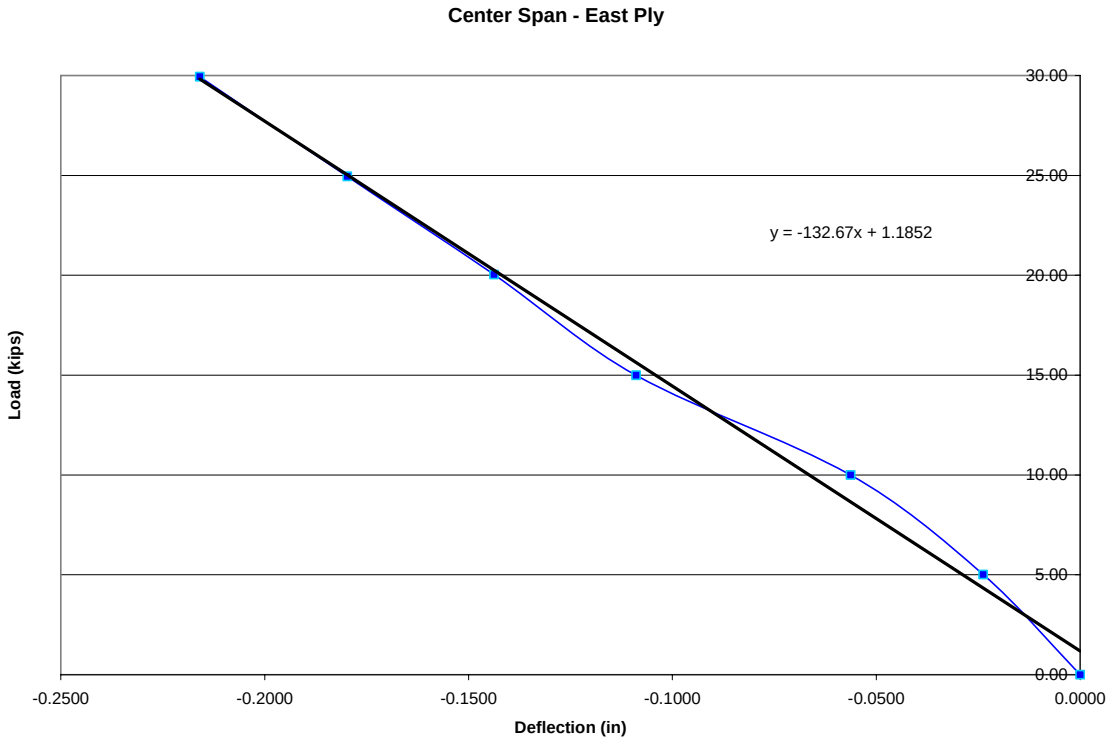

Figure C.44: C-E repaired center beams (south2)

Appendix D: North Damage Load-Deflection

(1 kip = 4.448 kN) (1 kN = 0.2248 kips)
(1 inch = 24.4 mm) (1 mm = 0.03937 inches)

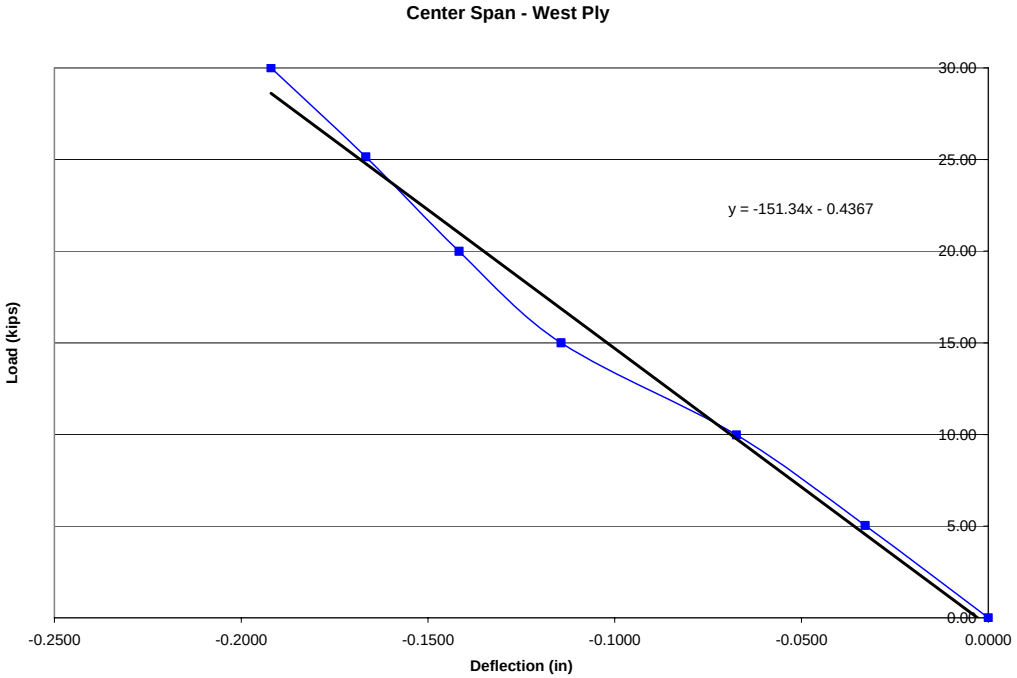

Figure D.1: C-W no damage

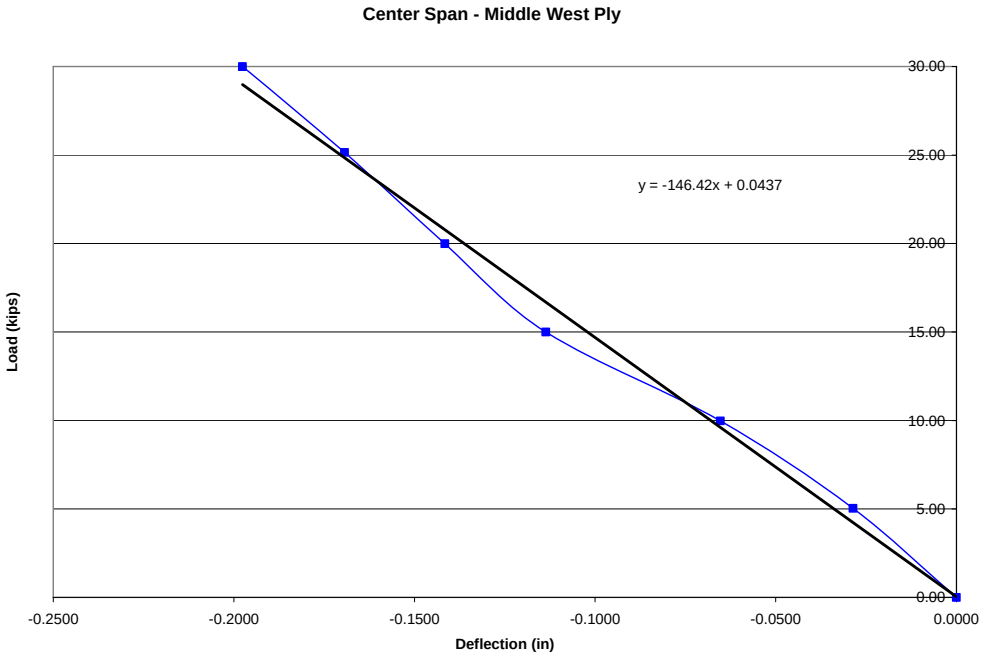

Figure D.2: C-MW no damage

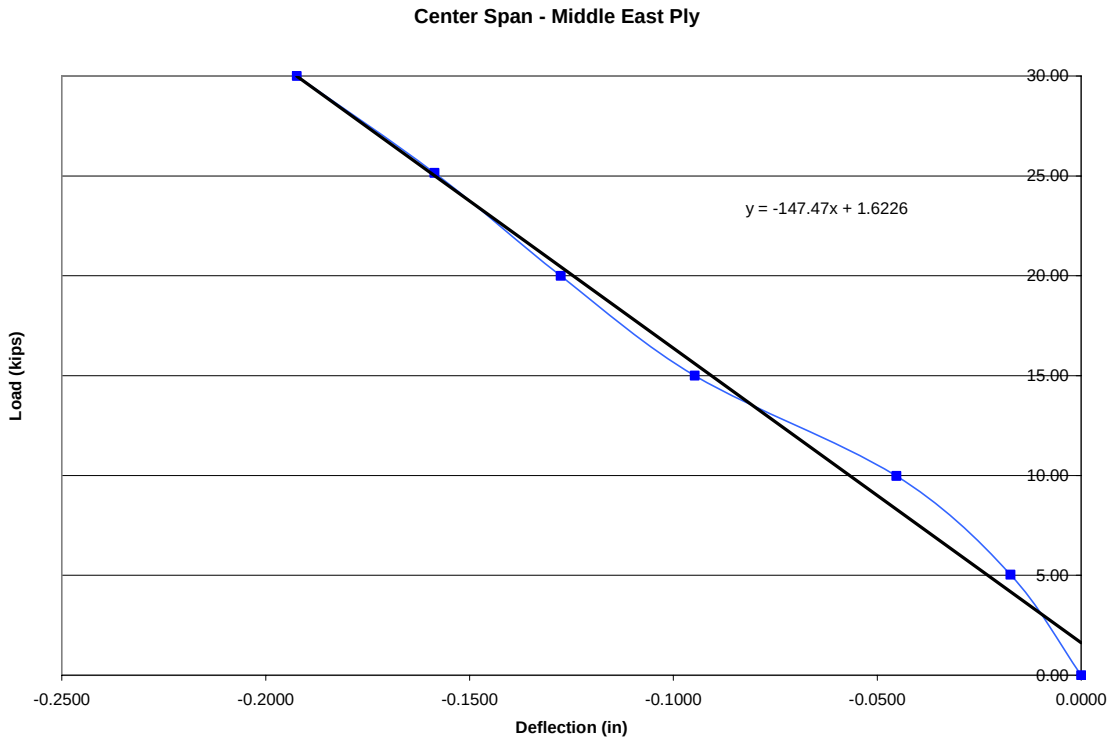

Figure D.3: C-ME no damage

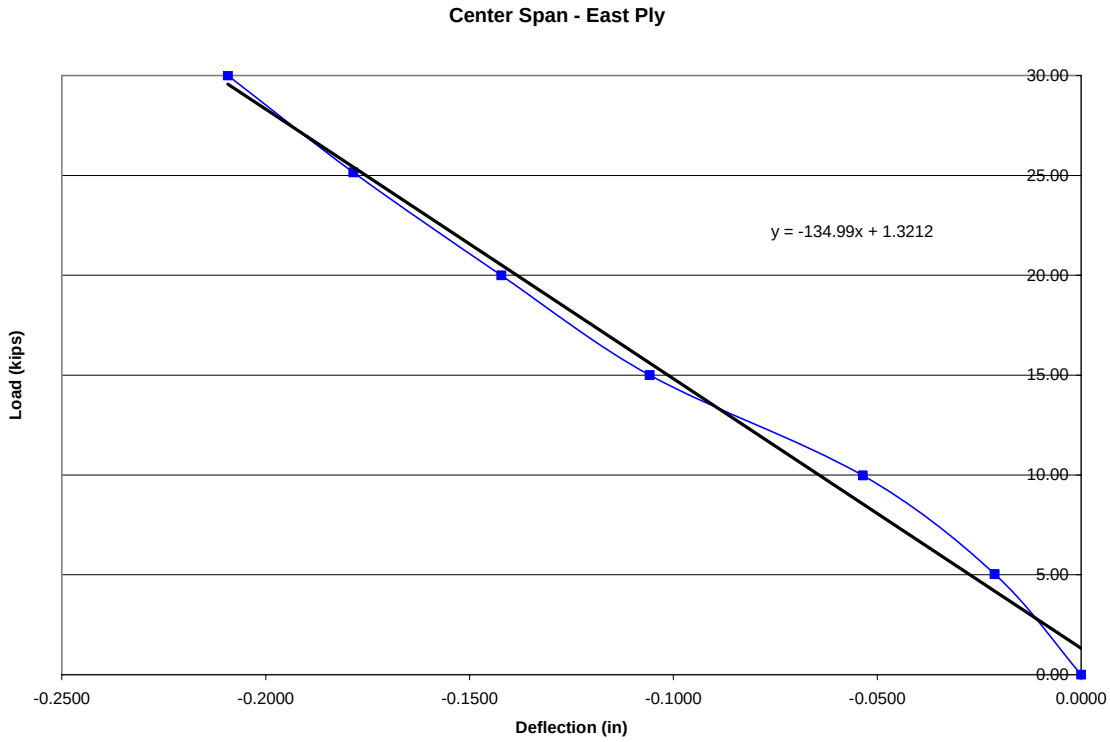

Figure D.4: C-E no damage

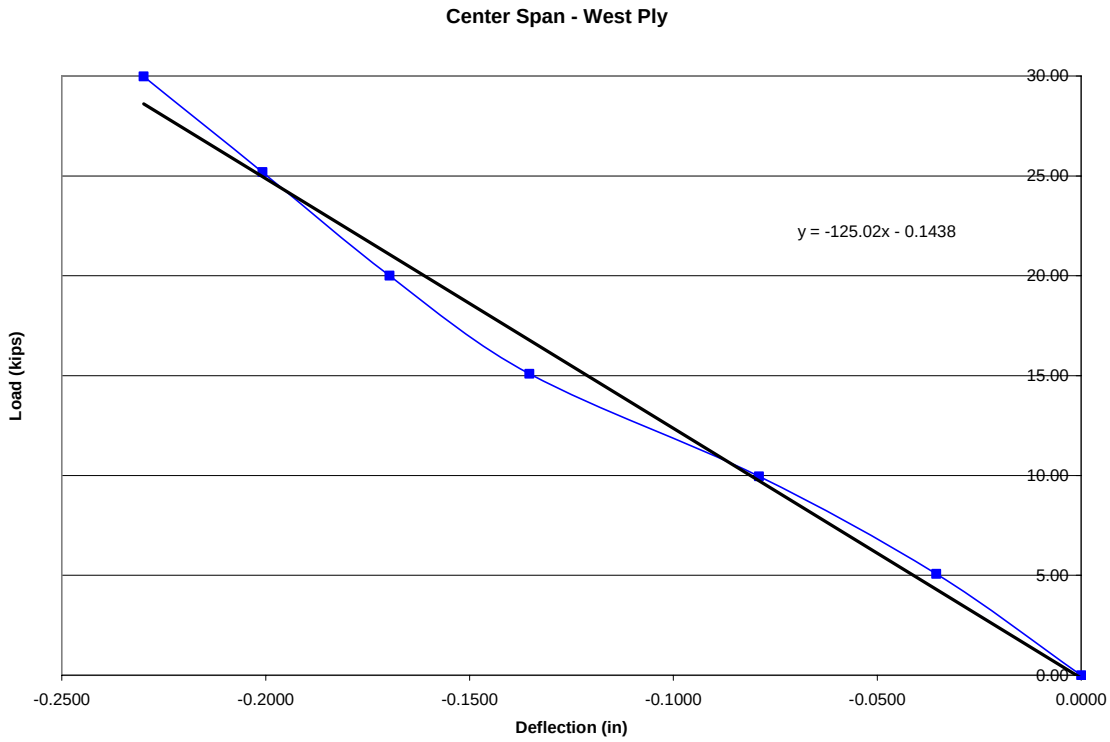

Figure D.5: C-W full damage

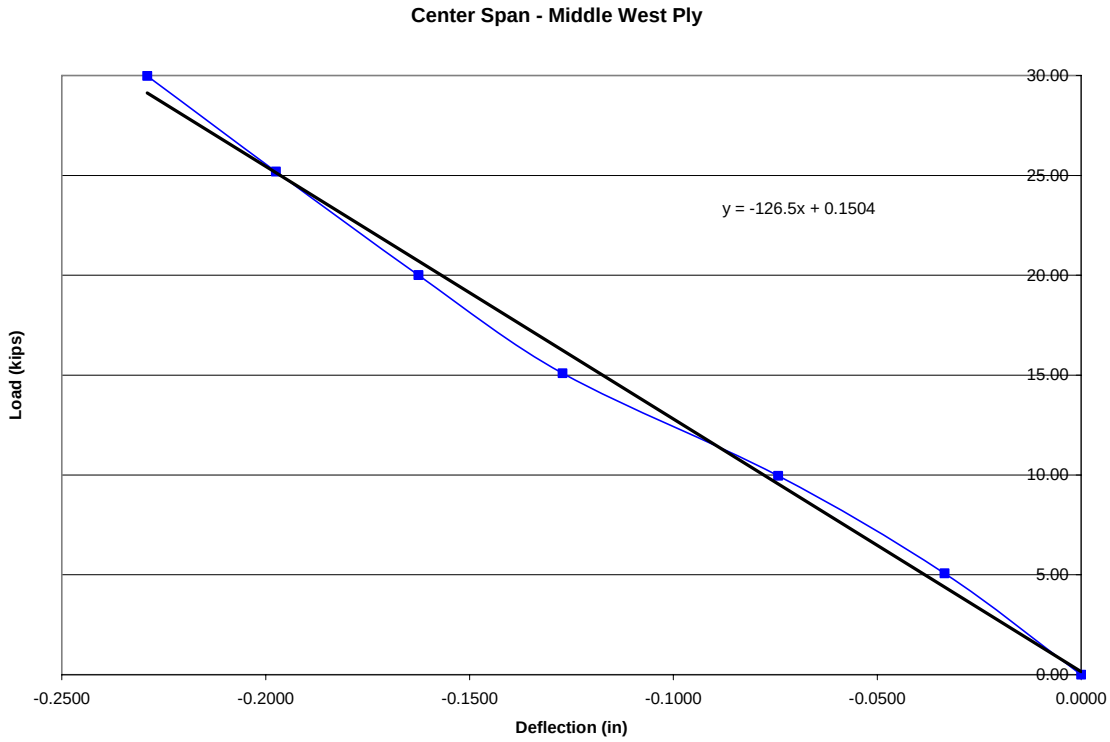

Figure D.6: C-MW full damage

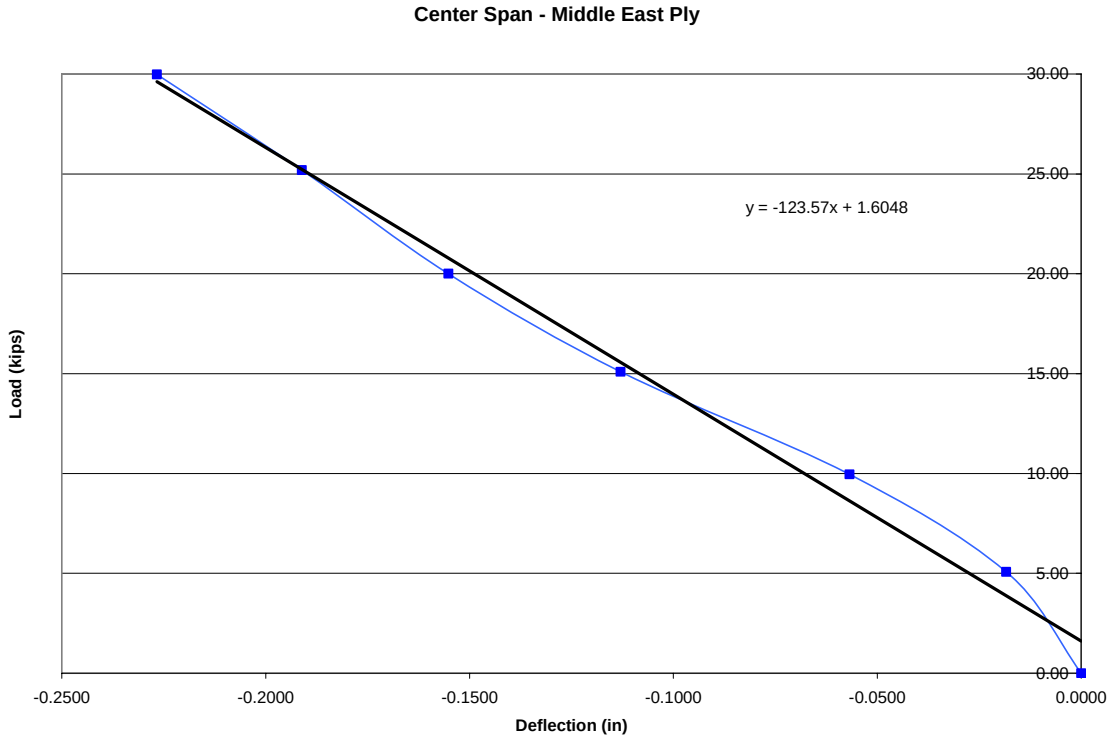

Figure D.7: C-ME full damage

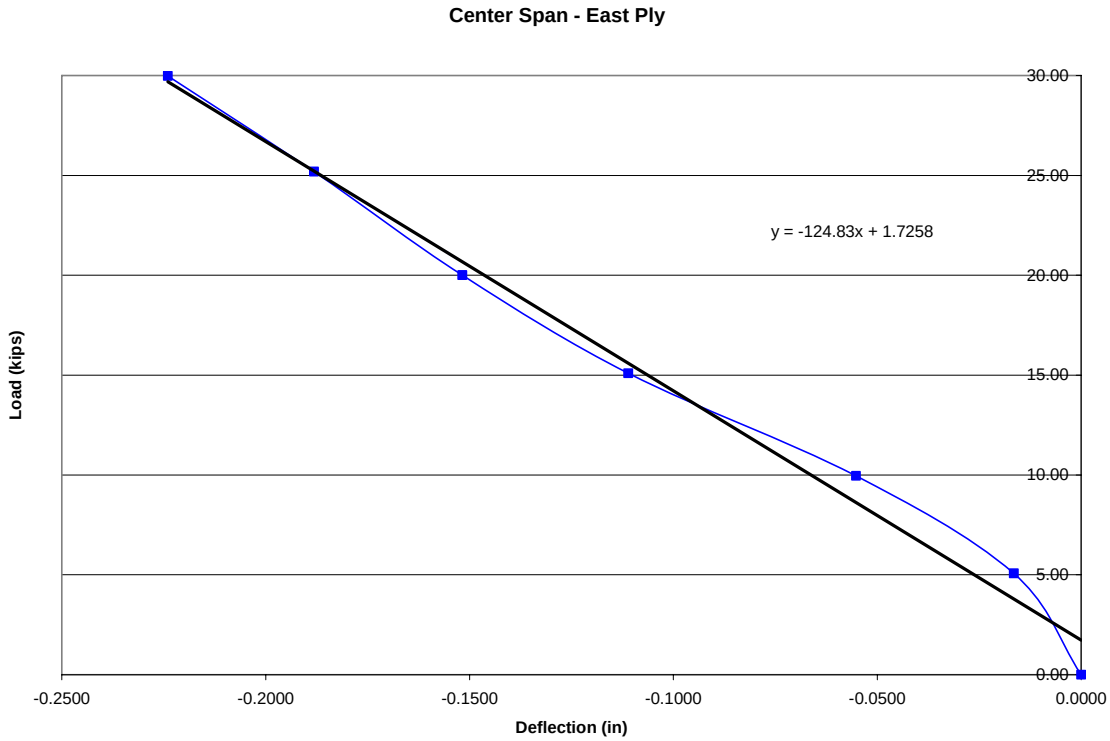

Figure D.8: C-E full damage

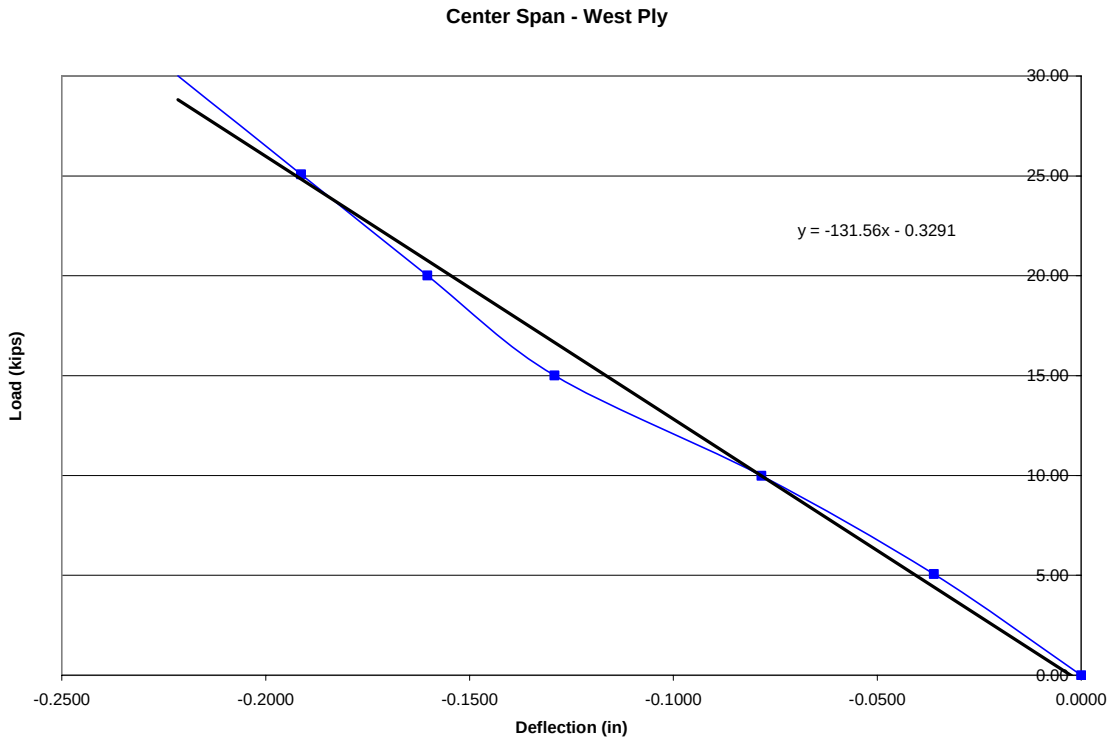

Figure D.9: C-W one set of Z-spikes

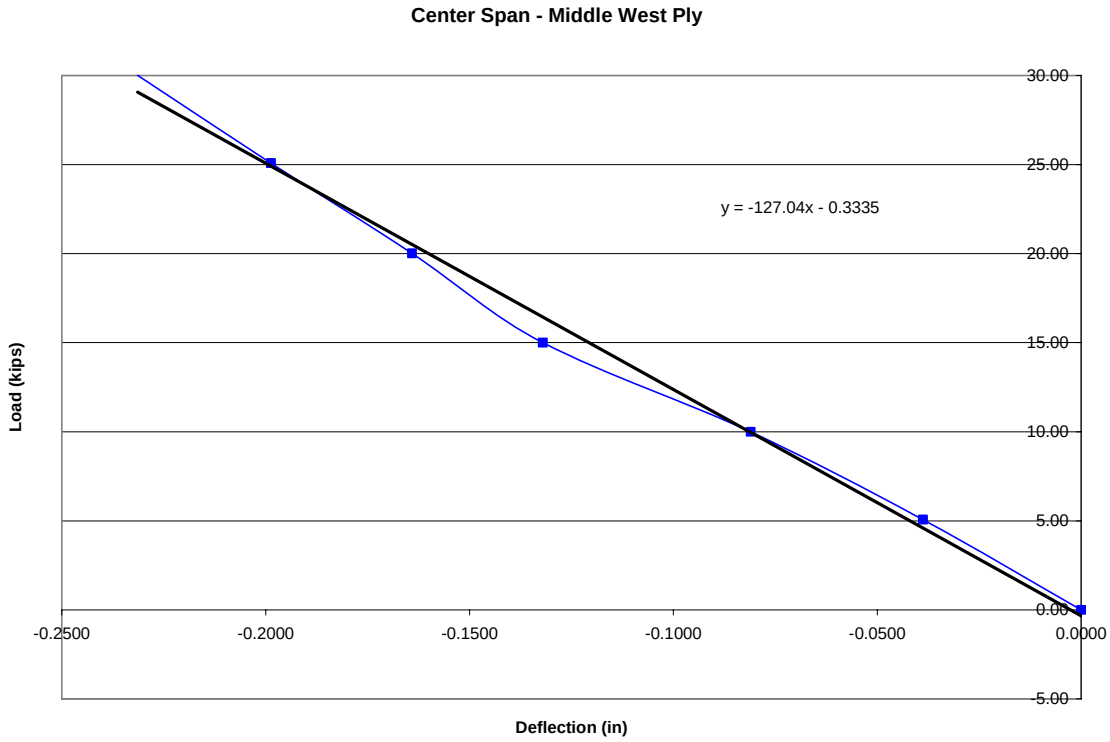

Figure D.10: C-MW one set of Z-spikes

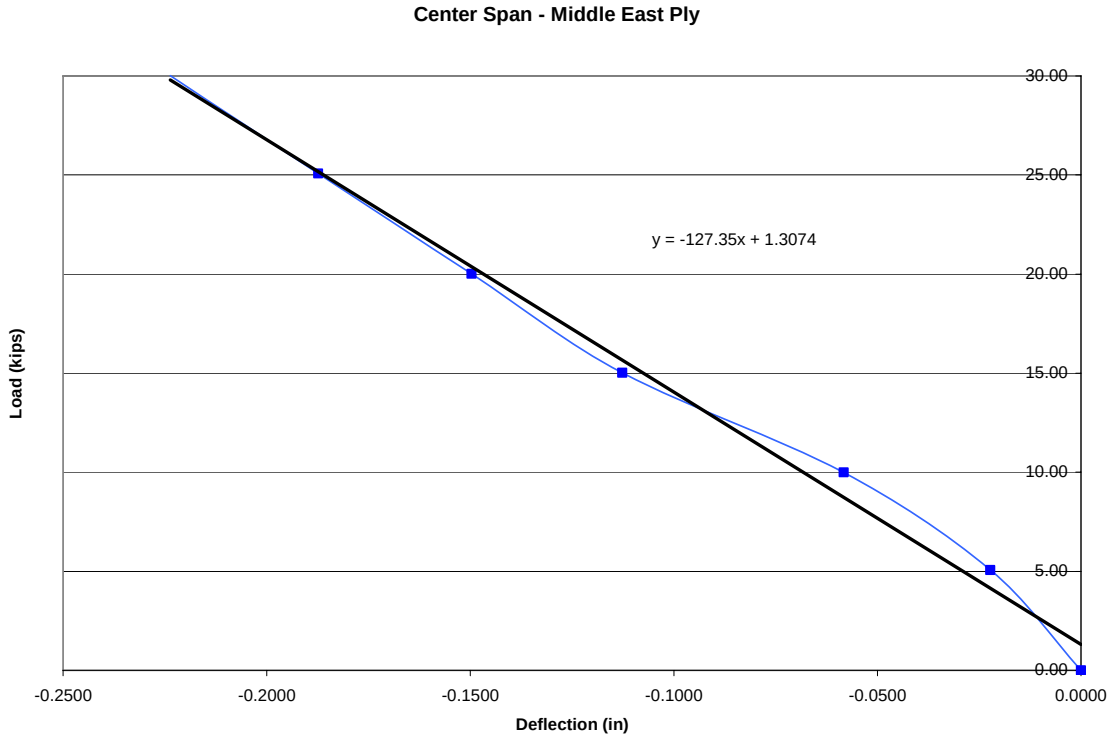

Figure D.11: C-ME one set of Z-spikes

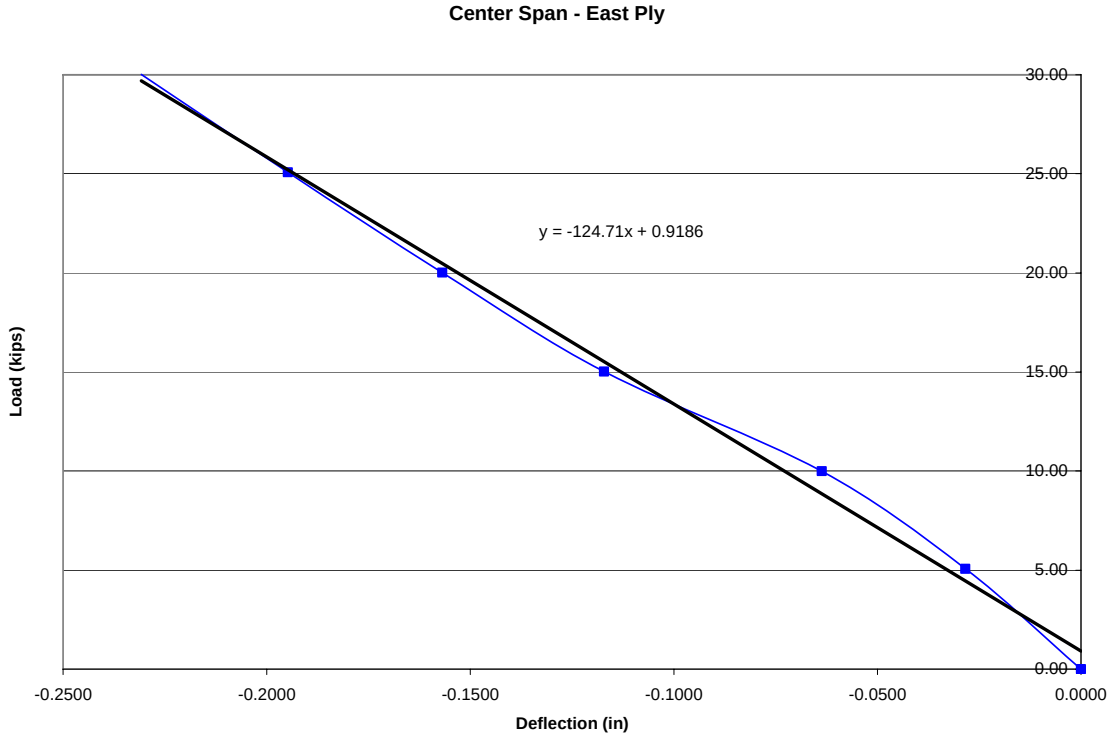

Figure D.12: C-E one set of Z-spikes

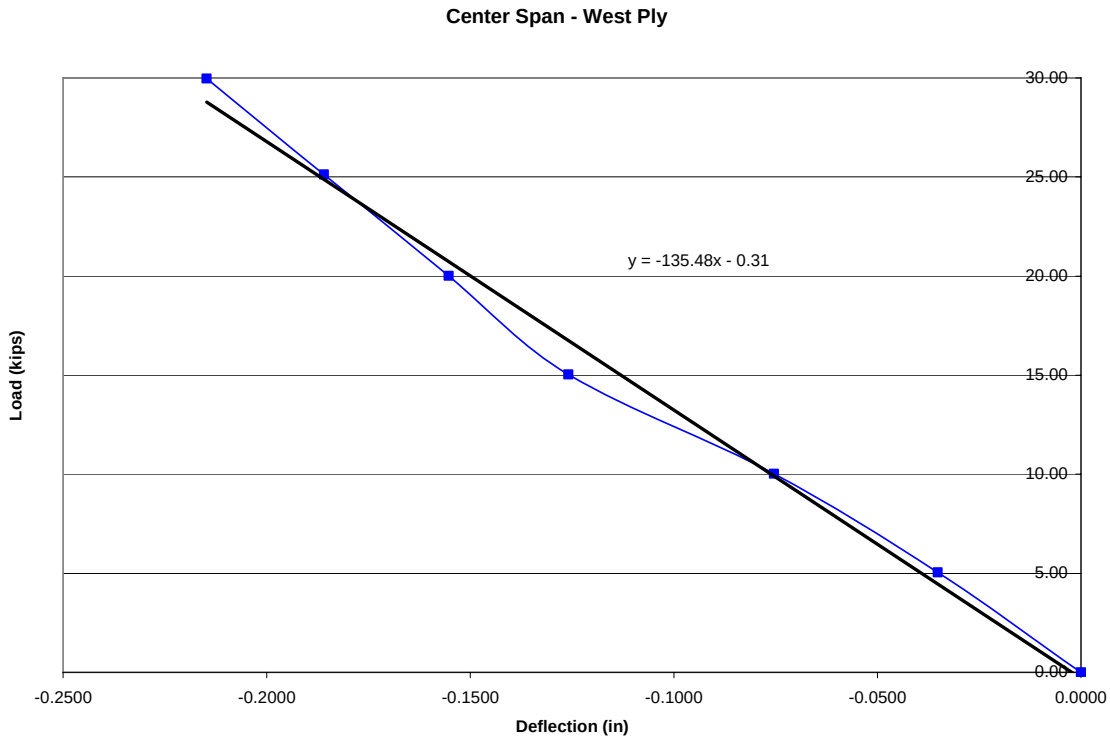

Figure D.13: C-W two sets of Z-spikes

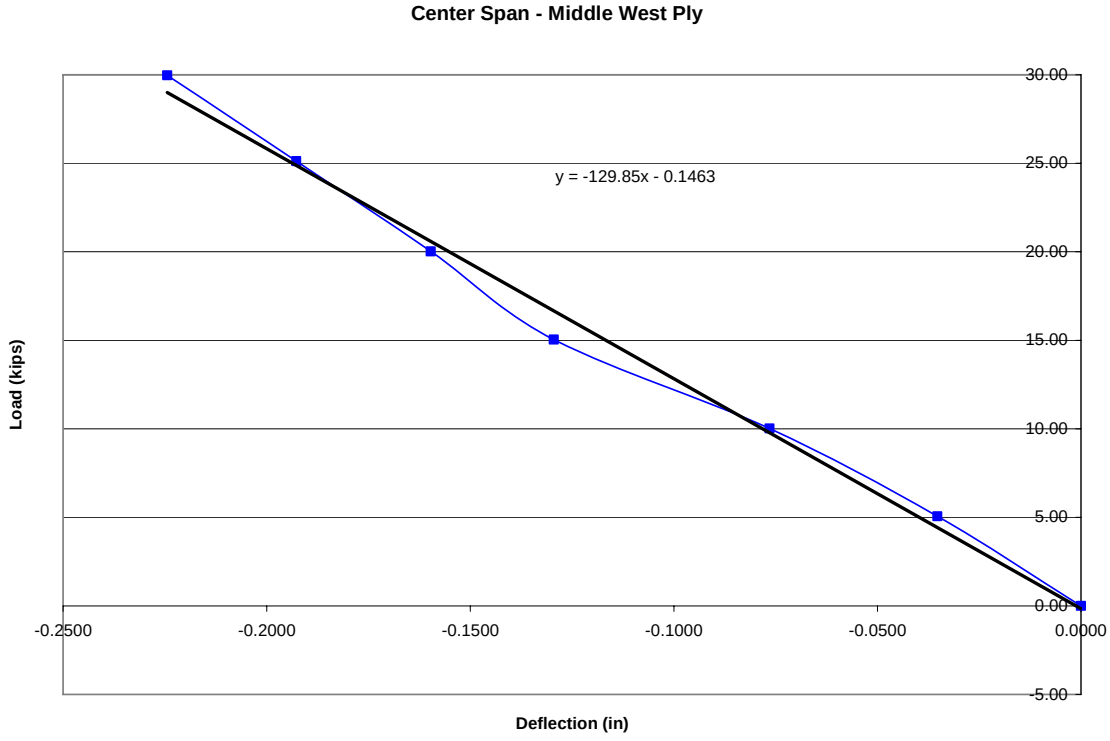

Figure D.14: C-MW two sets of Z-spikes

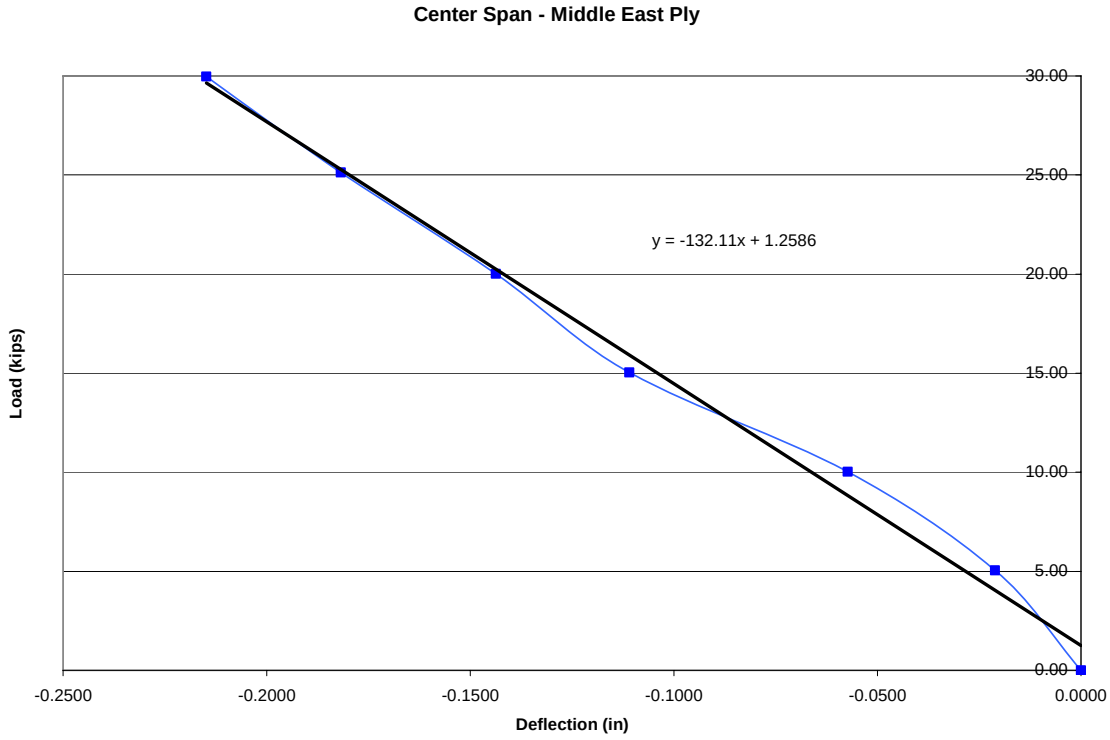

Figure D.15: C-ME two sets of Z-spikes

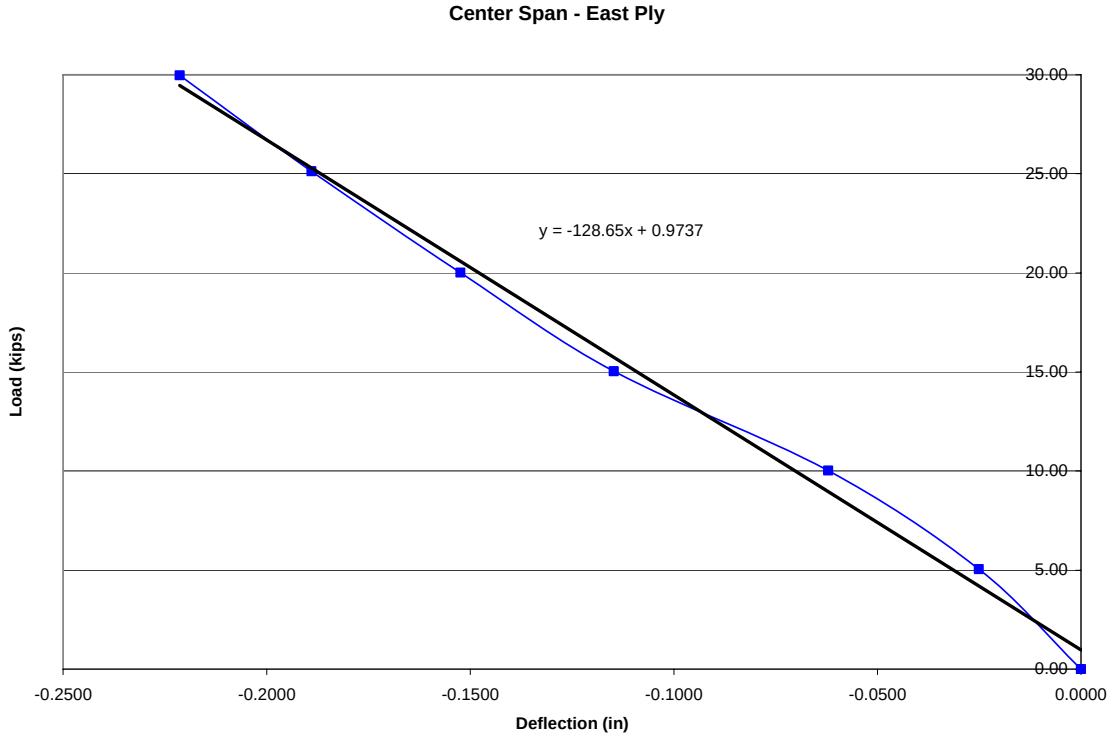

Figure D.16: C-E two sets of Z-spikes

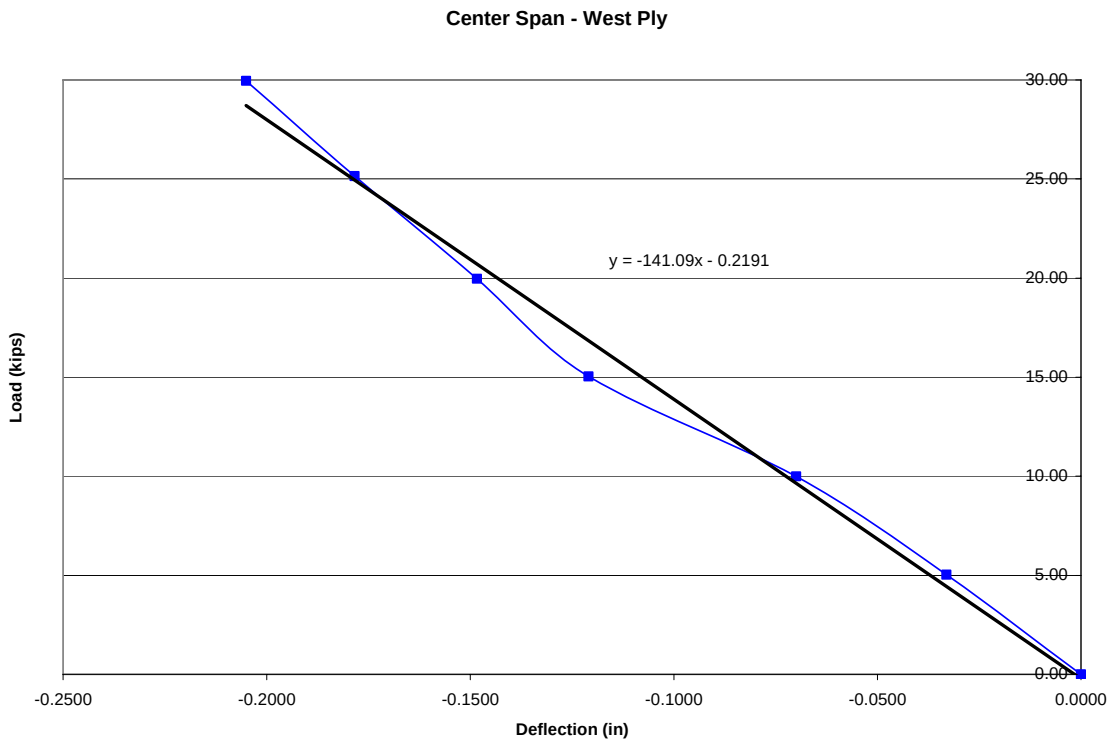

Figure D.17: C-W three sets of Z-spikes

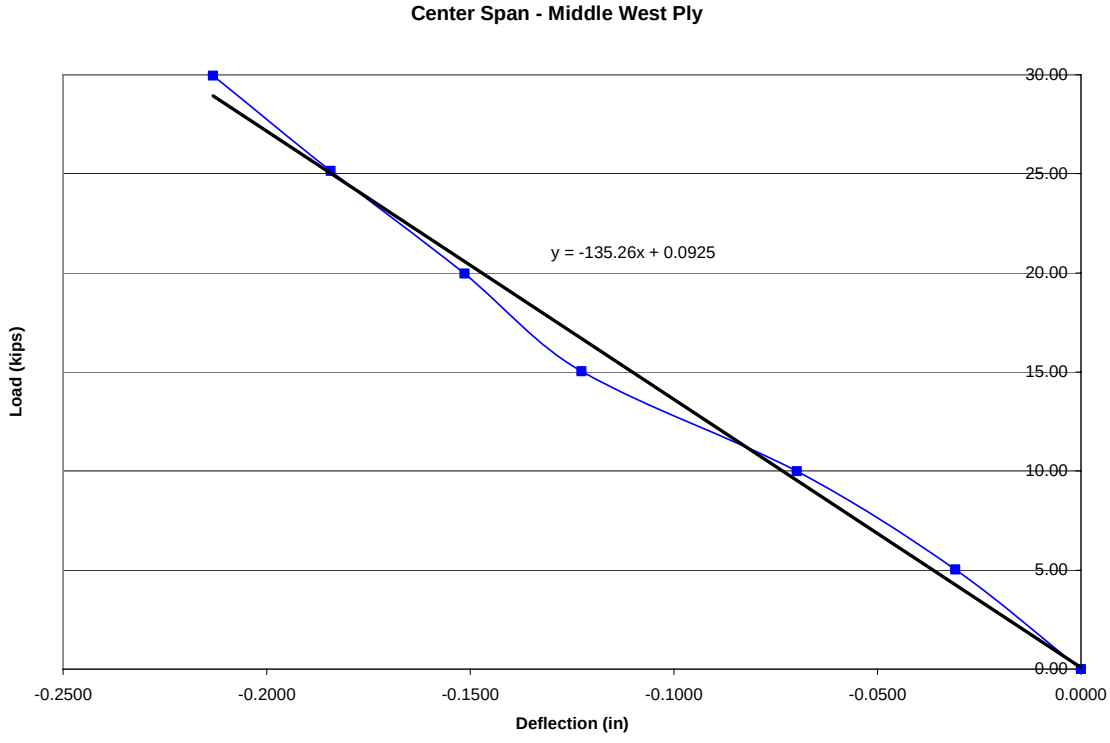

Figure D.18: C-MW three sets of Z-spikes

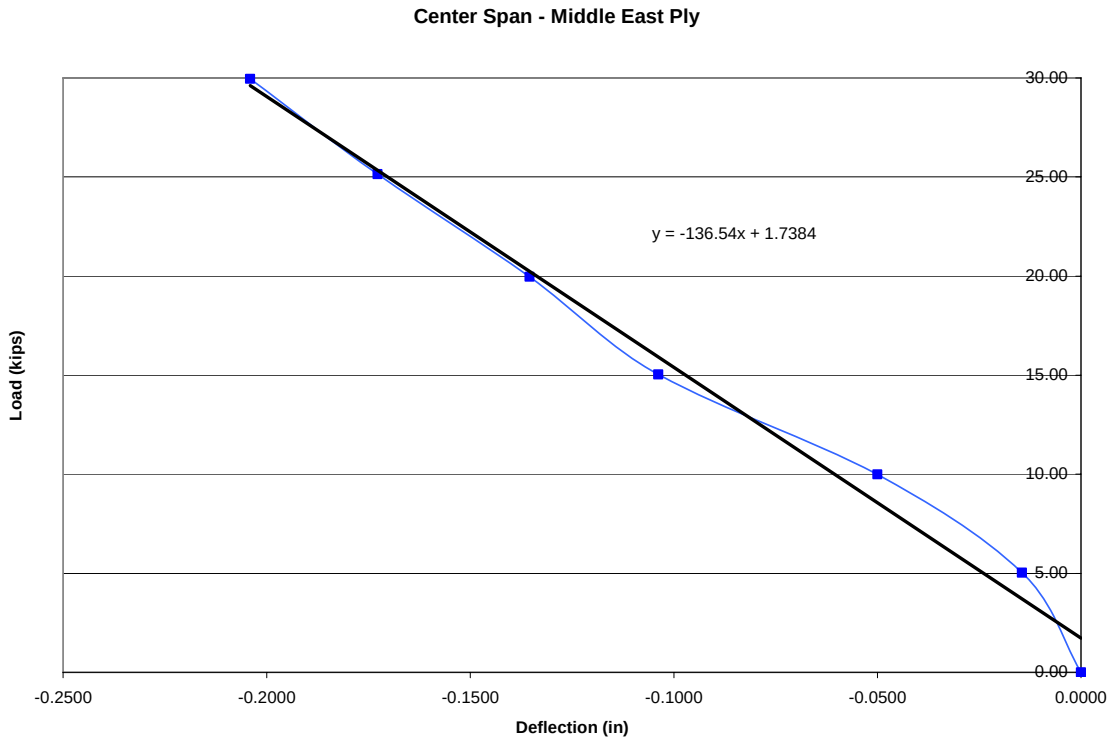

Figure D.19: C-ME three sets of Z-spikes

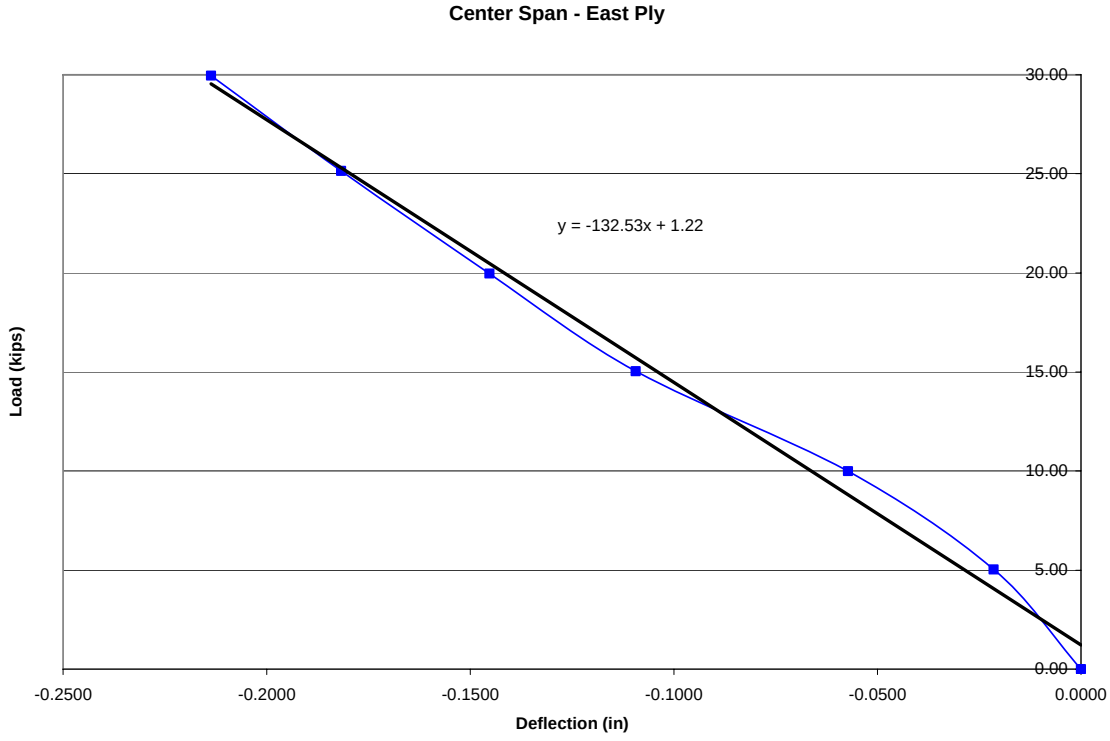

Figure D.20: C-E three sets of Z-spikes

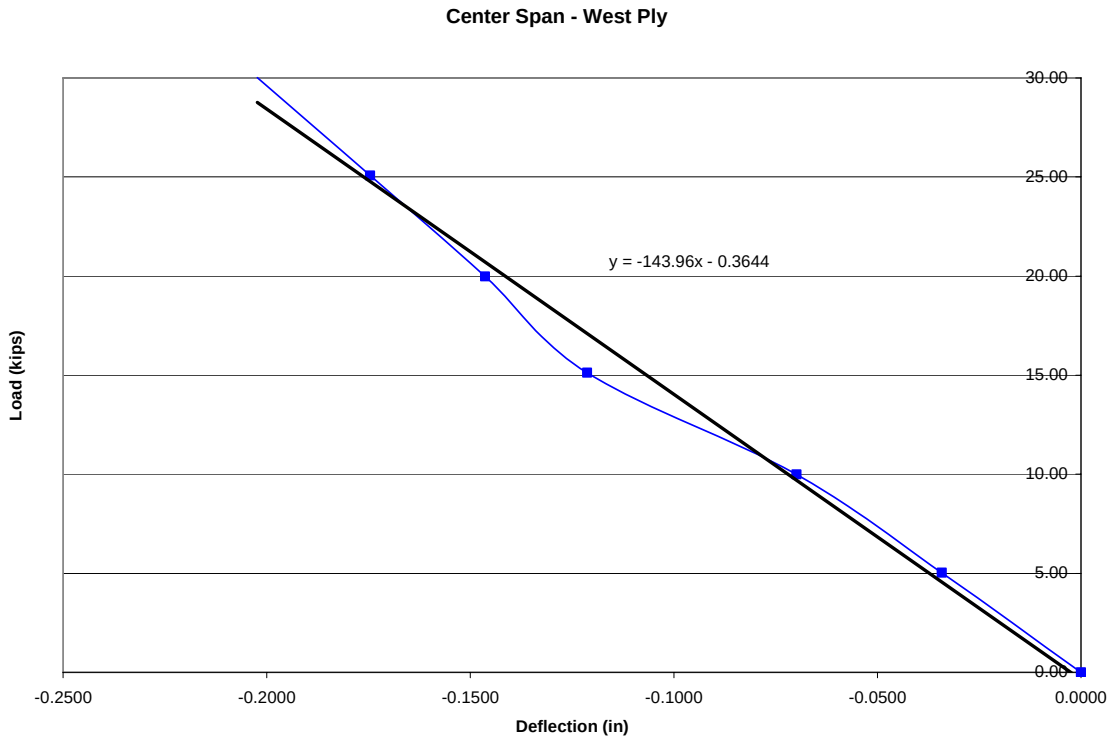

Figure D.21: C-W four sets of Z-spikes

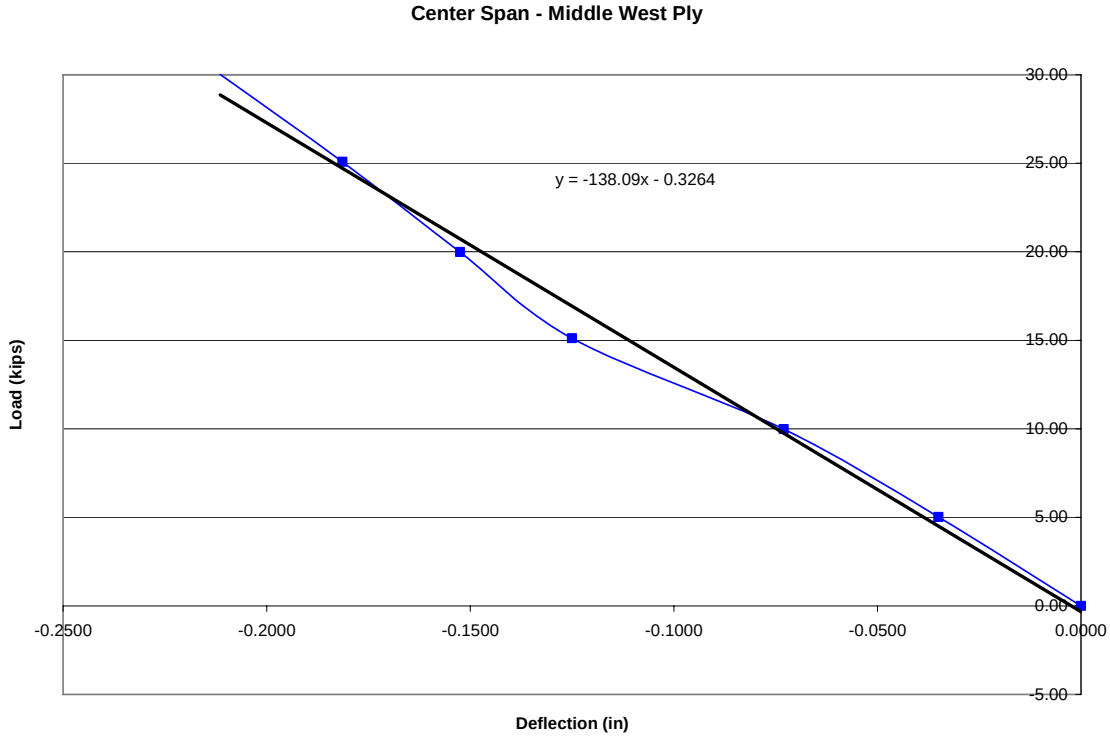

Figure D.22: C-MW four sets of Z-spikes

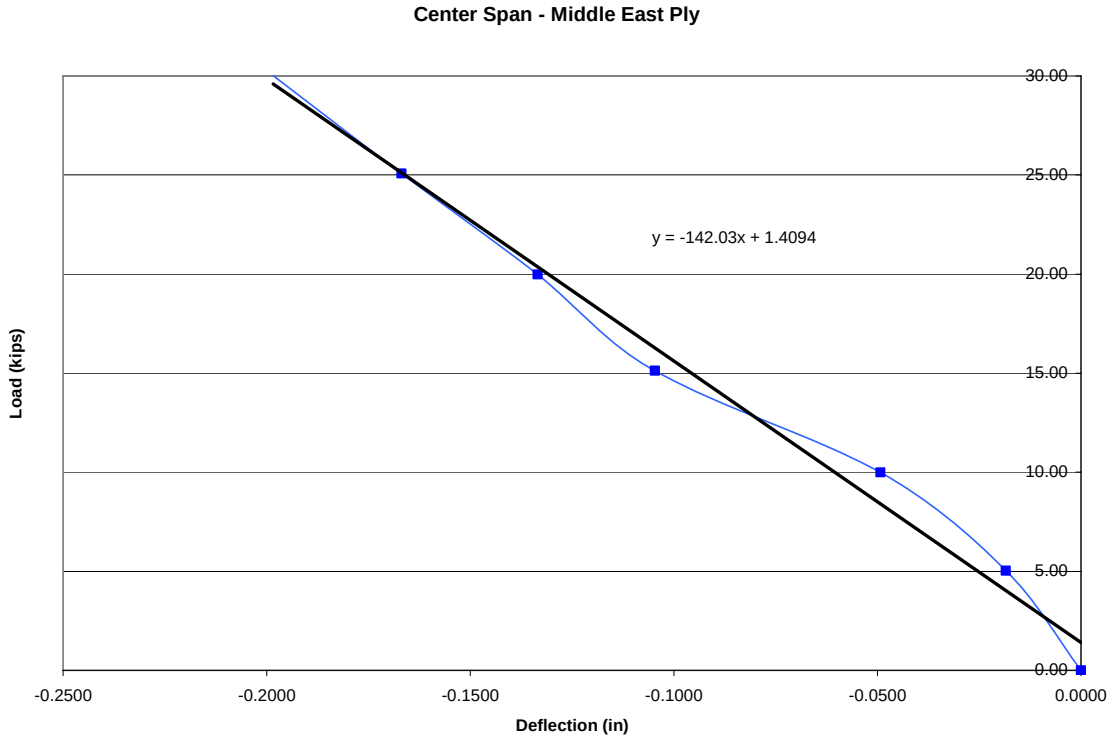

Figure D.23: C-ME four sets of Z-spikes

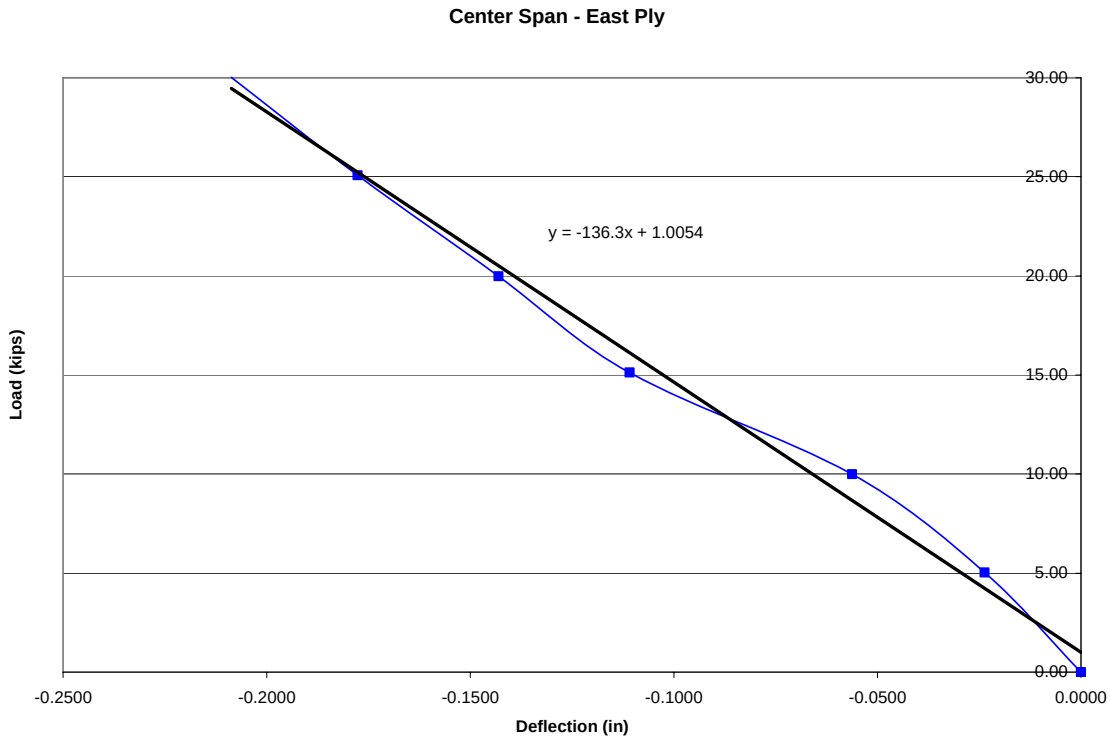

Figure D.24: C-E four sets of Z-spikes

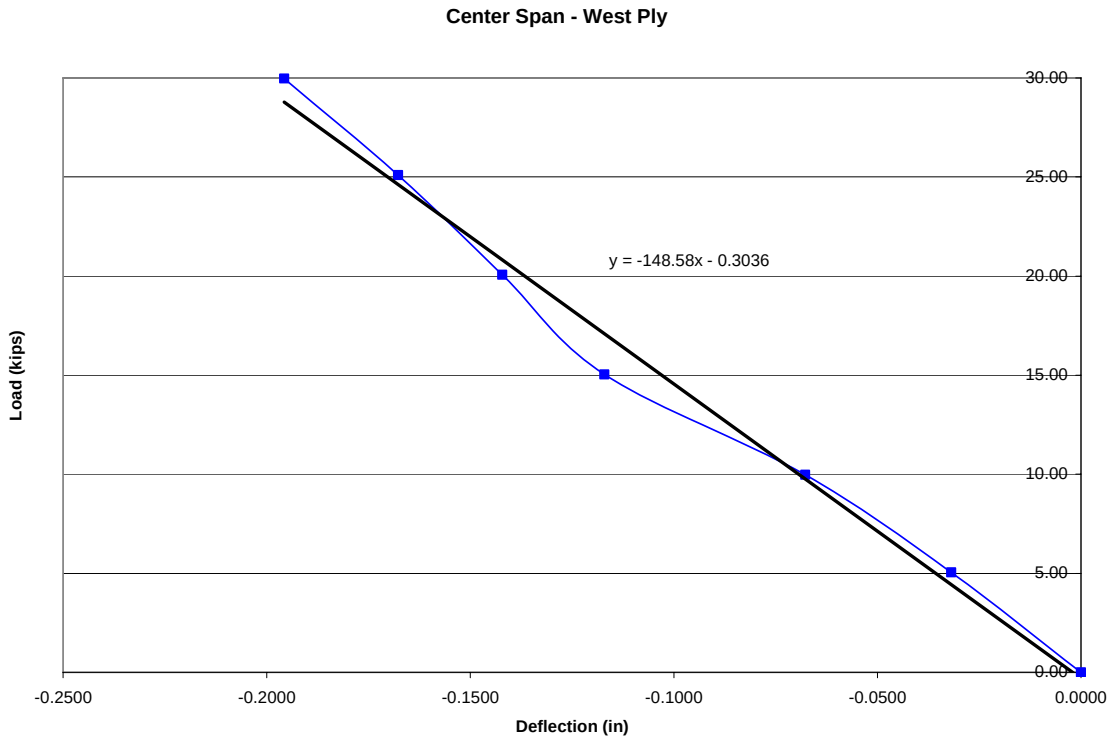

Figure D.25: C-W five sets of Z-spikes

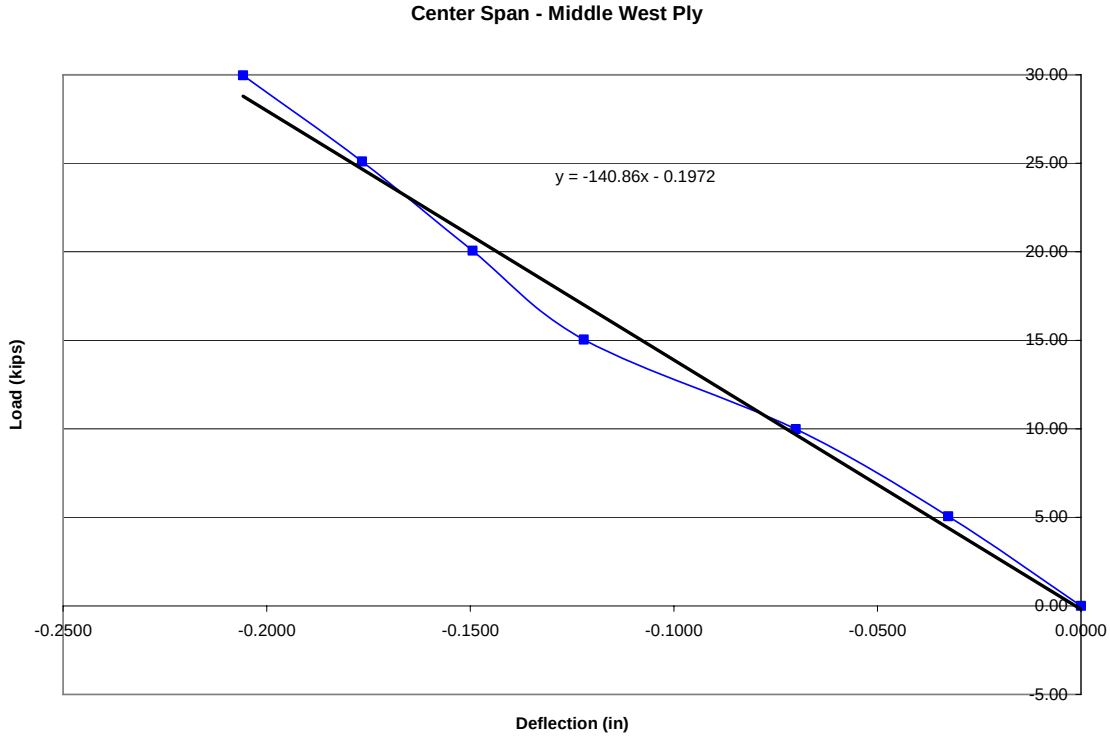

Figure D.26: C-MW five sets of Z-spikes

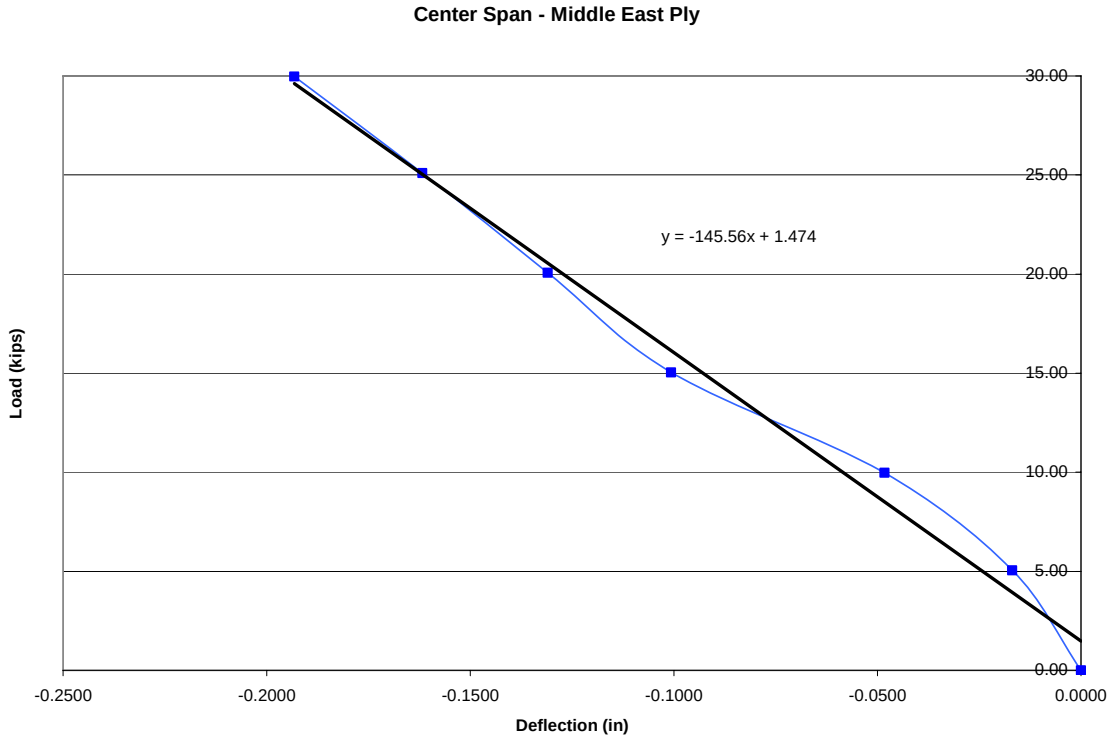

Figure D.27: C-ME five sets of Z-spikes

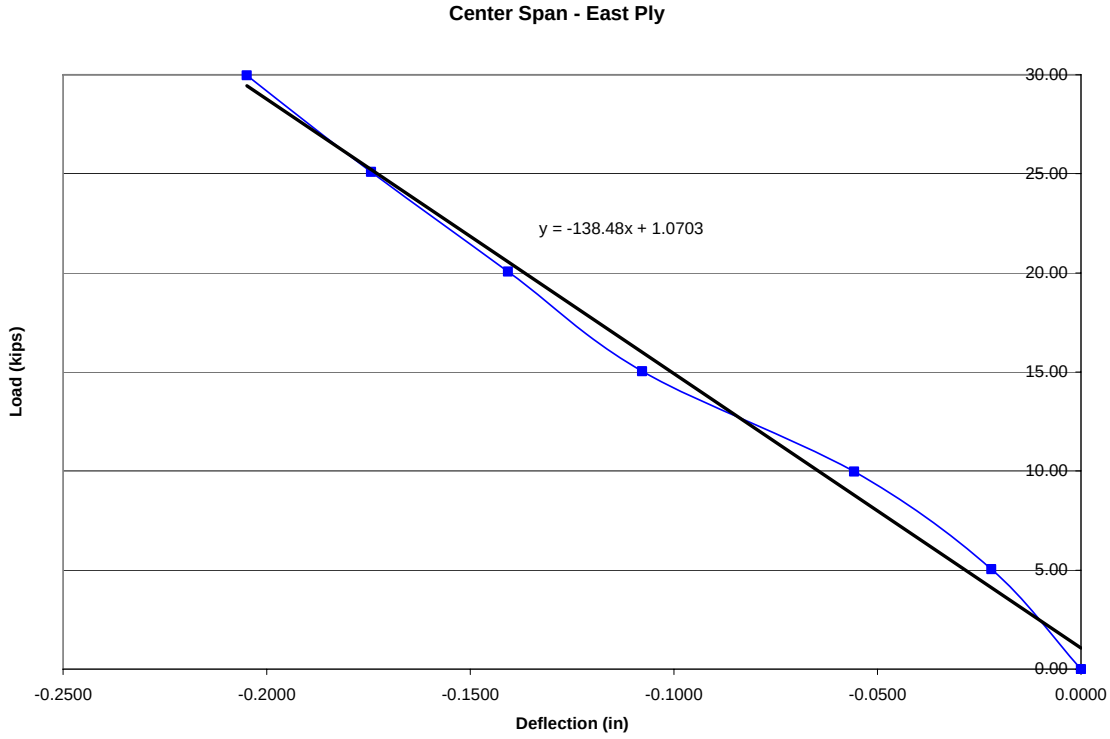

Figure D.28: C-E five sets of Z-spikes